SOUTHERN NEW MEXICO

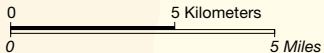## White Sands National Monument
Aden Lava Flow
Kilbourne Hole

21-23 NOVEMBER 2014

PTYS594: PLANETARY GEOLOGY FIELD STUDIES FALL 2014

UNIVERISTY OF ARIZONA LUNAR AND PLANETARY LABORATORY

Scale

0 — 5 Kilometers
0 — 5 Miles

North ↑

WHITE SANDS MISSILE RANGE
(no public access)

DOME DUNES

DUNES

DUNES

Lost River

ALKALI

FLAT

BARCHAN

PARABOLIC

HOLLOMAN
AIR
FORCE
BASE

SAN

Gardner
Peak
7533ft
2296m

DUNE FRONT

Visitor Center
to Alamogordo
15mi
24km

CO-OPERATIVE USE AREA BOUNDARY

Alkali Flat
Trail

Amphitheater

Heart of the Sands

Nature Center

🚹 🏕

🏕 **Interdune
Boardwalk**

ANDRES

ZONE OF
CO-OPERATIVE USE
(restricted area, permits required)

Dunes Drive

8mi
13km

🏕 **Playa
Trail**

TRANSVERSE-

**Big Dune
Nature Trail** 🏕

**Entrance
Station**

WHITE SANDS NATIONAL MONUMENT

Visitor Center
**Museum, bookstore,
gift shop, and
refreshments**

DOME DUNES

*LAKE
LUCERO
3890ft
1186m*

PARABOLIC

DUNES

MOUNTAINS

*LAKE
LUCERO*

DOME
DUNES

DUNE FRONT

San Andres Peak
8235ft
2510m

Twin
Buttes
4554ft
1388m

70

WHITE SANDS MISSILE RANGE BOUNDARY

WHITE SANDS MISSILE RANGE
(no public access)

Visitor Center to
Las Cruces
54mi
87km

Letter from the Editor

Hello and welcome (back) to another edition of the LPL Planetary Geology Field Studies trip field guide. This one could basically be called "Dunes and Volcanoes: Revenge of the Dust" but I frown on Star Wars references (plus we all know *Dune* and Lawrence of Arabia are go-to jokes on this one).

Given the collective knowledge of field trippers past and present, I thought I'd compile a short list of dos and don'ts for the upcoming trip. At this point, we're heading out so good luck if you haven't packed enough food or realize that your shoulders don't quite fit into your sleeping bag from the rec center (don't worry, someone will share or help you out). Here we go!

1. DON'T cook your meat with a red headlamp. This is the practical corollary to the "Don't let all the first years be in the same food group" doctrine.

2. DO make pop culture references as necessary over the CB.

3. DON'T walk over a'a. You think you can the whole way into putting glassy shards of rock into your hands and shins.

4. DO organize wake up songs for the camp (also DO be prepared to run if you play the wake up song before dawn).

5. DON'T wait to set up your tent at camp. It's much easier to cook with headlamps (see #1 for parameters) than set up a tent. Cactuses can be hiding in the underbrush.

6. DO remove any reflective vests before going into the wilderness "world's your toilet" washrooms. Camouflage is good in this case.

7. DON'T take things from National Parks or Monuments.

8. DO look up at the night sky. Our primitive camp sites are usually far away from city lights, and as the parks suggests, "half the park is after dark".

9. DON'T blow through yellow lights when caravan driving. We need to stick together, like in the Hunger Games or *The Walking Dead*.

10. DO enjoy the national parks and public lands that we visit. ☺

Here's to a good trip everyone!

Margaret Landis

Contents

Supplemental Geologic Material
Activities

About the cover
White Sands National Monument
shares airspace with the White Sands
Missile Range, famous in part for
developing rockets for the early NASA
manned space program. H.A.M. the
astrochimp is buried in Alamogordo,
NM, just northeast of the field trip
area.

Illustration: Eva A. Landis,
evalandis.tumblr.com

Day 1 – 11/21

8AM   Leave the loading dock. Drive south on Campbell, continue south on Kino. Take the I10 East towards El Paso – drive 245 miles.

Take exit 116, keep traveling East on NM 549 and continue when it becomes county road B004. This road parallels the freeway for 2-3 miles and then veers abruptly south and later veers back to head southeast. After ~9 miles form the freeway we take a right turn to cross the railroad and then a left to get back on B004. Continue driving SE on the south side of the tracks (roads B001 and B002). After a little over 7 miles we'll be at the Aden Lava flow. Take a right turn just before the flow reaches the tracks. Drive 200m SW to an 'intersection' and stop.

1PM   Lunch at the Aden lava flow
2PM   Check out inflated structures and polygons near the periphery of the flow

|	
Kenny	**Flora and Fauna & Human history of southern NM**
Josh	**Geologic history of southern New Mexico**
Catherine	**Lava flow inflation mechanism**
Mike	**Thermal contraction polygons**

Drive ~4 miles further SW down this dirt road. There's a turn-off to the left that leads up to the caldera. This road may or may not be drivable – either drive or walk about half a mile on this road to get to the rim – avoid stepping on any rattlesnakes (yes, seriously…).

4PM   Back to the vehicles and backtrack to the railroad. Take a right and drive 4 miles. There's a turn off to the right, take it and drive ~1.6 miles until the road dead-ends at our campsite. If this road is blocked we'll backtrack and use an alternate.

5PM   Camp at the Aden Lava Flow. Elevation: 4400 feet.
               (Sunset is ~5.04pm.)
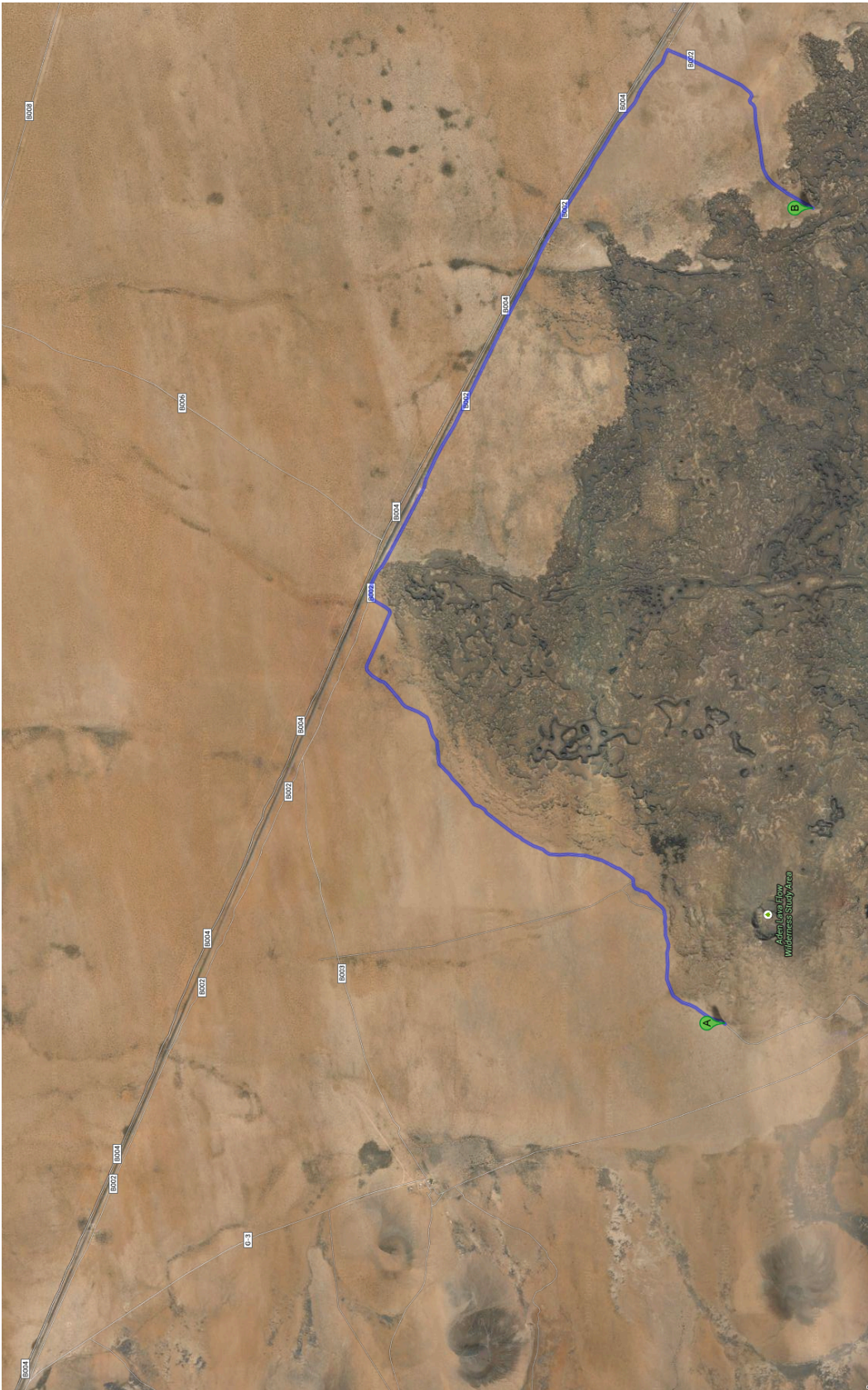
Day 2 – 11/22

8AM   Leave the campsite (sunrise is ~6.42am). Backtrack 1.6 miles to the railroad, take a right and drive SE 12 miles alongside the tracks. Take a right at Lanark onto county road A011and drive 8 miles to Kilbourne Hole.

9AM   Arrive at Kilbourne Hole.

Sondy	**Bombs**
Melissa	**Sediments at Meridiani Planum and Home Plate**
Tad	**Physics of volcanic surges**
Margaret	**Volcanic surge bedforms - analog to the MER sites?**
Jon	**Mantle and lower crustal xenoliths**

12PM   Lunch
1PM   Leave Kilbourne Hole

Backtrack to the railway line. Take a right and continue SE on county roads A12, A14 and A17 for 11 miles. Turn left on Industrial Drive and cross the railroad, take a right at the T-junction onto Airport Road and then a left onto NM136 E (later turns into TX 178 E/Artcraft Road). Join the I10W after about 7.5 miles. Drive 27 miles, transfer to I25N and drive another 6 miles. Take exit 6 onto US70; drive 49 miles to the White Sands Visitor Center.

(2.5 hrs driving – add 0.5 hour stop)

Hamish	**Rio Grande Rift history (somewhere along the road maybe San Augustin Pass)**

4PM   Arrive at White Sands (Gates Close at 6PM)

5PM   Camp at White Sands. Elevation: 4000 feet.
            (Sunset is ~5.04pm.)

Day 3 – 11/23

8AM   Leave the campsite.

Corey   Climate history of southern NM (past few hundred kyr)
Donna   Gypsum sources and sinks - including in martian dunes
Daniel   Determining dune/ripple migration rates from remote sensing
Ali   Dune geomorphology/Aeolian Stratigraphy

12PM   Lunch

Sarah P.   White Sands Missile Range

1PM   Leave White Sand National Monument

           Drive west on US 70 for 58 miles. Join the I10 West and travel 263
           miles, exit Kino Parkway. Go north, Kino becomes Campbell. Turn
           left into University Blvd ~4 miles after leaving the freeway.

6.00PM   Arrive back at LPL.

Participants

Atwood-Stone, Corey	Landis, Margaret
Baker, Vic	Lo, Daniel
Bapst, The	Lothringer, Josh
Bramson, Ali	Peacock, Sarah
Byrne, Shane	Sori, Mike
Dykhuis, Melissa	Spitale, Joe
Elder, Catherine	Springmann, Sondy
Furdella, Kenny	Viola, Donna
Hay, Hamish	Vriesema, Jess
Komacek, Tad	

Human History of New Mexico

Native People of New Mexico

The Clovis people were the first known people to inhabit New Mexico and much of North America. Their culture was geared towards big game hunting for food supplies and lasted from around 11,000 to 9,200 BCE. Their primary weapons were from animal bones called Clovis points. The Clovis people were named after Clovis, New Mexico due to the high number of artifacts found near the town. The disappearance of the Clovis people was thought to be from the loss of large game due to over hunting.

The Folsom people inhabited New Mexico from 9,000-8,000 BCE. Folsom people made up much of North America in this time period. Folsom, New Mexico is famous for a Folsom site where 23 bison were killed using Folsom points, similar to arrow heads. The Cochise people also inhibited parts of New Mexico from 10,000-500 BCE. They were the first people to show signs of agriculture. The Cochise people grew corn and beans.

The Anasazi people later inhabited New Mexico from 1-700 CE. Their culture was primary known for their arts. Evidence has been found of baskets, clothing, utensils, and sandals from this time period. The Anasazi primarily lived in the northwest section of the state. From 700-1300 CE, the Anasazi culture evolved into the pueblo Indians. The pueblo period is primarily known for their construction of stone structures. Two famous pueblos, not found in New Mexico, are Mesa Verde National Park and Canyon de Chelly National Monument. Much of central New Mexico was vacant until the 1200 CE, until the pueblo Indians started to occupy the areas along the Rio Grande River. The Navajo and Apache finally arrived in New Mexico in the 15th century, just before the Spanish arrive at the end of the 16th century.

Spanish Colonization of New Mexico

In 1595, Juan de Onate was granted permission by Spain to colonize New Mexico and spread Catholicism throughout the new world. His expedition started in 1598, exploring the Rio Grande area. He founded Santa Fe and was appointed the first governor. One of the most famous "battles" and a prime example of his harsh rule was the battle at Acoma in January of 1599. A fight broke out that led to the death of 11 Spaniards. Onate retaliated by killing over 800 men, women, and children. The foot of every 25 year or older Acoma man was cut off and females were sent off to be slaves for 20 years. Even with the harsh rule of Onate, the Spanish were still unable to completely control the pueblo Indians.

During the 1670s, drought, famine, and disease swept through the neighboring tribe of the pueblo Indians. These hardships provoked attacks from the pueblo Indians. There was a pueblo revolt was led by Pope in 1680 driving the Spaniards from all but southern New Mexico. The Spanish were driven into El Paso. Due to power struggles for Santa Fe and death of Pope in the 1680s, it left the pueblo Indians in disarray and vulnerable to attacks. In 1692, Diego Vargas led the Spanish forces to Santa Fe and forced the pueblo people to surrender and swear allegiance to Spain. This battle is known as the bloodless conquest, no lives were lost in this battle.

Mexican Rule and American war

The Mexican war started in 1808 and ended September 27th 1821, marking the freedom of New Spain, Mexico, from Spain. This war also marked the independence of New Mexico from Spanish rule but not from Mexican rule.

1841 marked the being of the Santa Fe expeditions. The republic of Texas felt that it had a claim to the land east of the Rio Grande and Santa Fe, that Mexico currently had control over. The Texan military expedition was led by Hugh McCleod and consisted of 320 troops and merchants. The expedition was poorly planned due to the harsh environmental landscape and Indian attacks. The Texans finally made it to Santa Fe, but were confronted with the Mexican army. Hughes and his troops had to surrender due to lack of supplies and man power. They were made prisoners and forced to march to Mexico City where they were held, until the US could rescue them the following year.

In 1846, during the Mexican-American War, Stephen W. Kearny took Santa Fe with around 2000 troops. The town fell without any opposition. In general, New Mexico was taken with little bloodshed. There was a revolt, Taos revolt, which only lasted a month and led to the death of around 300 New Mexican. By 1848, the Treaty of Guadalupe Hidalgo made Mexico concede New Mexico and west of the pacific the US.

New Mexico and the United States

The southeast corner of New Mexico was purchased through the Louisiana Purchase in 1803. The first exploration by the US was by lead by Lt. Zebulon Pike in 1807. In 1851, Santa Fe was made the capital of New Mexico. By 1848, New Mexico had become a US territory. In 1912, New Mexico became the 47th state.

Flora and Fauna:

State Flora and Fauna

State flower: Yucca flower
State tree: Two-Needle Pinon Pine
State grass: Blue Grama
State animal: black bear
State bird: Chaparral Bird (Greater Roadrunner)
State fish: Cutthroat Trout
State vegetable: Chilies

Fauna

The New Mexican wildlife population is very diverse due to the varying amount of climates in the region. There are over 1,100 different species of animals found throughout New Mexico. The majority of the land animals that live in New Mexico are found in the Rio Grande Valley. The large game found in New Mexico consist of elk, sheep, deer, antelope, oryx, javelin, turkey, black bear, ibex, and

mountain lion. There are also wolves, coyotes, gray foxes, white-tailed rabbits, gray squirrels, and bobcats. The birds found in New Mexico are the crow, hummingbird, raven, American goldfinch, cactus wren, 11 species of bats, great blue heron, chipping sparrow, and over 200 more species of birds. Due to droughts and lack of water in New Mexico, the diversity of fish has greatly decreased. Some of the common fish are rainbow trout, brown trout, kokanee salmon, large/smallmouth bass, pike, catfish, and cutthroat trout. There are also turtles, lizards, and snakes found throughout New Mexico.

Flora

The harsh climates in New Mexico can make it a challenging place for plant life. Most of the flora found in New Mexico are hearty drought resistant plants. Some of the cacti found in New Mexico are prickly pear, barrel cactus, cholla, and hedgehog cacti. The trees common to New Mexico are ponderosa pines, cottonwood, douglas fir, sagebrush, juniper, and many others. There is also a wide a sort of flowers like dogwood, dandelion, daisy, honeysuckle, and lily.

References:

New Mexico Office of the State Historian State Records Center & Archives, http://newmexicohistory.org,

New Mexico Department of Game and Fish, http://www.wildlife.state.nm.us/

Geological History of Southern New Mexico

By Joshua Lothringer
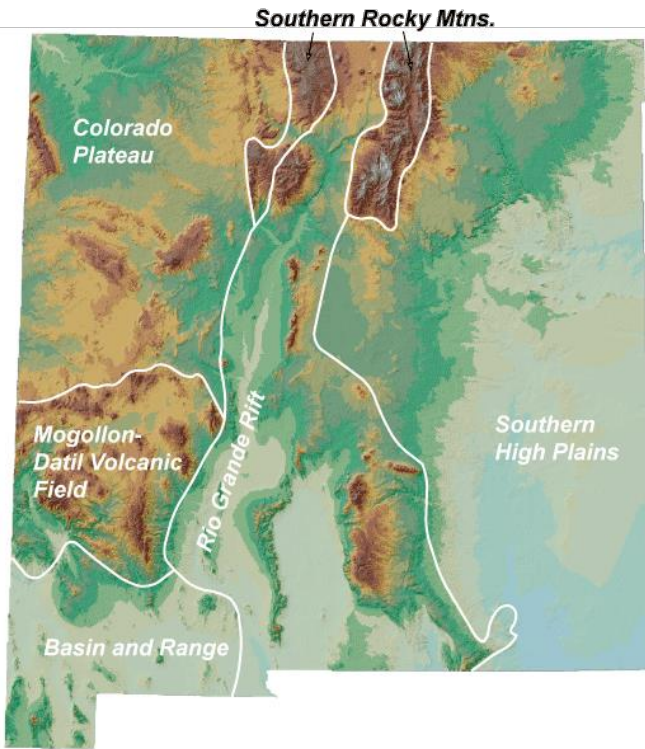
Figure 1 New Mexico Physicogeologic Provinces - New Mexico Bureau of Geology and Mineral Resources

Much of North America was periodically submerged under the ocean throughout much of the Paleozoic Era. As the continent began to uplift, this ocean retreated. This deposited large amounts of limestone, sandstone, and shale. Similarly, a great barrier reef around the Delaware Basin in southeastern New Mexico left evaporate deposits of salt, potash, and gypsum.

Entering the Mesozoic Era, the supercontinent Pangea began to break apart. During this time, rivers deposited colorful sandstones and shale. New Mexico was entirely above sea level at the beginning of the Mesozoic era, but towards the end, during the Cretaceous Period, a shallow inland sea developed through the middle of the North American continent. By the end of the dinosaur era 65 million years ago, this inland sea, too, had retreated. As the North American plate overrode the ancient oceanic Farallon plate, some tectonic activity began in the region 85 Mya. Some limited volcanic activity may have occured up to 75 Mya as bodies of magma reached the surface when the crust thinned as a result of the collision.
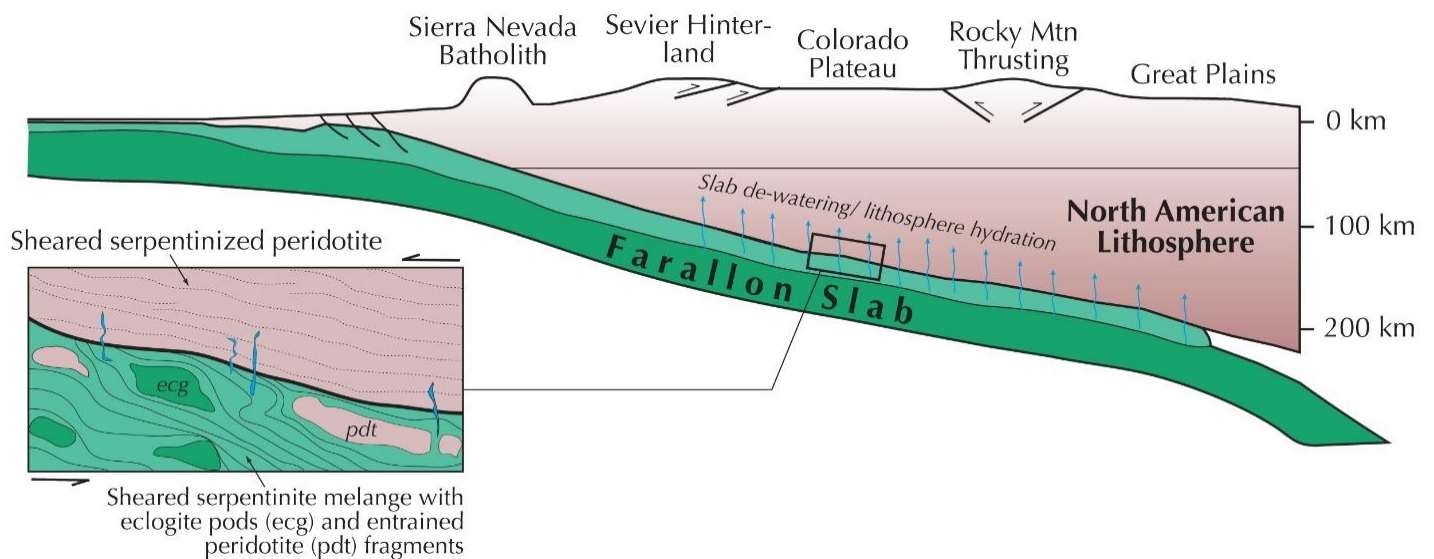
Figure 2 Farallon Plate Subduction - Behr, W.M

As the Cenozoic Era began, much of the western United States was covered in grassland, large lakes, and small mountain ranges. The intense tectonic changes due to the Farallon plate subducting under the North American Plate caused the formation of the North American Cordillera, the collection of mountain chains along the west of the continent. This process created the mountains, basins, and plateaus that we see today throughout the western United States. The Rocky Mountains began to form during the Laramide orogeny, a period of mountain-building in the western United States starting 70-80 Mya and ending 35-55 Mya. This plate collision also resulted in more volcanism in the New Mexico region. Some volcanism began towards the beginning of the Cenozoic Era, during the Paleocene epoch. Large-scale volcanism in the region began in the Late Eocene around 40 Mya and lasted until about 20 Mya. This deposited a thick layer of igneous rock throughout the region.

We will begin our trip by driving east through the Basin and Range Province. This geological physiographic region stretches across most of the western United States and extends north to the Columbia Plateau and south to northern Mexico. Basin and Range topography is characterized by narrow, rugged, and isolated fault-block mountains running North to South. This province is created by the extension of the Earth's
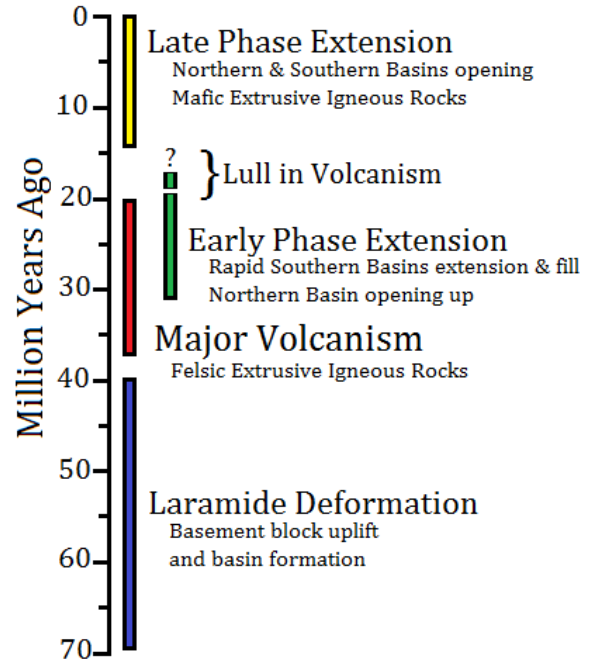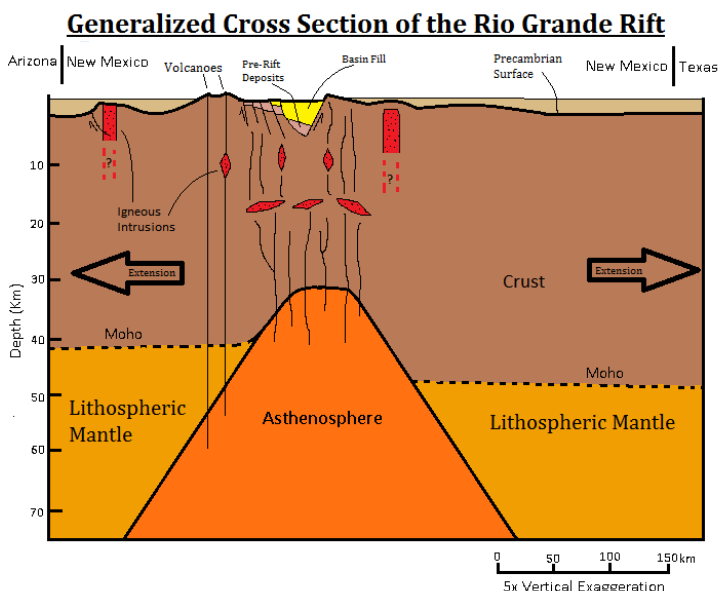

Figure 3 P. Morgan & M. Golombek

weakened crust due to injection of hot magma up to 30 Mya as the Farallon plate subducted underneath the North American plate during the late Oligocene epoch (the same process that created rifting in the bordering Rio Grande Rift discussed below). The shallow angle of subduction is thought to have caused the topography and decreased volcanism near the edge of the plates. Uplift to current elevations in this area is thought to have occurred by Epeirogenic movement within the last 10

Figure 4 W. Baldrige, K. Olsen & J. Callender

million years (Kues 1992). Collapse extension of this area continues to the present day.

As we continue our journey to south-central New Mexico, we will enter the Rio Grande Rift. This is an area of interconnected grabens created from the uplift of surrounding mountain ranges. Tertiary and Quaternary sediments filled these grabens as they subsided. The surrounding uplifts have exposed the Precambrian core and the Paleozoic sediments of the mountains.
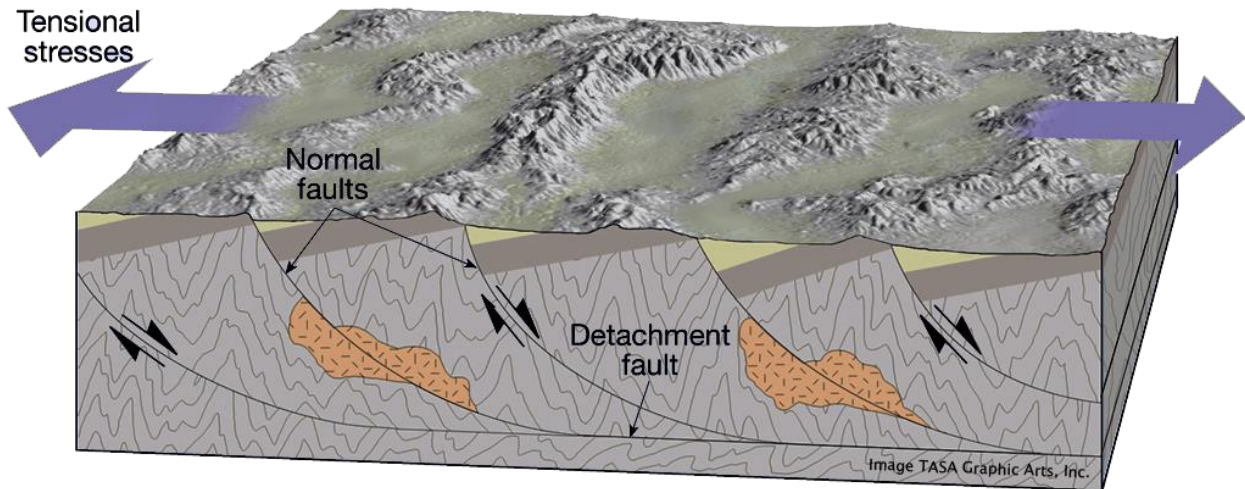
Figure 5 Basin and Range Terrain Formation - Idaho State University

References

Baldridge, W.; Olsen, K.; Callender, J. (1984). "Rio Grande Rift: Problems and Perspectives". *New Mexico Geological Society Guidebook, 35th field conference*. pp. 1–11.

Kues, Barry. "New Mexico: Geology." Rocks & Minerals 67.5 (1992): 340-9.

Morgan, P.; Golombek, M. (1984). "Factors controlling the phases and styles of extension in the northern Rio Grande rift". *New Mexico Geological Society Guidebook, 35th field conference*. pp. 13–20.

New Mexico Bureau of Geology and Mineral Resources. Virtual Geologic Tour of New Mexico: https://geoinfo.nmt.edu/tour/provinces/basin_and_range/home.html

University of New Mexico. Geologic History of New Mexico. http://www.unm.edu/~natsci/NM_history.htm

Idaho State University. Alamo Impact. http://geology.isu.edu/Alamo/rocks/basin_range_uplifts.php

Lava Flow Inflation
Catherine Elder

1 Background on Lava Flows

- Variety in lava flows occurs because of differences in viscosity and stress. Viscosity is controlled by temperature, water content, bubble content, crystal content, and chemical composition (primarily silica content). Stress is determined by effusion rate, fountain height, lava speed, slope, and channel width (Productions 2004).

- A'a is more viscous, so it's more resistant to movement and forms loose rubble on the surface and flow front (Productions 2004)

- Pahoehoe flows advance at least 10 times more slowly than a'a flows. This allows their surfaces to develop smooth and continuous crusts at the beginning of emplacement (Houghton *et al.* 1999).

- Inflation is the injection of molten lava underneath a solidified crust. It primarily occurs in pahoehoe flows when lava continues to be added beneath the solid continuous crust.

Figure 1: Left: An a'a flow front advancing over pahoehoe on the coastal plain of Kilauea Volcano, Hawaii. Right: Pahoehoe toes fed by lava that broke out from a lava tube (out of view) also at Kilauea Volcano, Hawaii. Images are from USGS Volcano Hazards Program photo glossary of volcano terms.

2 Inflation

- Pahoehoe forms when toes/tongues/lobes break out from the crust at the flow front. These toes quickly form a crust, but if more lava is added, more toes will break out. Toes can merge to form larger toes.

- These initial toes are thin (<50 cm), but can grow with continued lava input. As they are filled with more lava, they inflate like a balloon and push the crust upwards (Self *et al.* 1998, Productions 2004).

1

- If there is a low lava supply or uneven terrain, inflation occurs only locally. This creates tumuli (Figure 2) and inverted surface topography (Figure 3). The resulting terrain is called hummocky pahoehoe.

Figure 2: A tumulus. Michelle and James for scale.

- If there is a larger lava supply and smooth terrain, the toes coalesce and inflate together becoming part of the main flow (Productions 2004).

- This process can convert a 20 to 50 cm thick lobe into a sheet many meters thick in a period of weeks (Self *et al.* 1998).

- It can inflate flows on Hawaii to thicknesses of $\sim$ 6 m and more viscous continental flows to thicknesses of $\sim$ 25 m (Productions 2004).

- The inflation of the lobe can last days, months, or years (Self *et al.* 1998 and references therein).

- Inflation can also form tree molds (Figure 4).

3 Pahoehoe Flows in the Western United States

- The Basin and Range province has many small inflated hummocky pahoehoe flows fed from scoria cones like the Amboy and Pisgah flow fields in the Mojave Desert, California.

- The Colorado Plateau has many basaltic flow fields with inflated pahoehoe. The Taos volcanic field and the Potrillo maar field (including Kilburn Hole) in the Rio Grande Rift contain many pahoehoe sheet flows (Self *et al.* 1998).

2
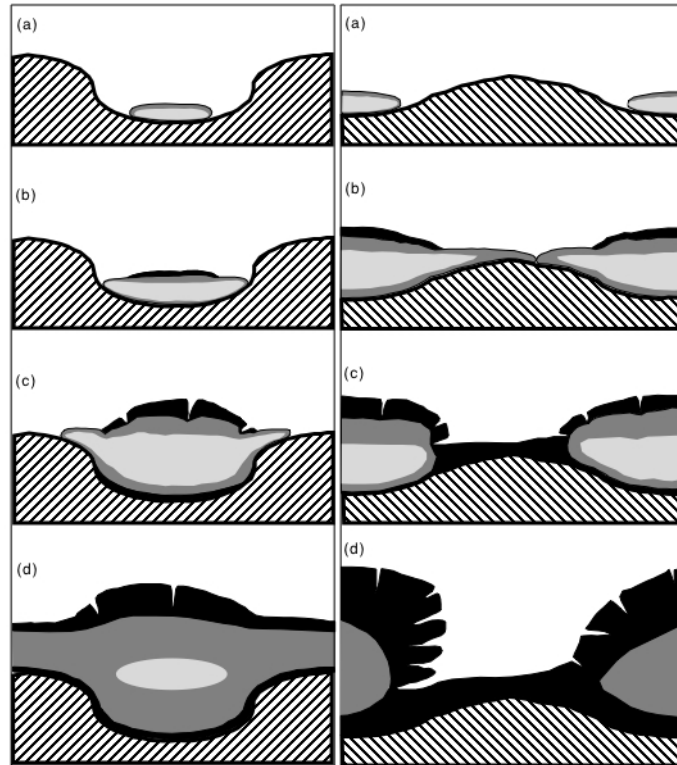
Figure 3: Cartoon of the inversion of topography during inflation from Self *et al.* (1998). a) The initial pahoehoe lobes are confined to the lowest areas. b,c) The flows advance, inflate and spread laterally filling the depressions. The thickest crust and the core of the flow is on the oldest part of the sheet, so the highest inflation is over what was originally the lowest ground. Breakouts from the inflation features eventually cover the earlier higher ground. d) A continuous sheet or an inflation pit forms over the previous high points depending on the rate of inflation relative to the rate of crust growth (Self *et al.* 1998).

4   Lava Flows on Other Planets

- Lava flows stretching hundreds of kilometers are commonplace on the Moon, Mars, and Venus and sometimes cover a larger area than the ancient flood basalts on the Earth (Houghton *et al.* 1999).

- Lava flows cover 90 % of the surface of Venus, 50 % of Mars, at least 20 % of the Moon, and 70 % of the Earth including the ocean floor (Houghton *et al.* 1999).

- The shape and size of extraterrestrial lava flows can provide insight into the properties of the crusts and mantles of other planets (Houghton *et al.* 1999).

- On Earth, pahoehoe lava flows are the dominant type of basaltic lavas in terms of both areal coverage and total volume (Self *et al.* 1998), and several large flows on other planets seem to be pahoehoe (Self *et al.* 1998, Theilig and Greeley 1986, Bruno *et al.* 1992, Campbell and Campbell 1992).

3

Figure 4: A hollow tree mold formed when lava chilled and solidified around the cooler tree trunk and incinerated the tree. The pahoehoe inflated to the highest point on the tree mold, and then deflated as lava drained out from beneath the solidified pahoehoe crust. Alfred for scale.

References

Bruno, B. C., G. J. Taylor, S. K. Rowland, P. G. Lucey, and S. Self 1992. Lava flows are fractals. *Geophys. Res. Lett.* **19**, 305–308.

Campbell, B. A., and D. B. Campbell 1992. Analysis of volcanic surface morphology on Venus from comparison of Arecibo, Magellan, and terrestrial airborne radar data. *J. Geophys. Res.* **97**, 16293–+.

Hon, K., J. Kauahikaua, R. Denlinger, and K. MacKay 1994. Emplacement and inflation of pahoehoe sheet flows: Observations and measurements of active lava flows on Kilauea Volcano, Hawaii. *Geological Society of America Bulletin* **106**, 351–370.

Houghton, B., H. Rymer, J. Stix, S. McNutt, and H. Sigurdsson 1999. *Encyclopedia of Volcanoes*. Academic Press.

Productions, V. V. 2004. Lava Flows and Lava Tubes.

Self, S., L. Keszthelyi, and T. Thordarson 1998. The Importance of Pahoehoe. *Annual Review of Earth and Planetary Sciences* **26**, 81–110.

Theilig, E., and R. Greeley 1986. Lava flows on Mars: Analysis of small surface features and comparisons with terrestrial analogs. *J. Geophys. Res.* **91**.

4

Thermal Contraction Polygons
Mike Sori

Solids that experience cooling or drying tend to contract according to thermal physics. This results in tensile stress, and where the local stress exceeds the tensile strength of the material, fractures from to suddenly relieve the stress [e.g., Mellon, 1997]. The resulting pattern of fractures often looks polygonal in planform, and this process is generalizable to different materials; see Figure 1.
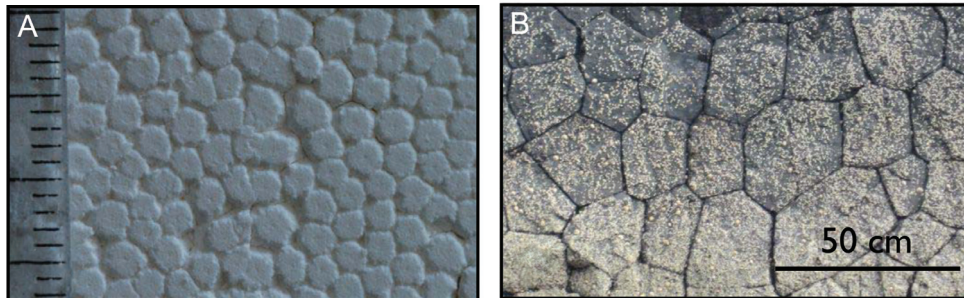
Figure 1: Contraction polygons seen in drying corn starch (A) at the mm scale and cooled lava flow (B) at the tens of cm scale. From [Goehring et al., 2008].

In the case of cooling basalt, fractures propagate several meters to tens of meters in depth. This results in a set of parallel vertical polygonal prisms knowns as columnar joints (Figure 2). Such formations have been reported and studied as early as the late 17th century for the case of the Giant's Causeway in Northern Ireland [Bulkeley, 1693]. Quantitative studies of the geometry of basalt columns have been aided by experiment [e.g., Goehring et al., 2008] and observations of the Kilauea Iki lava lake [e.g., Ryan and Sammis, 1978; Hardee, 1980].

Figure 2: Columnar jointing in the Columbia River Basalt Group in Washington. From [Goehring and Morris, 2008].

The hexagonal nature of basalt columnar joints is a result of different modes of deformation [e.g., Rice, 1967], and that fracture opening is a sudden and discrete process (though downward continuation of fractures is probably incremental) [Ryan and Sammis, 1978]. Consider a cooling lava surface that is yet unfractured. The first fracture to open will be a result of pure tensile stress. However, this opening will relax material adjacent to this fracture, and subsequent contraction will cause both a tensile and a shear component of stress. See Figure 3. The important point is that positions of previously open fractures influence the next fracture opening [Ryan and Sammis, 1978; Goehring et al., 2010]. Note that a purely hexagonal pattern is a simplification, and other materials may experience a more rectangular pattern [e.g., Corte and Higashi, 1960; Goehring et al., 2010].
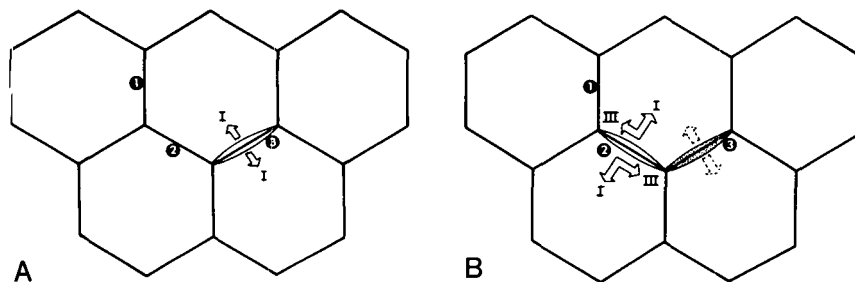
Figure 3: Formation of two cracks in what will eventually become a hexagonal fracture pattern. The first crack (A) forms a result of purely tensile stresses, but the second crack (B) forms as a result of both tensile and shear stresses because of the influence of the first crack. From [Ryan and Sammis, 1978].

Note that in the case of lava flows, polygonal patterns can also form in tumuli. A tumulus is a positive topographic feature typically on the scale of meters high that is formed by uplifted and up-tilted crustal plates [Walker, 1991]. See Figure 4. One can distinguish said polygons from thermal contraction polygons that form on lava lakes by the meter-scale topography.
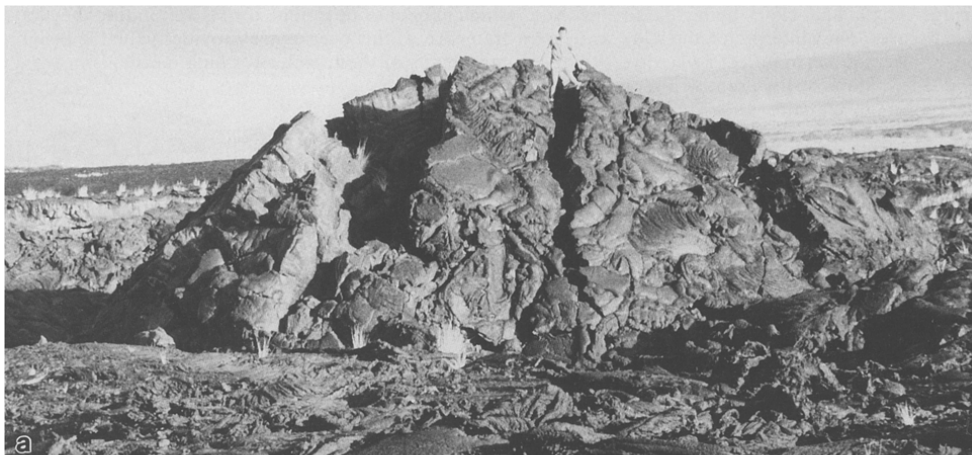
Figure 4: Image of a 2.8-m high tumulus in Hawaii. From [Walker, 1991].

Thermal contraction polygons are also important elements of the landscape in glacial settings. In this case, the cracks that form as a result of thermal contraction may fill with meltwater; in this case, the subsurface permafrost may then freeze the water, forming an ice wedge [e.g, Black, 1976]. Warmer months then cause the ice wedge to thermally expand, causing compressive stresses and microtopography on the landscape. See Figure 5. Annual cycles repeat this process and cause cracks to grow over time. In non-glacial environments, sand may take the place of ice and form sand wedges [e.g., Pewe, 1974].

Figure 5: Ice wedge polygons in Northwest Territories, Canada.

Polygonal landscapes have also been observed on Mars from multiple spacecraft since they were first detected in Viking Orbiter images [Evans and Rossbacher, 1980]. Such polygonal landscapes are now known to come in a wide variety of morphologies [Levy et al., 2010] and span a large range of latitudes. Authors have interpreted equatorial polygons to be thermal contraction polygons indicative of recent (within the past ~10 Myr) Martian periglacial landscapes, and argue that their location inside erosional basins is unlikely to support a volcanic origin [Balme and Gallagher, 2009]. However, many outstanding questions remain concerning polygonal landscapes on Mars at all latitudes, and lander data would be especially valuable in interpretation of formation mechanisms of the polygons themselves and implications for Martian history [Levy et al., 2010].
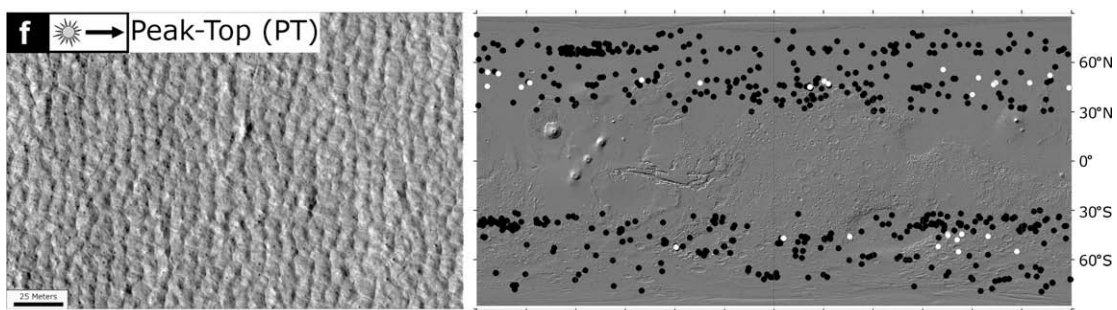
Figure 6: Polygonal landscape of a certain morphological group on Mars. White dots indicate HiRISE images contained these polygons. From [Levy et al., 2010].

References

Balme, M. R., and C. Gallagher (2009), An equatorial periglacial landscape on Mars, *EPSL, 285*, 1-15.

Black, R. F. (1976), Periglacial features indicative of permafrost: Ice and soil wedges, *Quarternary Res., 6,* 3-26.

Bulkeley, R. (1693), Part of a letter from Sir R.B.S.R.S. to Dr. Lister, concerning the giatns causeway in the county of Atrim in Ireland, *Phil. Trans. R. Soc. Lond., 17*, 708-710.

Corte, A., and A. Higashi (1960), Experimental research on dessication cracks in soil, *US Army Snow Ice and Permafrost Research Report, 66,* 48.

Evans, N., and L. A. ROssbacher (1980), Reports of the Planetary Geology Program, *NASA Tech. Memo. TM 82386,* 376-378.

Goehring, L., L. Mahadevan, and S. W. Morris (2008), Nonequilibrium scale selection mechanism for columnar jointing, *PNAS, 106,* 387-392.

Goehring, L., and S. W. Morris (2008), The scaling of columnar joints in basalt, *J Geophys Res,* 113-129.

Goehring, L., R. Conroy, A. Akhter, W. J. Clegg, and A. F. Routh (2010), Evolution of mud-crack patterns during repeated drying cycles, *Soft Matter, 6*, 3562-3567.

Hardee, H. C. (1980), Solidification in Kilauea Iki lava lake, *J. Volcanol. Geotherm. Res., 7,* 211-223.

Levy, J. S., D. R. Marchant, and J. W. Head (2010), Thermal contraction crack polygons on Mars: A synthesis from HiRISE, Phoenix, and terrestrial analog studies, *Icarus, 206,* 229-252.

Mellon, M. T. (1997), Thermal contraction cracks in Martian permafrost: Implications for small-scale polygonal features, *LPSC XXVIII,* Abstract 1495.

Pewe, T. L. (1974), Geomorphic processes in polar deserts, *Polar Deserts and Modern Man,* University of Arizona Press, Tucson, pp. 33-52.

Rice, J. R. (1967), Mechanics of crack tip deformation and extension by fatigue, *Fatigue crack propagation: Philadelphia, Am. Soc. Testing and Materials, 415* , 247-309.

Ryan, M. P., and C. G. Sammis (1978), Cyclic fracture mechanisms in cooling basalt, *Geol. Soc. Am. Bull., 89,* 1295-1308.

Walker, G. P. L. (1991), Structure, and origin by injection of lava under surface crust, of tumuli, "lava rises", "lava-rise pits", and "lava-inflation clefts" in Hawaii, *Bulletin of Volcanology, 53,* 546-558.

Xenoliths and Lava Bombs

Volcanic History of Kilbourne Hole

Kilbourne Hole is a maar crater that formed in the Late Cenozoic due to a phreatomagmatic eruption, an interaction with magma and water without igneous extrusion. Maars in this area are well preserved, and Kilbourne hole is an excellent example of this type of volcanic steam eruption (Crumpler and Aubele 2001).

Bombs

Volcanic bombs (Figure 1) form during eruptions and are igneous rocks that solidify into pieces larger than about 2.5 inches; they can acquire aerodynamic shapes during their flight from the volcano. As they cool they can take on elongated shapes. Bombs can pose a hazard to humans around volcanos as they can travel for kilometers away from the volcano (the recent eruption of Mount Ontake in Japan earlier this year. In addition, bombs can also embed themselves in lava flows surrounding the volcano.

We see bomb sags in pyroclastic surge beds, results of volcanic gas and steam moving onto a surface leaving layers. Bombs indent the surge beds at Kilbourne Hole and other maar volcanoes(Kelley 2014), Figure 2.

Xenoliths

The word *xenolith* comes from Greek and means "foreign stone", a fragment of a foreign rock enveloped in a larger host rock with a different composition. We see xenoliths in meteorites as well as in sedimentary and igneous terrestrial processes. Igneous xenoliths form when lava tears surrounding rocks from the edges or margins of magma chambers, giving us samples of the mantle. Thus, mantle xenoliths provide us information about mantle conditions and mineral stability at depths far below what we can easily sample, including unite, peridotite, and kinds of spinel. The xenoliths we see at Kilbourne Hole include peridotite, made of olivine and eclogites (garnet and green pyroxene) (Fuhrbach 1992).

Some Mineral Compositions

Basalt: amphibole and pyroxene, sometimes plagioclase, feldspathoids, and/or olivine
Olivine: $(Mg,Fe)_2SiO_4$
Peridotite (Dunite): generally olivine with lesser pyroxene (augite); dunite is dominantly olivine; some metallic minerals (chromite, magnetite, etc.)
Plagioclase: $NaAlSi_3O_8$ to $CaAl_2Si_2O_8$
Pyroxenes: $XY(Si,Al)_2O_6$

Figure 1: A lava bomb from Kilbourne Hole. Credit: Kelley (2014).

Figure 2: A lava bomb in a surge bed at Kilbourne Hole. Credit: Kelley (2014)

Figure 3: Xenobomb from Kilbourne Hole showing peridotite surrounded by basalt. Credit: Niranjan Khalsa, `http://davetzold.com/2013/02/10/kilbournes-hole/`

Xenolith Bombs

When Kilbourne Hole erupted it ejected liquid magma into the atmosphere, which then cooled into elliptical shapes allowing the center to cool slowly and form crystals, or preserve mantle minerals and form "xenolith bombs" (Fuhrbach 1992). The olivine present in xenolith bombs at Kilbourne Hole is often of gem quality forsterite, the magnesium-rich olivine endmember. Weathering exposes the bombs from their surge beds for easy collection, and breaking open a bomb reveals a xenolith interior, often full of green peridotite (Figure 3).

Some of the xenoliths we see in bombs at Kilbourne Hole in addition to gem-quality peridotite include granulite, charnokite, and anorthosite, perhaps from the lower to middle crust (Hamblock et al. 2007). The granulite may contain garnet and sillimantite, or pyroxene, suggestive of metasedeimentary or igneous origin, respectively Hamblock et al. (2007).

Analogue to Home Plate on Mars?

Kilbourne Hole is believed to be a terrestrial analogue for Home Plate on Mars due to its explosive origin. Squyres et al. (2007) proposed that the Home Plate feature visited by the Spirit Mars Exploration Rover on Mars shows evidence of pyroclastic activity, and that observations from orbit and by Spirit "indicate that the lower strata were emplaced in an explosive event, and geochemical considerations favor an explosive volcanic origin over an impact origin." Kilbourne Hole shows lava bombs and bomb sags, which "are found in volcaniclastic deposits on Earth ... causing downward deflection of layering" (Squyres et al. 2007).

References

Crumpler, L. S. and J. Aubele (2001). Volcanoes of New Mexico: An Abbreviated Guide for Non-Specialists. In L. S. Crumpler and S. G. Lucas (Eds.), *Volcanology in New Mexico*, Volume 18, pp. 5–15. New Mexico Museum of Natural History and Science Bulletin.

Fuhrbach, J. R. (1992). Kilbourne Hole Peridot. *Gems & Gemology*, 16–27.

Hamblock, J., C. Andronicos, K. Miller, C. Barnes, M.-H. Ren, M. Averill, and E. Anthony (2007). A composite geologic and seismic profile beneath the southern rio grande rift, new mexico, based on xenolith mineralogy, temperature, and pressure. *Tectonophysics 442*(14), 14 – 48.

Kelley, S. A. (2014, August). Kilbourne Hole. Technical report, New Mexico Bureau of Geology & Mineral Resources.

Squyres, S. W. et al. (2007). Pyroclastic activity at home plate in gusev crater, mars. *Science 316*(5825), 738–742.

Sediments at Meridiani Planum and Home Plate
Melissa J. Dykhuis

which is on Mars

which is also on Mars

who is totally just posing as an expert on Mars
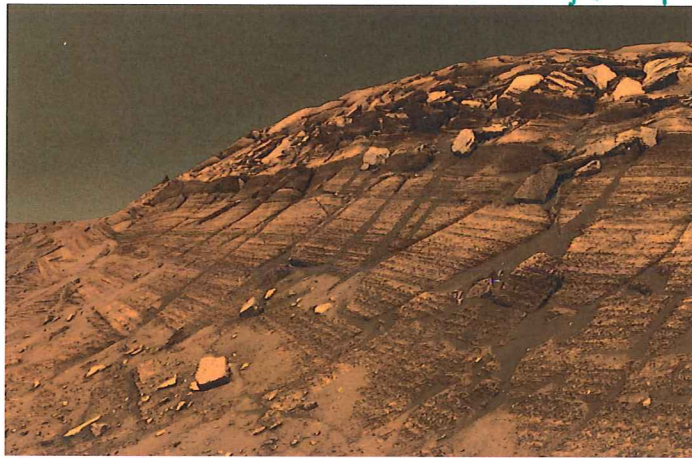
Above: Sediments at Meridiani Planum of course.

A dry lakebed?

Squyres et al. (2004) see evidence at Meridiani Planum for a pattern of episodic shallow inundation, evaporation, and then movement of sediment over dry ground.

Inundation: Festoon cross-lamination
(i.e., "curvy tilted lines")

Evaporation: Sulfur → sulfate salts

(i.e. quartz sandstone)

Dry movement: Siliciclastic material and larger-scale cross-bedding

Above: Festoon cross-lamination (arrow), image scale 40 cm across
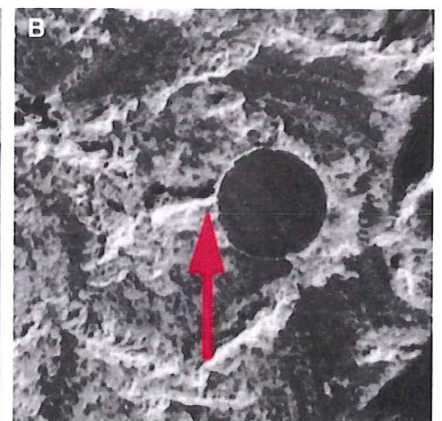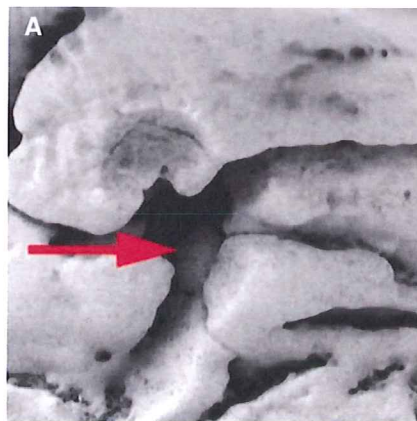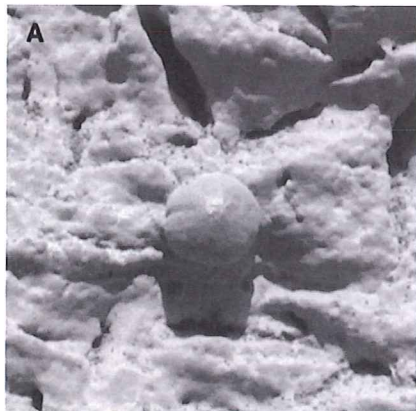
Left: A spherule with lines across it that parallel the surrounding laminae, *image scale 15 mm across.* Try squinting, it helps?
Above: Spherules impinging on vugs, *images 12 mm across.*
found under rugs, exact nature unknown but scary (cf. Seuss 1974)

When did this happen?

Squyres et al: "Nothing in our observations at Eagle crater places useful bounds on the duration of aqueous activity at Meridiani."

Definitely on my list of what *not* to say during orals.

24

Home Plate

Squyres et al. (2007) interpret some Home Plate geology in terms of volcanic activity. *(or maybe impact)*

Mineralogy: alkali-rich basalts; Inner Basin

I hate it when that happens

Formations: bomb sags, high-angle cross-bedding, coarse-to-fine gradation

HiRISE Image

Tracks

Home Plate

Low Ridge

Tyrone

Spirit's Winter Campaign Site

Tracks

50 m
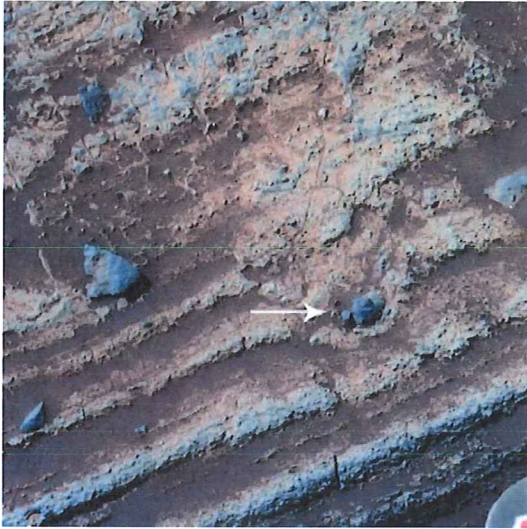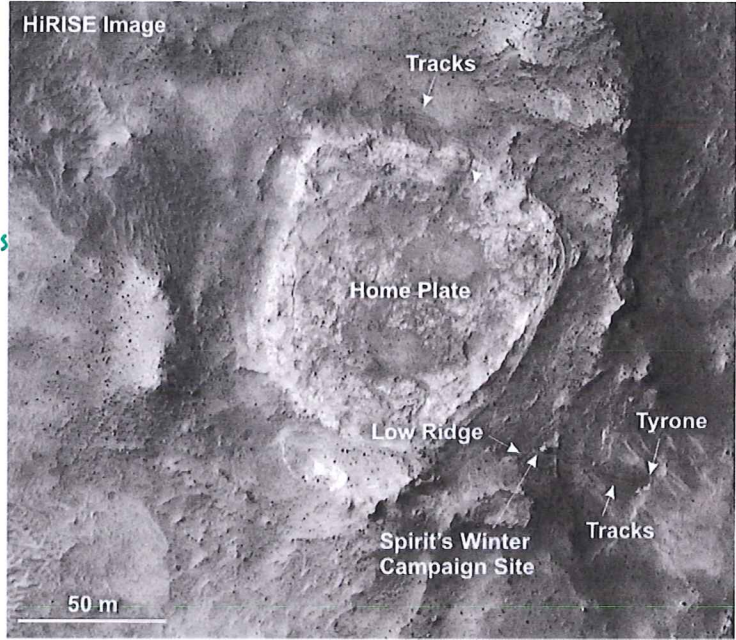
Above: *A bomb sag near Home Plate, ~4 cm across*
Right: *High-angle cross-bedding near Home Plate, 1-2 m across, interpreted as "scouring during flow bursting, migration of three-dimensional bedforms with frontal scour pits, and at times when the sediment concentration of a flow is decreased."*

→ *Reinterpreted by MJD to mean "a Volcano was here".*

Means "associated with lakes"... not outdoor toilets.

Lacustrine vs. volcanic/impact surge origin

Knauth et al. (2005) reinterpreted Meridiani Planum geology in terms of explosive surge origin, with analogies to our very own Kilbourne Hole.
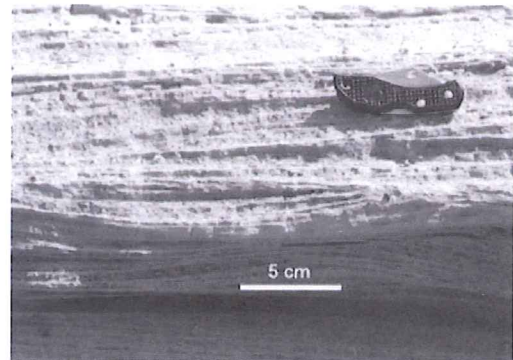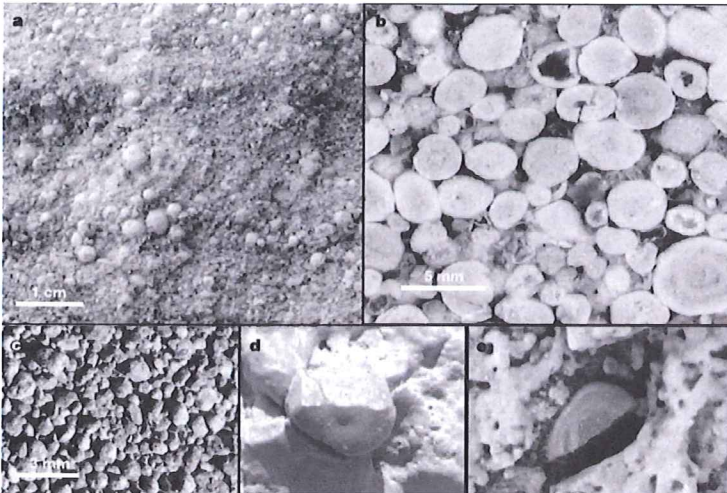
Above: *Festoon cross-beds at Kilbourne Hole*

Left: *Spherules from a) Kilbourne Hole; b) Onverwacht Formation, South Africa; c) Meteor crater; d) Mars, broken 4 mm spherule; e) Mars, broken 4 mm spherule*

25
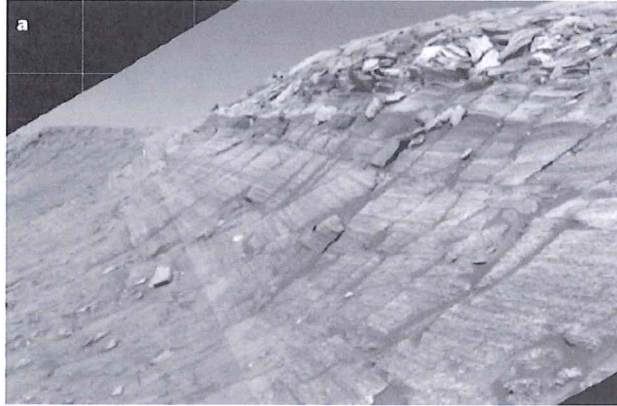
Mars vs. Kilbourne Hole ↖ Guess which is which?

On Earth, nuclear test sites and volcanic landmarks like KB Hole show similar strutures as observed in Meridiani Planum, particularly festoon cross-bedding and spherules (previous page figures).

Impact surges on Mars create "fluidized" ejecta aprons, so it's worth considering surge origin for Meridiani Planum as well as Home Plate.

Problems solved by impact surge hypothesis
(as emphasized by Knauth et al.)

- Mixing of highly soluble salts with less soluble salts: Not likely with evaporation
- High sphericity of spherules: More common for surge events
- No evident basin boundary

Problems with impact surge hypothesis
(less emphasized by Knauth et al.)

- Big enough nearby impact?
    Schiaparelli crater, 450 km wide, 1000 km away?
    Or perhaps multiple crater events?
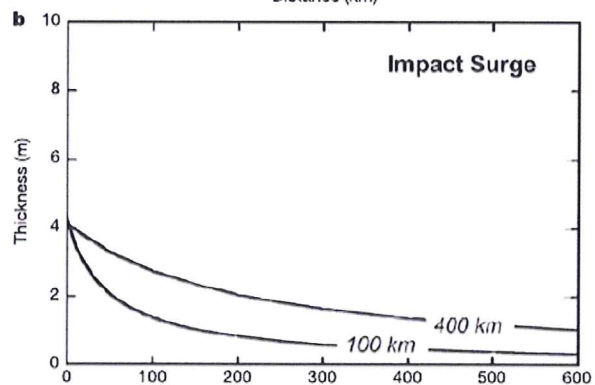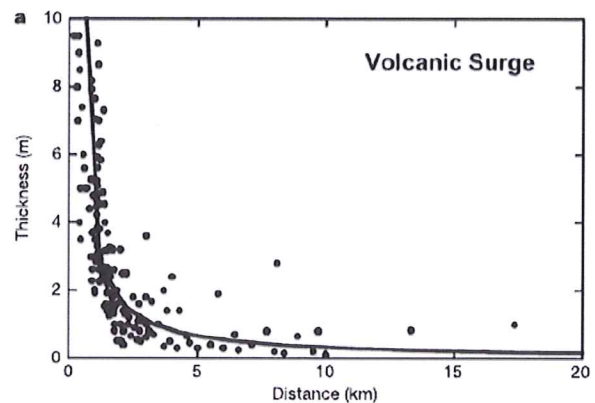
Above: Martian crater ejecta thickness estimated via terrestrial volcanic surge deposits.

Morals

The moral of the story: The same geologic evidence can be interpreted in many different ways.
The other moral of the story: Remote exploration of another planetary surface is *hard*.

MJD is deeply indebted to Google for a crash course in geology vocab.

26

PHYSICS OF VOLCANIC SURGES

T.D. KOMACEK

1. PYROCLASTIC DENSITY CURRENTS: OBSERVATION

Pyroclastic Density Currents (PDCs) are aggregations of gas and rock that spread laterally at speeds up to $\sim$ 700km/hr, with temperatures of order $\sim$ 1000 Kelvin. An example of the generation of a pyroclastic density current in the Tonga eruption of 2009 is shown in Figure 1 (Doronzo et al. 2011). An image of a pyroclastic density current itself, from the Mount St. Helens eruption of 1980, is shown in Figure 2 (Druitt 1998). This PDC traveled $\sim$ 25 km from the caldera. An image of a pyroclastic surge deposit (from the Upper Laacher See Tuff, in Germany) is shown in Figure 3. A common surge bedform called "sandwaves" are seen in Figure 3. These have wavelengths up to 20m and can be up to 2m high. The wavelengths of sandwaves decreases with distance from the vent, pointing towards the dynamics inherent in pyroclastic surges. Additionally, the deposit thickness of a PDC decreases with distance from the vent (Wohletz & Sheridan 1979), see Figure 4. Though there are more complicated aspects to PDCs, I will now

FIG. 1.— Generation of pyroclastic density current from collapse of eruption column in the Tonga eruption of 2009, adapted from Doronzo et al. (2011).
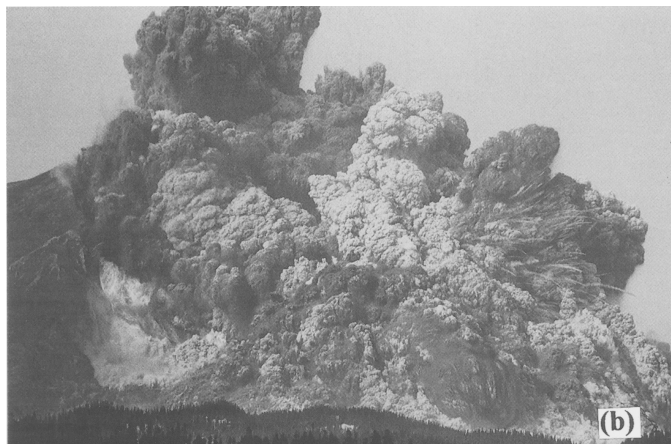
FIG. 2.— Image of Mount St. Helens pyroclastic density current, adopted from Druitt (1998).
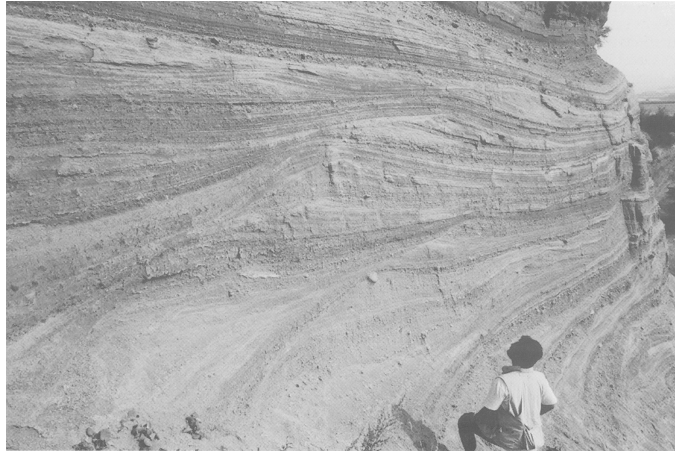
FIG. 3.— Image of surge deposit from Upper Laacher See Tuff in Germany, adapted from Druitt (1998).
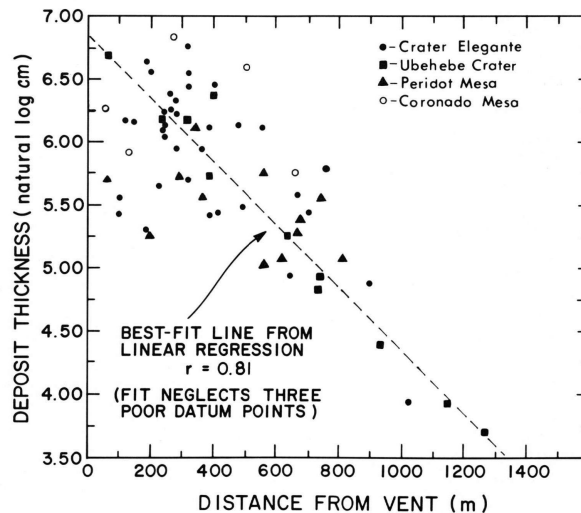
FIG. 4.— Empirical relation from Wohletz & Sheridan (1979) of pyroclastic deposit thickness vs. distance from vent. Note the clear linear trend of decreasing thickness with increasing distance.

turn to models and interpretation of these surge deposits, as everybody likes results.

2. PYROCLASTIC DENSITY CURRENTS: MODELS

A basic model for ignimbrite (PDC deposit) emplacement, developed by Druitt (1998), is shown in Figure 5. It is clear from this model that the multi-flow structure of PDCs requires complicated physics for detailed understanding. There is a differential settling of large and small clasts, leading to a stratified suspension current. The smaller particles are lofted in an ash cloud, while larger clasts can combine and form "layer 1" deposits. A somewhat more physical description of this, from Burgisser & Berganz (2002), is given in Figure 6. Three dimensionless numbers govern the dynamics of a PDC: the Stokes number, $\text{St} \propto \tau_v \Delta U d_{\text{eddy}}^{-1}$, Froude number $\text{Fr} \propto \Delta U d_{\text{eddy}}^{-1/2}$ Stability Factor $\Sigma = \text{St}/\text{Fr}$, and dense-dilute concentration $\text{DD} \propto \tau_c \tau_v^{-1}$. Here τ_c is the time between particle collisions in the flow, τ_v is the e-folding timescale of the particle velocity in the viscous medium, ΔU is the eddy speed of the turbulent flow, and d_{eddy} is the eddy diameter. Hence, it should be clear that pyroclastic density currents are controlled by turbulence, which makes it clear why smaller particles are more easily lofted in such a flow. Hence, the model shown in Figure 6 can be interpreted as the expectation that turbulent flow will have both dilute (DD >1) and granular (DD <1) components, where the dilute component is the "surge" and the granular component is the main pyroclastic flow. In between these two regimes one expects to find stratified deposits, which are homogenized throughout the flow thickness.

PDCs are also controlled by the concentration gradient, see Figure 7. It is clear that an increase in concentration gradient in the flow leads to faster and smaller eddies, enabling the flow to stay closer to the ground and flow over longer length scales.

A numerical simulation of pyroclastic density current formation, compared to experimental simulation of the same phenomena from Doronzo et al. (2011), is shown in Figure 8. The stages shown are early eruptive column formation through column collapse and current generation (this whole process only takes ∼ 5 sec to occur!). The simulation was done using a nasty-sounding Euler-Lagrange multiphase approach by solving the three-dimensional incompressible
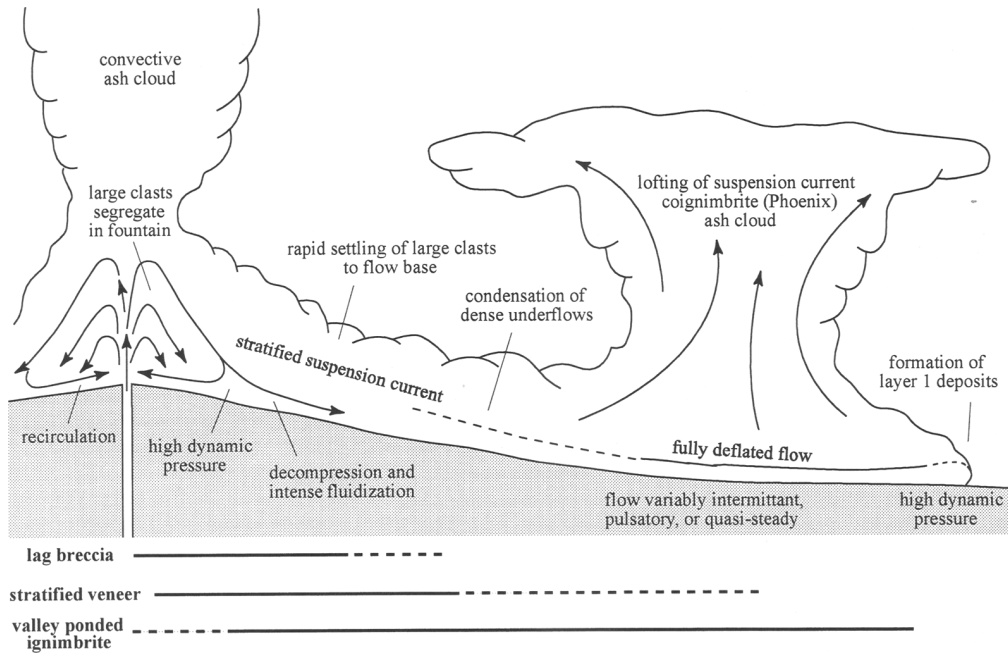
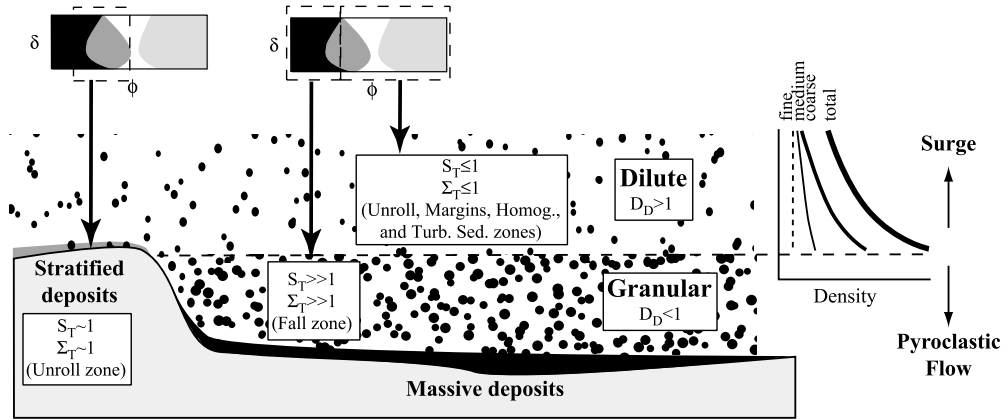Fig. 5.— Model for the eruption and emplacement of ignimbrite from Druitt (1998).

Fig. 6.— Schematic cross section of pyroclastic density current from Burgisser & Bergantz (2002).
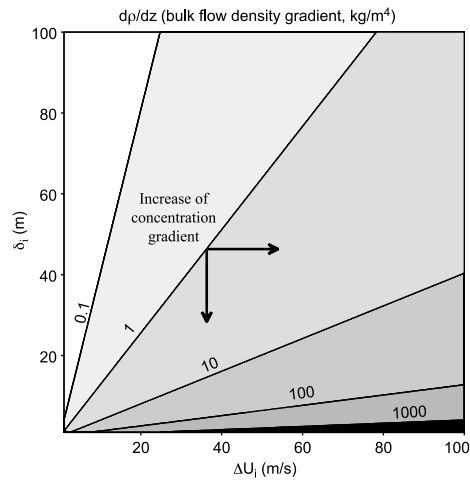

Fig. 7.— Change in eddy length scale and velocity as a function of concentration gradient, from Burgisser & Bergantz (2002).
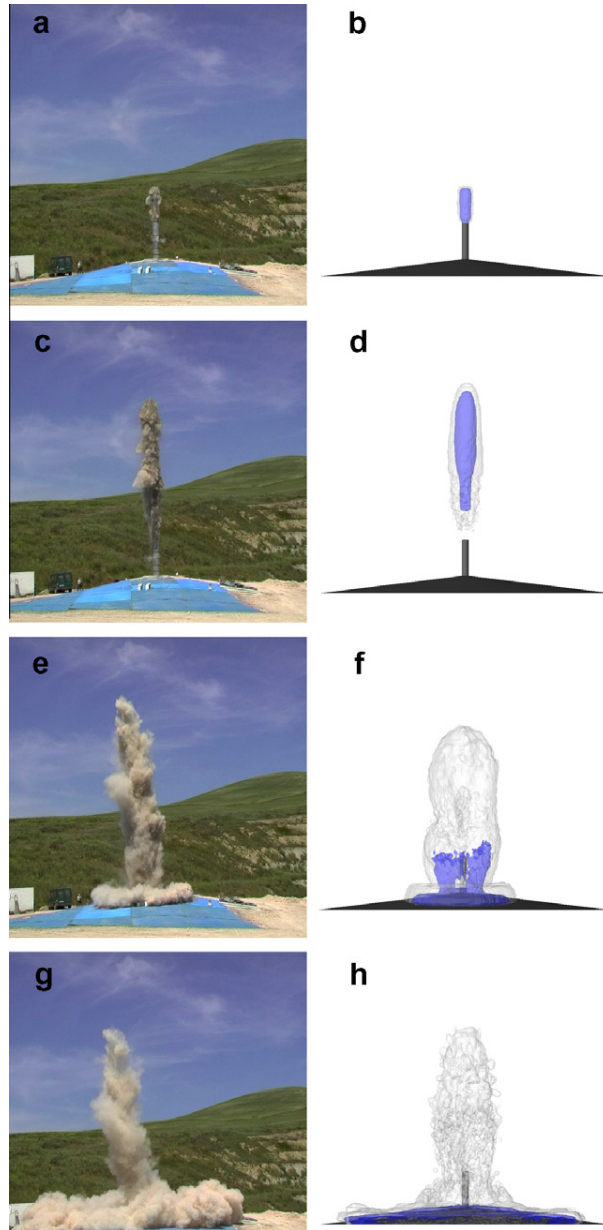
FIG. 8.— Images of experimental (left) and numerical (right) simulations of pyroclastic density current formation, from Doronzo et al. (2011).

Reynolds Averaged Navier-Stokes equations via a finite volume method. The experiments are done by sticking a bunch of nitrogen and fine particles in a tube that is pressurized to 190 bars and then let go, leading to velocities of up to 15 m/s and pressures ∼ 500 Pa within the flow. Pretty cool!

3. PLANETARY CONNECTION

Pyroclastic density current deposits are potentially expected to be found on Venus, Mars, and the Moon (in addition to Earth, of course) in our Solar System (Cameron 1964; Carter et al. 2012; Ghail & Wilson 2013; Spohn et al. 2014). The early application, from Cameron (1964), interpreted Sinuous rilles on the Moon as PDCs, using telescopic observations from Earth. An image from the Lick observatory is shown in Figure 9. Basically, the argument goes that because a channel is seen near a crater, there must have been nuées ardentes (ash flows) forming smooth deposits over great distances on the surface. It is agreed that Sinuous rilles were likely formed by lava action, but their exact formation process is unknown.

The venus application is born from Magellan data, with radar imagery of Tuli Mons (Carter et al. 2012) shown in Figure 10. Even though this is shield volcanism, smooth pryroclastic deposits can still form (note that Plinan-type eruptions are not expected to have occurred on Venus and Mars). The argument is that the polarization is similar to that expected from lunar pyroclastic deposits. There is a correlation between low circulation and high linear polarization areas, which points to fine-grained pyroclastic deposits. There is also evidence of pahoehoe flows in the
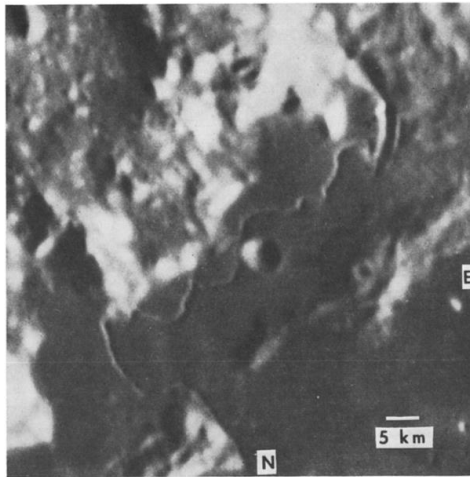
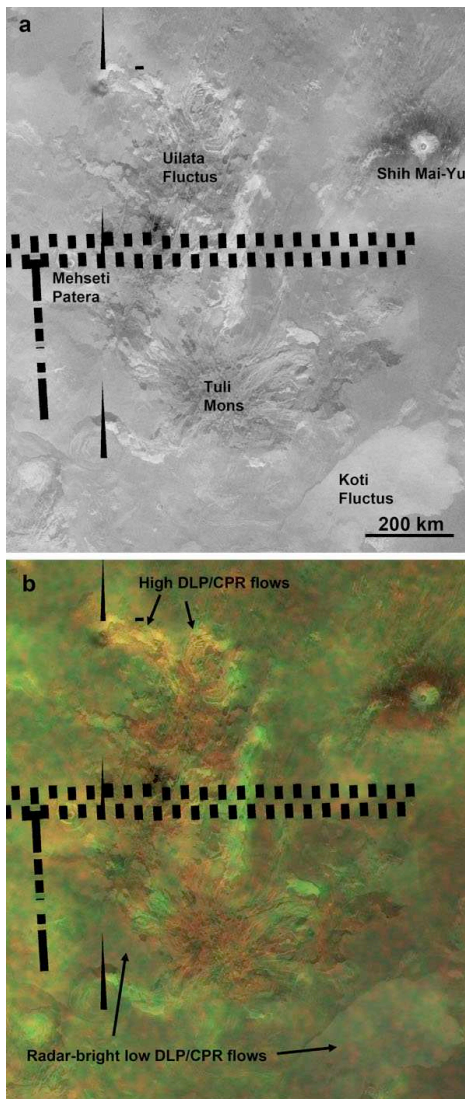FIG. 9.— Hadley rille on the Moon, from Cameron (1964).

FIG. 10.— Top: Magellan SAR image of Tuli Mons. Bottom: Radar polarimetry overlaid, red represeting linear polarization and green circular polarization. Adapted fromCarter et al. (2012).

radar-bright regions.

REFERENCES

Burgisser, A. & Bergantz, G. 2002, Earth and Planetary Science
  Letters, 202, 405
Cameron, W. 1964, Journal of Geophysical Research, 69, 2423
Carter, L., Campbell, B., & Glaze, L. 2012, in Comparative
  Climatology of Terrestrial Planets
Doronzo, D., de Tullio, M., Dellino, P., & Pascazio, G. 2011,
  Computers & Fluids, 44, 56
Druitt, T. 1998, Geological Society of London Special
  Publications, 145, 145

Ghail, R. & Wilson, L. 2013, Geological Society of London
  Special Publications, 401
Spohn, T., Breuer, D., & Johnson, T., eds. 2014, Encyclopedia of
  the Solar System (Elsevier)
Wohletz, K. & Sheridan, M. 1979, Geological Society of America
  Special Papers, 180, 177

Volcanic surge bedforms: Analog to the MER sites?
Margaret Landis

At a glance

- Surge bedforms are caused by particles falling out from an explosive release of particles and fall into two dominant categories: flow and fallout
- Particles sort themselves by size based on the type of flow they were embedded in
- The bedforms appear in the field to have dune-like structures and cross-bedding
- Common around maar volcanoes where water has explosively interacted with magma
- Can lead to interpretive difficulty given that similar structures can arise from large explosions of different origins (explosive volcanism, impacts, and bomb detonations)

Surge bedform formation

Surge bedforms occur when an explosive eruption or other event that lofts small particles of material into the air. For example, Figure 1 shows the volcanic plume in the blast driven surge in a volcanic eruption, where the area of dune deposition is along the interface between the surge and the surrounding topography.
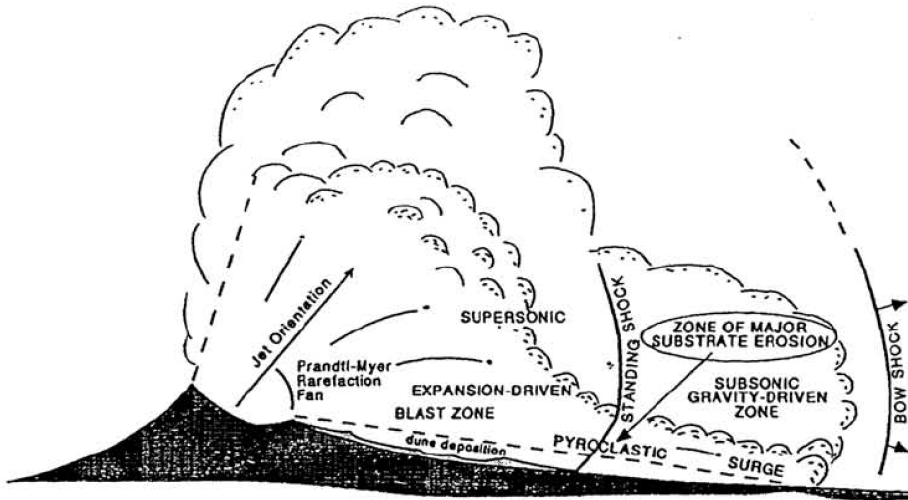
Figure 1 From Wohletz (1998), this figure shows an in-progress volcanic eruption with an ash cloud with the pressure wave from the explosion. It also shows the area of erosion and deposition caused by the base surge.

Due to the interplay between the particles in the surge runout (the physical particles in the surge) and the blast wave, the deposition that occurs sorts the particles by size. Other objects, like volcanic bombs or leaves, can be imbedded in the layered deposits that result.
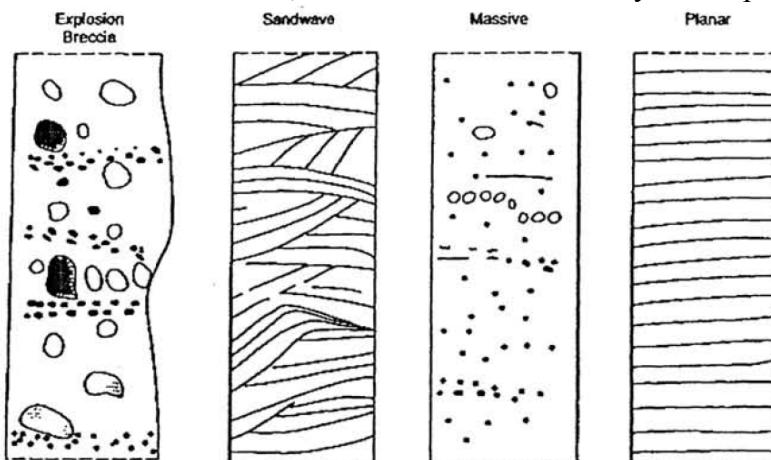

Figure 2 Soil profiles for a selection of surge bedform types (Wohletz, 1998).

These deposits can have layers, apparent dune forms, or can be mostly comprised of explosion breccia depending on the style of eruption and proximity to the eruption. Some examples of soil profiles that can arise in surge bedforms are shown in Figure 2. Sandwaves can also occur with a variety of cross-bedded morphologies as well. These are due to the introduction of turbulence within the base surge (Figure 3).
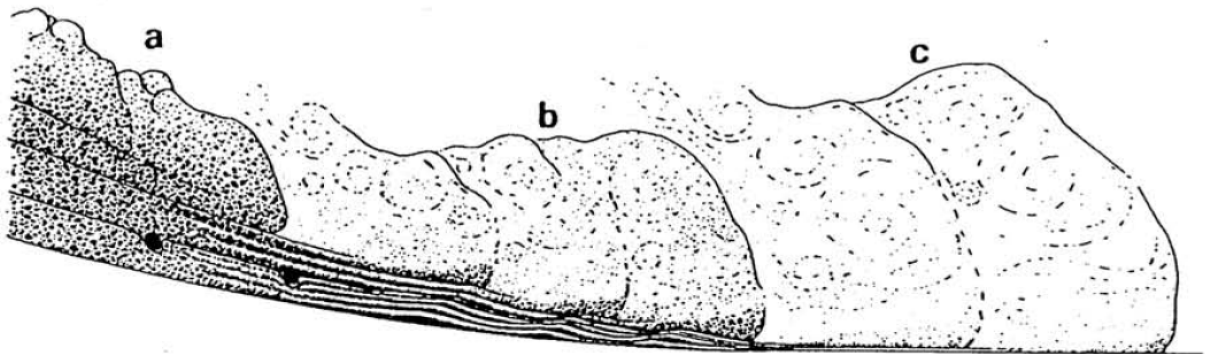

Figure 3 Adapted from Sohn and Chough (1989), three stages (a-c) of a base surge development showing how the turbulence increases and particle density decreases with radial extent (left to right) from the vent (Wohletz, 1998).

Volcanic surge bedforms in the field

Surge bedforms were first identified after the nuclear tests at the Nevada Test site where they could be carefully studied knowing the exact explosive yield of the bomb detonations. In nature, volcanic surge bedforms can occur in different eruption regimes, but some of the most distinctive and earliest recognized are those around maar volcanic craters (Fisher and Walters, 1970 and references therein). Maar volcanic craters occur when water interacts with a magma

Figure 4 Panel to the left shows a close up view of the maar crater deposit stratigraphy (with the author's boot for scale) and, on the right, in context along the rim of the volcanic crater.

causing a series of explosive eruptions. Each explosive eruption drapes a new set of material over previous sediments, causing the cross-bedding and layering described above (Figure 2).

Figure 4 shows photographs from Rattlesnake Crater in northern Arizona (35.226364, -111.333528). This example of maar crater only has a partial rim but occurs in the larger volcanic field around Flagstaff, AZ in the San Francisco volcanic field.

Analog to the MER landing sites?

The dominant interpretation of MER Opportunity landing site is that a volcanic landscape was heavily modified by the evaporation of a highly acidic shallow lake. For Gusev Crater, the landing site of MER Spirit, the dominant interpretation is that the deposits are pyroclastic in nature. In two Science papers, Squyers and co-authors make the case for these interpretations (Squyers et al. 2004 for Opportunity and Squyers et al. 2007 for Spirit). For further discussion, see M.J. Dykhuis' discussion, this field guide.

For Spirit and Gusev Crater, there is cross-bedding consistent with the fine-grained units in the upper section. In addition to the cross-bedding in the upper layers, the rover captured an image that suggests a bomb sag, leading to the interpretation of clear base surge deposits in the crater. The volcanic bomb sag (Figure 5) and other evidence has lead to the conclusion that Home Plate and other deposits are volcanic in nature and therefore analogs to the volcanic surge deposits present on Earth.
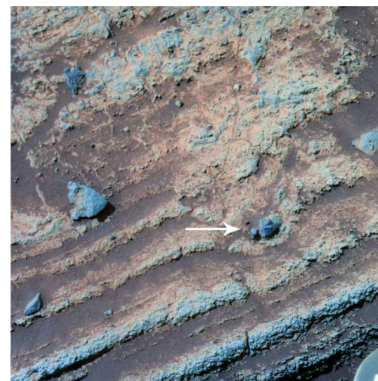

Figure 5 An arrow in the figure points to what Squyers et al. (2007) interpret to be a volcanic bomb sag. These types of bomb sags are common in terrestrial volcanic surge deposits like those in Kilbourne Hole Hole, New Mexico.

The interpretation for the Opportunity landing site are less clear-cut. Layered terrains as well as hematite blueberries lead Squyers et al. (2004) to conclude that there was long-term aqueous alteration by a reservoir of water that, while sustained for a long period of time, was of a non-neutral pH and of high salinity. While this is the common consensus interpretation, an alternative interpretation by Knauth et al. (2005) suggests that alternatives to aqueous alteration, for instance the large number of small impacts in Meridiani Planum, could have generated an impact base surge history sufficient to explain the layered deposits.

References

Fisher, R. V. & Walters, 1970. A. C. Am. J. Sci. 268, 157–180.

Knauth, L.P, D.M. Burt, K.H. Wohletz, 2005. Nature 438.

Squyers, S.W. et al., 2007. Science 315, 738.

Squyers, S.W. et al., 2004. Science 306, 1709.

Wohletz KH, 1998. In: *From MAGMA to TEPHRA Modeling Physical Processes of Explosive Volcanic Eruptions*, A Freundt (Ed.), 247-312.

Mantle and lower crustal xenoliths

By: The Bapst

What are xenoliths?

Xenoliths (Greek for "foreign rock") are rock/mineral fragments that are enveloped in a larger "host" rock during the development, solidification, or transport of the host material.

Mantle Xenoliths

Mantle/lower crustal xenoliths (which originate at depths of 30-200 km) are hosted and transported to or near the surface in volcanic rocks (see example in Figure 1). Xenoliths are typically embedded in rapidly erupted material (e.g., phreatomagmatic) and thus "lock in" mineralogical and chemical signatures of their depth of origin.

These fragments are a snapshot of the mineralogy, chemistry, and physical nature of the lower crust/mantle and provide samples of typically unreachable parts of the Earth (or any differentiated planetary body, generically). Our knowledge of the composition of the upper mantle is largely a result of xenolith analyses. The alternative process for bringing upper mantle material to the surface involves tectonic processes (e.g., orogenic peridotites, ophiolites or abducted oceanic crust).
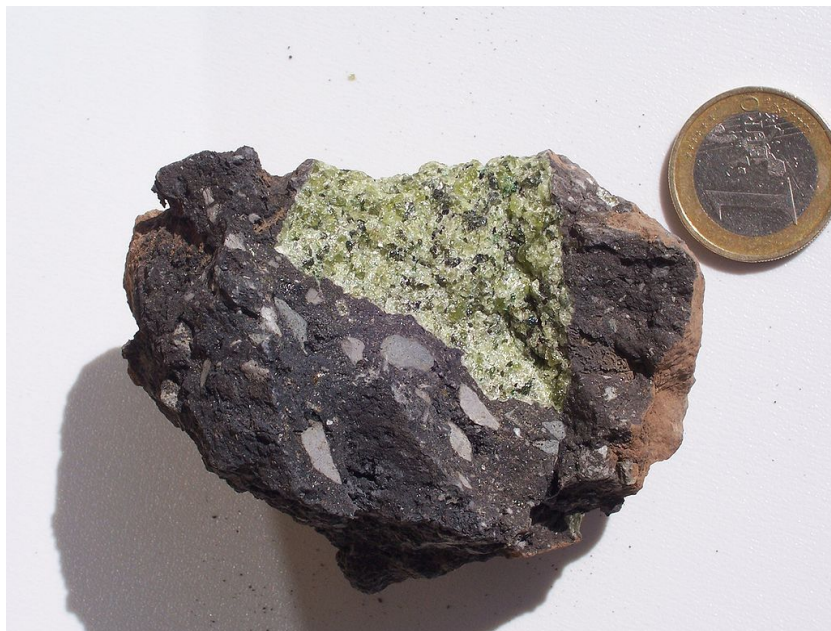
Figure 1. Peridotitic mantle xenolith (green, olivine and pyroxene rich ultramafic rock) within a volcanic bomb (dark) from the Vulkan-Eifel, Germany. *Source: Wikipedia (CC BY-SA 1.0)*

Geologic Occurrences
- Cratonic xenoliths
    - Continental volcanic rocks
        - Dominated by garnet-facies peridotite
        - Different plate setting results in different lithologies and chemical signatures
            - Cratonic
                - Thickest, oldest continental crust
                - Deeper equilibrium depth
            - Circum-cratonic
                - Shallower equilibrium depth
            - Rift-related magmatism
                - Marginal to cratons
                - Very shallow equilibrium depth compared to cratonic and circum-cratonic
                - More consistent with "non-cratonic" xenoliths
- Non-cratonic xenoliths
    - Oceanic volcanic rocks
        - Xenoliths much rarer compared to continental environments
            - Contained in exclusively alkalic potassic mafic magma
            - Most sample the oceanic lithosphere not the mantle lithosphere
                - Good exception: Soloman Islands (margin of Ontong Java Plateau)
    - Subduction zone environments
        - Only recently recognized
        - Detailed relationship to subduction zone is a matter of debate
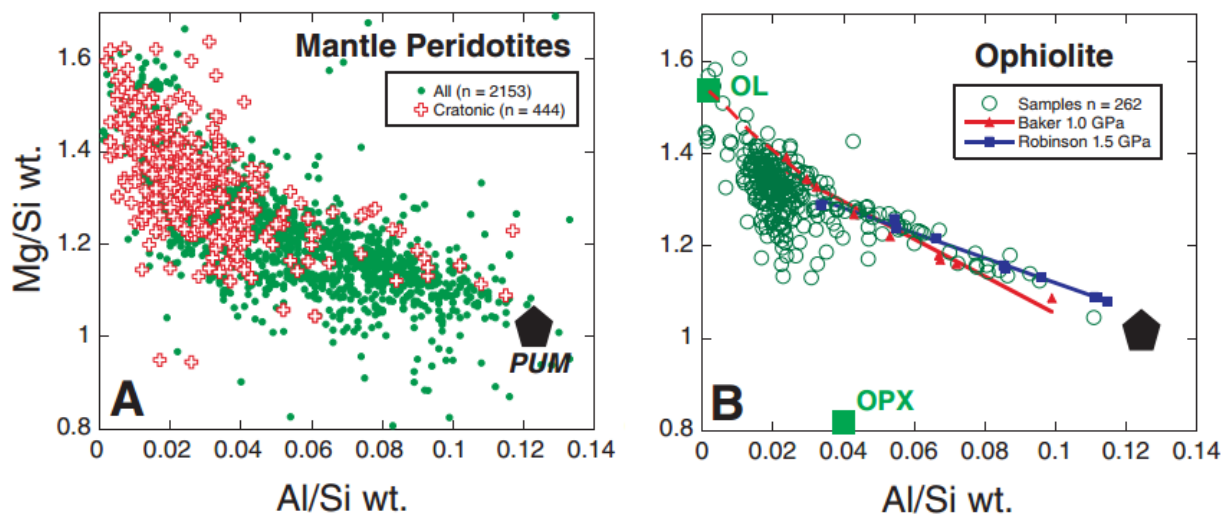
Figure 2. Plots comparing silicon enrichment for different sources of mantle peridotite; black pentagon represents primitive upper mantle (PUM) and is based on chondritic composition **(A)** Mantle peridotites from xenoliths from cratonic zones (red) and all other sources (green); note non-cratonic mantle xenoliths lie closer to PUM **(B)** Ophiolite peridotite (non-xenolith), with partial melting modeled compositions for two pressures (~depths); note similarity to cratonic xenoliths in A; *Source: Canil and Lee, 2009*

Fluid Inclusions

Mantle xenoliths can also contain melt-phase and fluid inclusions, which provide another sample of conditions and composition of the mantle. Fluid inclusions are largely composed of CO_2 but have minor constituents as well such H2O, CH4, N2, noble gases, CO, sulfur species, and carbonates. The distribution of minor volatile species in inclusion fluids can provide information on the oxidation state of the upper mantle, on mantle degassing processes and on recycling of subducted material to the mantle. Melt inclusions in ultramafic xenoliths give information on silicate–sulphide–carbonatite immiscibility relationships within the upper mantle.
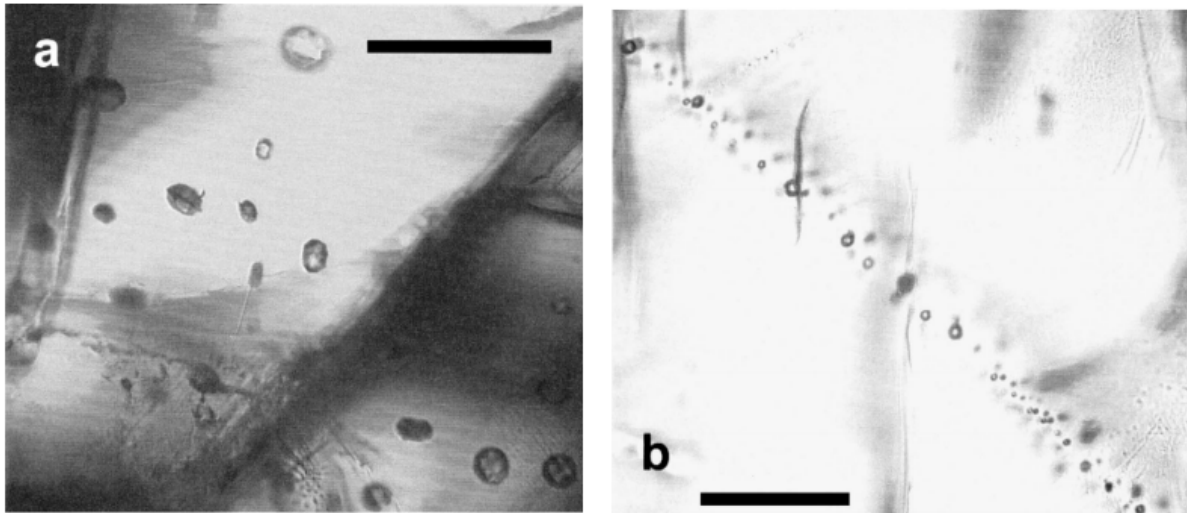
Figure 3. Carbon dioxide fluid inclusions in mantle xenoliths. Scale bar is 100 microns. *Source: Anderson and Neumann, 2001*

Alteration

Mantle xenoliths are susceptible to alteration given various melt events that might occur while the xenolith is present in the crust, e.g., magma chamber. For this reason, certain chemistry may be altered, including possible reset of specific radioactive elemental series. Alteration has to be considered when performing petrologic analysis of xenoliths.

References:

Andersen, T., Neumann, E.-R., 2001. Fluid inclusions in mantle xenoliths. *Lithos* 55, 301–320.

Canil, D., Lee, C.-T. a., 2009. Were deep cratonic mantle roots hydrated in Archean oceans? *Geology* 37, 667–670.

Pearson, D., Canil, D., Shirey, S., 2003. Mantle samples included in volcanic rocks: xenoliths and diamonds. *Treatise on geochemistry*.

History of the Rio Grande Rift Valley

Hamish Hay

1. Introduction

The late Cretaceous marked the beginning of a series of tectonic events that would later sculpt some of the distinguishing geological structures in the southwestern United States. The combined action of subduction, fault reactivation, and erosion resulted in these structures, including the Grand Canyon, Colorado Plateau, and Rio Grande Rift Valley.

Separating the Colorado Plateau and the North American craton, the Rio Grande Rift Valley is a north-south trending rift basin located through central Colorado, New Mexico and into northern Mexico at the rift's southern most extent (Figure 1). The exact mode of rift formation (i.e. passive or active) is still under debate, and requires detailed understanding of the regional tectonic setting, as well as the asthenospheric mantle flow beneath the rift itself.

2. Geological History

The first episode of rifting began 32-27 Ma, with extensional reactivation occurring along the southern Rocky Mountains. Sufficient thinning of the crust at around 26 Ma resulted in extensive mafic extrusions and volcanic ash emplacement, with intermittent quiescent periods where alluvial fill appears to dominate the sedimentary sequence. The rift itself can be conveniently split up into three segments as each segment shares different characteristics, although the broad extensional history remains the same [1].

The northern most segment of the Rio Grande Rift valley began rifting 27 Ma, and is almost entirely void of any volcanic synrift sediments. Extension in this segment is accommodated by a broad zone of block faulting [1].

Figure 1: Map view of the Rio Grande Rift Valley. Three distinct segments can be identified, the largest of which is the sourthern most segment, extending far into northern Mexico.

En echelon style basins are found offset from each other in a transverse manner throughout the central segment. These basins, trending north-northeast, are lacking in prerift volcanic sediments. There are, however, large deposits of late synrift volcanics, with some areas showing active volcanism as recently as 5 Ma [1]. This rift segment sits atop a Precambrian basement [2].

The largest extension associated with the Rio Grande Rift Valley is evident in the most southern segment, where the basin width is approximately 2.5 times greater than the largest basins in the north [1]. Large amounts of pre and synrift volcanism are also apparent in this segment. Extension here is accommodated by extensive normal faulting and rotated fault blocks. This segment was the first to undergo rifting, with extension beginning 32 Ma [1].

Basaltic-andesitic volcanism make up the main volcanic extrusions throughout the entire early rift history, although these are interbedded with episodes of felsic pyrocalstic deposits from between 32-26 Ma. Mafic extrusions, and indeed volcanism itself, ceased 20 Ma in the middle Miocene lull. Following this lull, bimodal basaltic-rhyolitic eruptions began around 13 Ma. Extensive uplift of the southern Rocky Mountains began 7 Ma, and this uplift continues today, albeit at a slower rate [1].

3. Rifting Mechanisms

Rifting can either occur as a passive or active process. When passive, regional tectonic forces in the lithosphere cause significant crustal thinning and extension. In an active regime, rifting is instead driven by upwelling asthenosphere in the mantle directly beneath the rift, as is thought to be the case in the Afar Triangle in Ethiopia [3].

It is not clear, given the regional tectonic setting of the southwestern United States, what the driving force behind rifting actually is. Certainly, from the west, much of North and South America has been under a compressional tectonic regime from flat-slab subduction of the Farallon plate since at least the beginning of rifting [4]. Thus, it seems more plausible that extension associated with the Rio Grande Rift Valley is active.

A large seismic low velocity zone lies beneath the Rio Grande Rift Valley in the upper mantle, and this is interpreted by almost all to indicate a positive thermal anomaly [5]. This would represent the source of much of the volcanism in the rift valley. Moucha et al. [5] computed the viscous mantle flow field for the mantle surrounding the rift valley (Figure 2). Here, mantle flow is coupled with the descending and detached Farallon slab, which in turn appears to
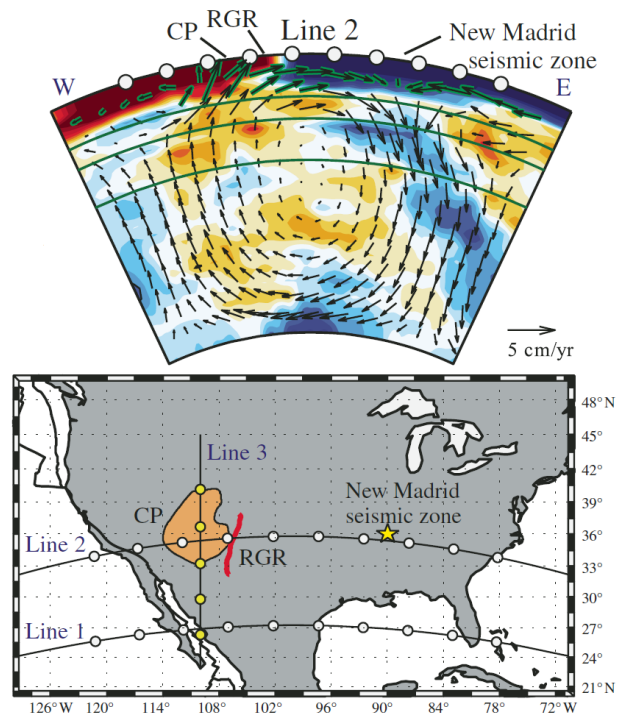

Figure 2: Computed flow field for a modelled seismic and geodynamically coupled velocity structure across the southern United States [5]. The section extneds from the surface to the CMB.

drive both uplift associated with the Colorado Plateau and some of the extensional activity observed in the Rio Grande Rift Valley. This phenomenon is known as "dynamic topography", and is essentially the transfer of stress from the downgoing slab through the viscous mantle, leading to the mantle flow field shown in Figure 2. This flow and its accompanied viscous stresses are expressed at the surface through dynamic, topographical changes. In the case of the Colorado Plateau, upwelling asthenosphere drives its recent and rapid uplift, whereas asthenospheric flow, oblique to the lithosphere, is thought to be the main driving mechanism behind extension and crustal thinning at the Rio Grande Rift Valley [5].

References

[1] C. E. Chapin, Evolution of the rio grande riftsummary, Special Publications 14 (1979) 1–6.
[2] C. E. Hedge, Z. E. Peterman, J. Case, J. D. Obradovich, Precambrian geochronology of the northwestern uncompahgre plateau, utah and colorado, US Geological Survey Professional Paper (1968) C91–C96.
[3] I. D. Bastow, G. W. Stuart, J.-M. Kendall, C. J. Ebinger, Upper-mantle seismic structure in a region of incipient continental breakup: northern ethiopian rift, Geophysical Journal International 162 (2005) 479–493.
[4] E. D. Humphreys, Post-laramide removal of the farallon slab, western united states, Geology 23 (1995) 987–990.
[5] R. Moucha, A. M. Forte, D. B. Rowley, J. X. Mitrovica, N. A. Simmons, S. P. Grand, Mantle convection and the recent evolution of the colorado plateau and the rio grande rift valley, Geology 36 (2008) 439–442.

Quaternary Climate of New Mexico
Corey Atwood-Stone – Fall 2014 Field Guide

Climate dominated by Ice-Age/Milankovitch cycles, even in unglaciated New Mexico.

We can use the most recent cycle as a good proxy for how climate varies over the 2.5 million years of the Quaternary. Although the cycle frequency changes 1 million years ago from 41ky to 100ky periodicity.
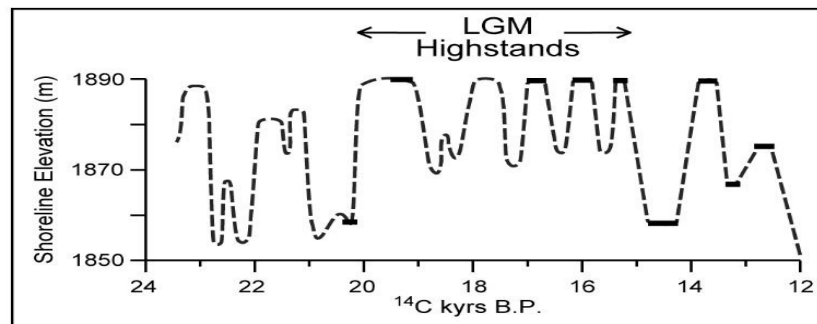

Composite CO2 record (0-800 kyr BP)
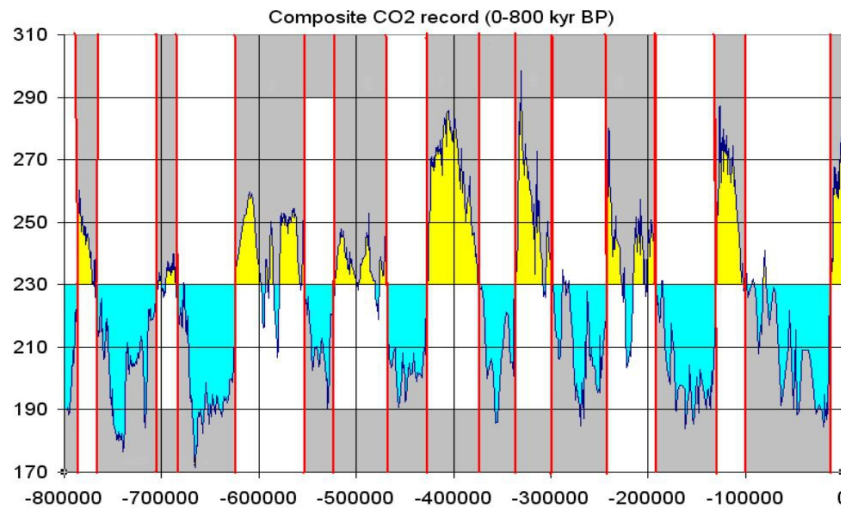
Climate Information from Lake Estancia (Central NM)
>   ~45kya – change from playa conditions to shallow lake and marsh
>   ~24kya – onset of periodic major expansions of the lake
>   ~12kya – full desication of the permanent lake (xcept a brief expansion 10-11kya)

Climate Information from Pack Rat Middens (In current southwest NM Desert)
>   Late Pleistocene vegetation is Pinion & Juniper with uderstories of flowering
>   annuals and grasses – indicative of significant winter and moderate summer
>   rainfall
>   ~10-11kya – move to warmer drier climate inferred by change to Oak and Juniper
>   ~8-4kya – decline in tree population over this period, but still wetter than today
>   ~4kya – arrival of desert scrub vegetation marks beginning of the modern climate

White Sands Area – Lake Otero and Lake Lucero

     In the late Pleistocene Lake Otero is a large permanent lake

     Otero undergoes three major episodes of deflation at 11, 7, and 4 kya

     Built up gypsum in closed basin lake is deposited as evaporites during deflation
        and then eroded to source white sands dunes

     Finally ending up as a small transient lake in its SW corner called Lake Lucero,
        and a large alkali flat
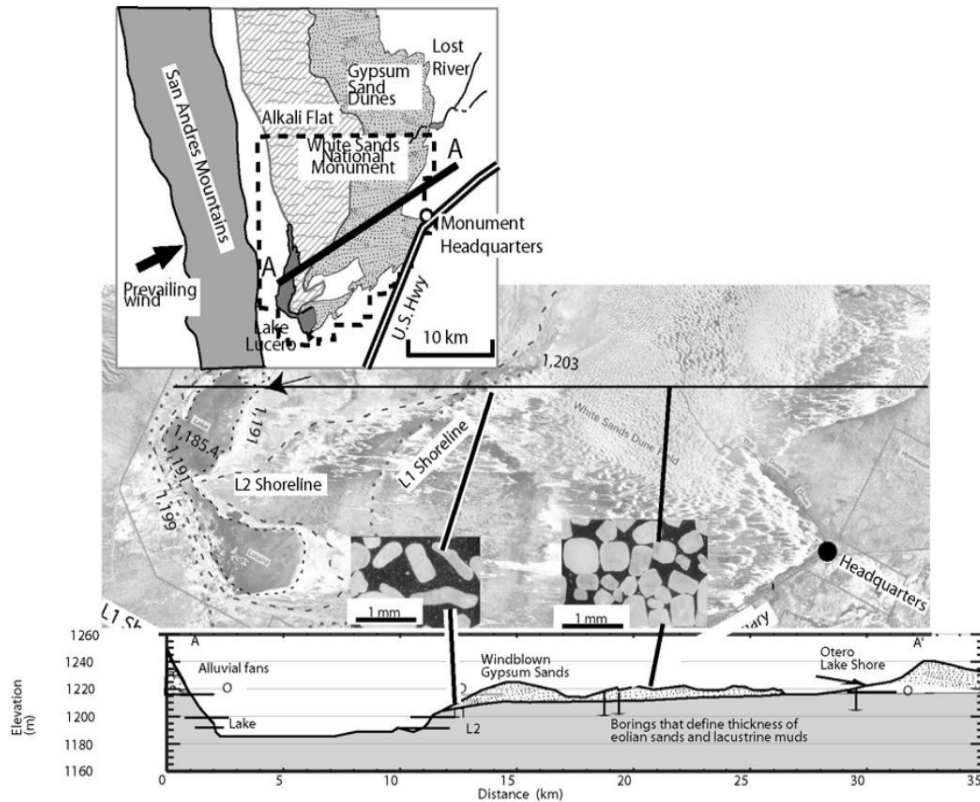
Climate on Other Timescales
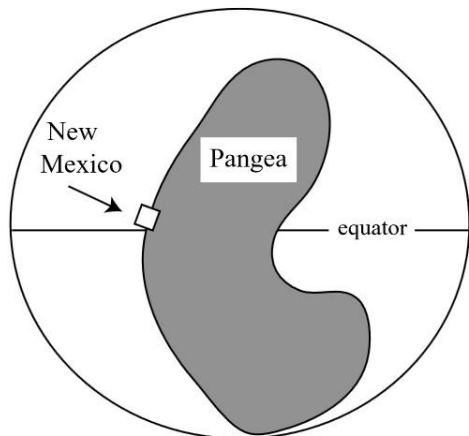
Very Long   Shorter
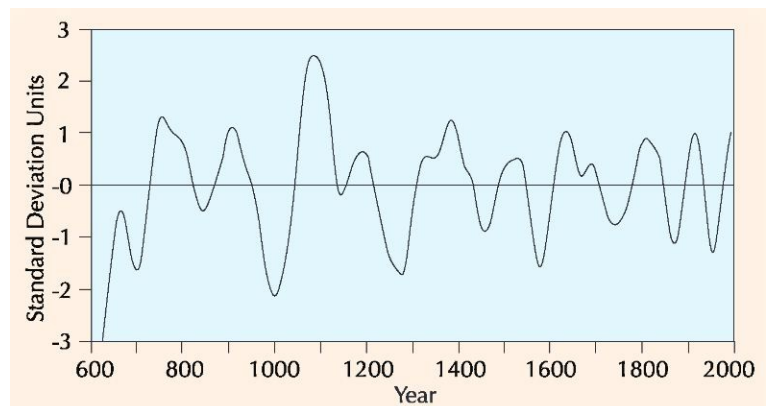
Gypsum Sources and Sinks

Donna Viola
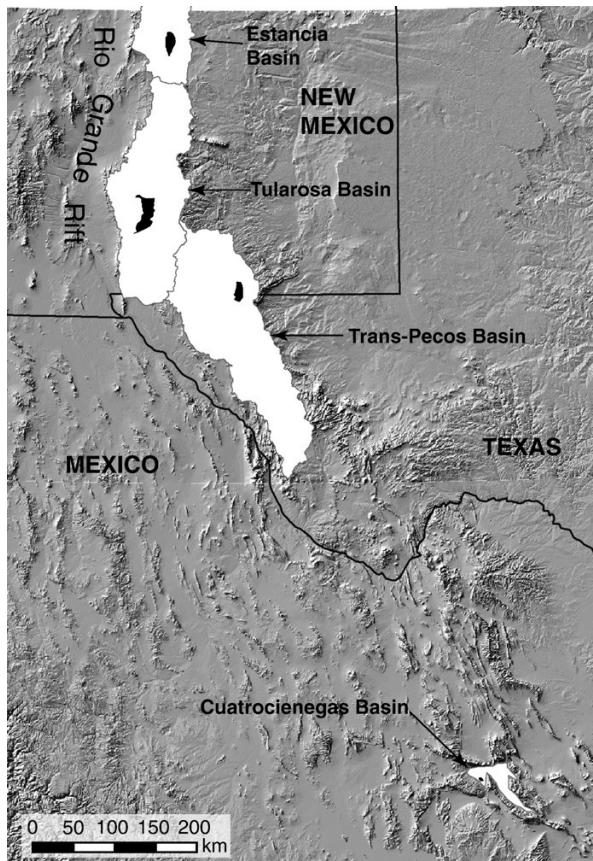
Figure 1: Map of gypsum dune fields (black) and the basins in which they are located (white). From Szynkiewicz et al (2010).
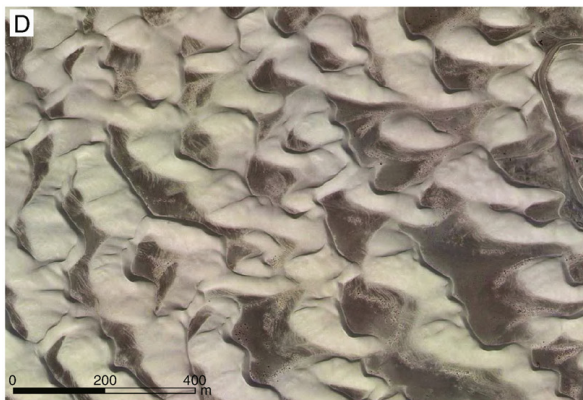
Figure 2: Crescentic ridges common in White Sands Dune Field. From Szynkiewicz et al (2010).

Several large gypsum dune fields are found in southern New Mexico, western Texas, and northern Mexico (Figure 1): Estancia Dune Field, White Sands, Guadalupe Dune Field and the Cuatrocienegas Dune Field. Each of these is found within closed basins located along the eastern margin of the Rio Grande Rift.

White Sands Dune Field

The White Sands dune field has an area of ~500 km^2, and is the largest gypsum dune field in the world. It is located within the topographically-closed Tularosa Basin. During most of the late Pleistocene, there was a lake present in the basin (Lake Otero), which dried to form playa lakes and underwent deflation near the end of the last glacial maximum and the early Holocene (~12-9 kyr ago). The dune field itself is part of a wet aeolian system, where dune accumulation is dependent upon fluctuations in the groundwater table; cementation can occur within the capillary fringe due to periodic dissolution and re-deposition of gypsum. Figure 2 shows some of the gypsum dunes that are common in White Sands.

Sources and Sinks of Gypsum in White Sands

Gypsum is a hydrated calcium sulfate ($CaSO_4 \cdot 2H_2O$), and is an evaporitic mineral that typically forms by precipitation out of salty water. In the case of White Sands, gypsum formation was tied to the evaporation of Lake Otero after the Tularosa Basin became closed. The dune field evolved due to the stepwise deflation of this gypsum-rich Lake Otero sediment, which allowed for the accumulation of sand-sized gypsum grains that were transported northeast along the primary wind direction.

Szynkiewicz et al. (2010) analyzed $\delta^{34}S$ values along transects in the White Sands dune field and use these isotope ratios to differentiate between various events of gypsum sand production and dune accumulation to piece together the history of the region, which includes at least three events of deflation and dune formation (Figure 3). Currently, Lake Lucero, a playa southwest of the White Sands

dunes, is also gypsum-rich, and continues to act as a source for gypsum into the dunes at a much smaller scale than Lake Otero. Figure 4 shows the location of Lake Lucero relative to the current dune field.
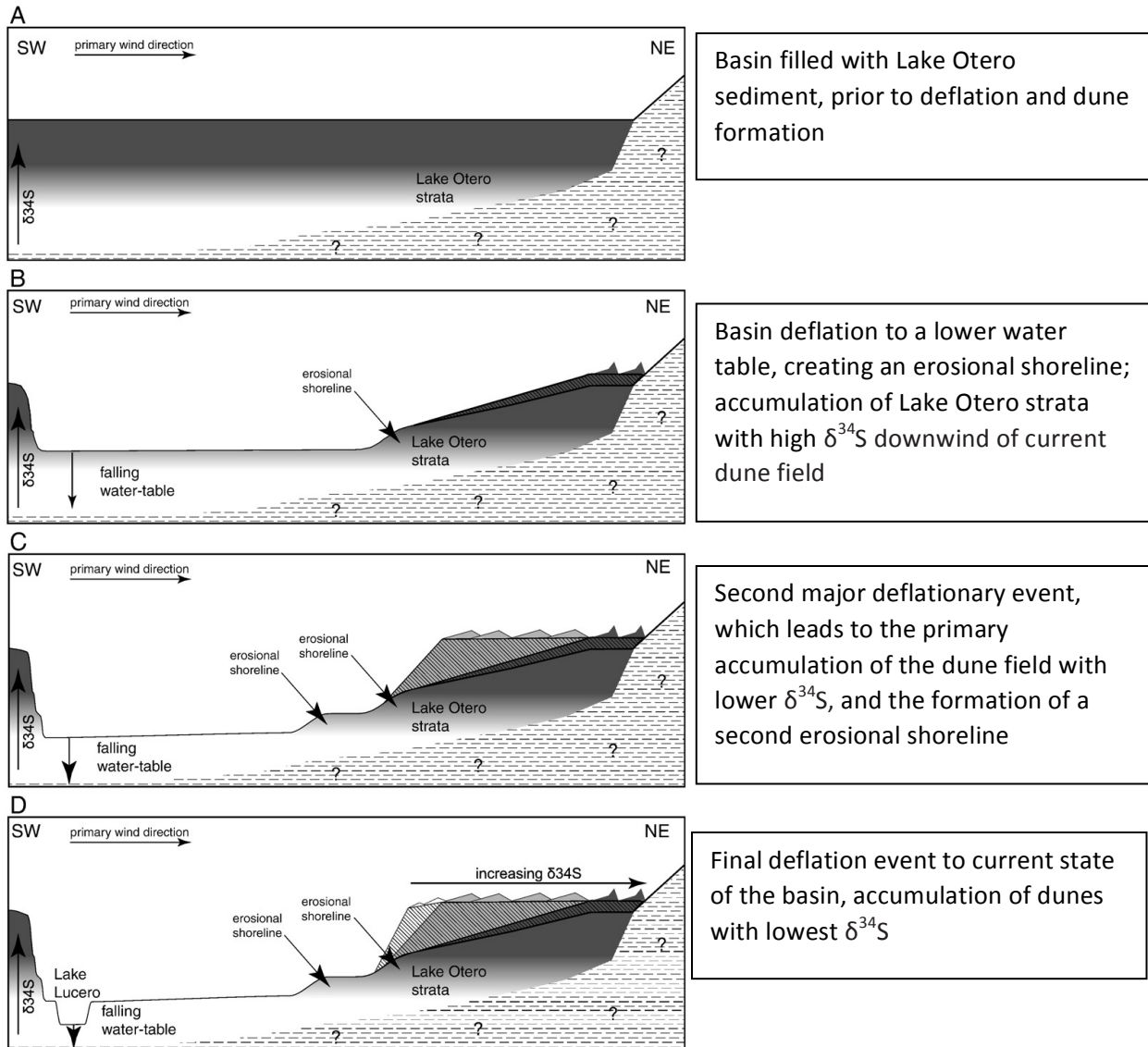
A — Basin filled with Lake Otero sediment, prior to deflation and dune formation

B — Basin deflation to a lower water table, creating an erosional shoreline; accumulation of Lake Otero strata with high $\delta^{34}S$ downwind of current dune field

C — Second major deflationary event, which leads to the primary accumulation of the dune field with lower $\delta^{34}S$, and the formation of a second erosional shoreline

D — Final deflation event to current state of the basin, accumulation of dunes with lowest $\delta^{34}S$

Figure 3: Simple model of the evolution of White Sands dune field. From Synzikiewicz et al (2010).
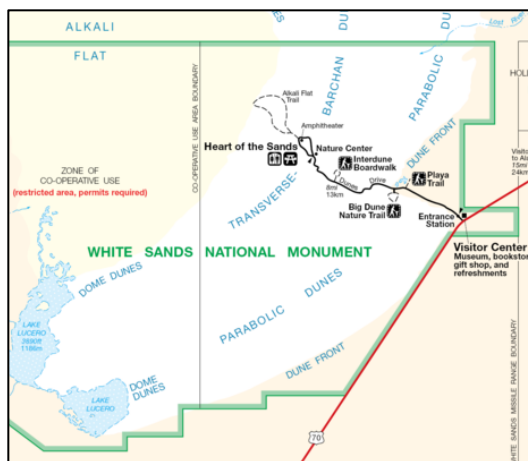
Figure 4: Map of White Sands National Monument, showing the relationship between present-day Lake Lucero and the White Sands dune field.

45

Planetary Analog: Gypsum Dunes on Mars

There is a large dune field located in the north polar region of Mars, Olympia Undae, which extends for over 1000 kilometers within the Borealis (or north polar) basin. High concentrations of gypsum were discovered in the eastern region of Olympia Undae (Figure 5) using the OMEGA instrument on ESA's Mars Express orbiter. Peak gypsum concentrations are seen centered around 240°E, 85°N, and decrease westward across the Olympia Undae dune field. The gypsum signature is correlated with dark, longitudinal dunes, and the crystals themselves are thought to have been derived from materials within the polar cap itself since the dunes are found downwind from scarps that cut through the north polar layered deposits. Figure 6 shows a map of the NPLD and the likely source regions for the gypsum-rich dunes, as well as a conceptual model for the formation of the gypsum dune fields on Mars.

Figure 5: Map of gypsum concentrations detected by OMEGA (where red is >25% and purple is ~6%), superposed on an albedo map (white indicates surface water ice) from Langevin et al. (2005). The gypsum signature is found within the expanse of dunes that surround the north pole of Mars.
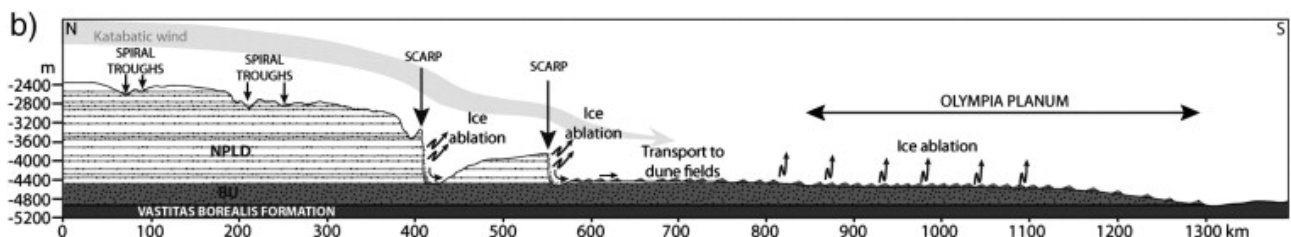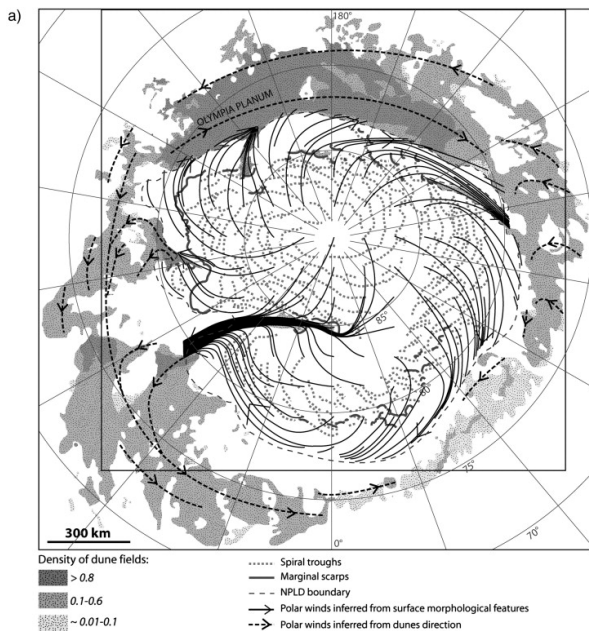
References

Langevin et al. (2005). Science, 307, 1584-1586.
Masse et al. (2012). Earth and Planetary Science Letters, 317, 44-55.
Szynkiewicz et al. (2010). Geomorphology, 121, 69-83.

Figure 6: (a) Map of the NPLD and Olympia Planum region on Mars, and (b) a conceptual model showing the likely source region for gypsum-rich sand, where ice ablation releases gypsum-rich sediments from the NPLD and is transported to the Olympia Undae dune field via the katabatic winds. From Masse et al (2012).

Introduction

The White Sands Dune Field, situated within the Tularosa Basin in southern New Mexico, is the world largest known field of gypsum dunes at 500 km^2. The gypsum sand is sourced from the leaching of evaporite-rich Permian strata flanking the basin into the Late Pleistocene Lake Otero, which then dried up and underwent basinal deflation at 7 ka. Lake Lucero is the largest of the resulting playas, occupying the topographically lowest area of the basin at the southwest. Downwind from Lake Lucero, dune morphology changes from transverse/barchans/crescentic at the center of the field to parabolic at the northern, eastern and southern flanks.

Controls on Dune Migration

Mechanistically, dune migration rates are determined by the surface shear stress τ and the availability of sediment. This surface shear stress results in the erosion and transportation of sediment from the windward side of the dune to the leeward side, where the sediment is then deposited. Typically, the surface shear stress is calculated by measuring wind velocity u at various heights above the surface, and fitting the measurements to the law of the wall:

$$\frac{u}{u_*} = \frac{1}{\kappa}\ln\frac{yu_*}{\nu} + C, \quad u_* = \sqrt{\tau/\rho}$$

where $\kappa = 0.41$ is the von Karman constant, y is the height from the surface, ν is the kinematic viscosity of the air, ρ is the density of the air and C is a constant. The sediment flux Q can then be determined via $Q \propto \tau^{3/2}$, a relationship determined empirically through wind tunnel studies on general sediment transport. The availability of sediment manifests quantitatively as an upper bound on the value of Q and the size of the dunes. For a dune with a slipface surface area S, the migration rate is then $M = Q/S$, assuming all eroded sand is deposited. Thus larger dunes migrate more slowly with the same sediment flux.

However, dunes do not merely respond to the wind regime, but create secondary flow regimes that interact with the dunes. Studies have found that while erosion of the windward stoss side is dominated by the mean streamwise accelerations assumed in the simple model above, turbulent structures and eddies are significant at the crestal region of the dune. Wind tunnel experiments with transverse dunes found the reversed flows associated with eddies generated significant stresses of approximately 30-40% of the maximum, and shear stress variability continued to increase until a peak value at the point of flow reattachment. Consequently, while streamwise shear stress is low, the high shear stress from the turbulent flow can inhibit sediment deposition. This is further supported by the similarities in flow characteristics on the lee side of aeolian dunes with those in the wake of fluvial bedforms, which are generally regarded to be the result of turbulent flow. A successful quantitative model for predicting dune migration rates, taking into account this turbulence, has yet to emerge.

Measurement of Migration Rates

Understanding the local wind conditions is essential in the study of dune migration. For the White Sands Dune Field, wind data comes from the nearby Holloman Air Force Base. The strongest winds blow from the southwest between December and May (Fig. 1). In October and November, relatively strong winds also blow from the north. Thus, the dune field may be described as being under dominantly unidirectional wind control, but subject to a brief shift in wind direction.
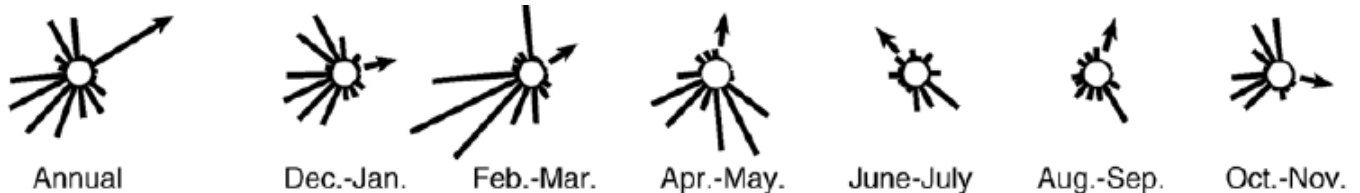

Figure 1: Wind regime from Holloman AFB (Kocurek et al, 2007)

A number of studies have been conducted to measure the migration rates of the White Sands dunes. One of the earliest was conducted by McKee (1966), utilizing aerial photography taken by the United States Air Force at 6-month intervals over a 2-year period. The study found that dune migration rates can vary significantly over the dune field, with dunes on the downwind end of the field migrating more slowly. While a particular barchan dune exhibited overall forward movement, with migration of as much as 7 m at some parts (Fig. 2a), a parabolic dune further downwind in the field not only moved less at its forward end, but has actually retreated on part of its upwind curve (Fig. 2b). This variation in migration rates was believed to be due to the dissipation of energy over the dune field.
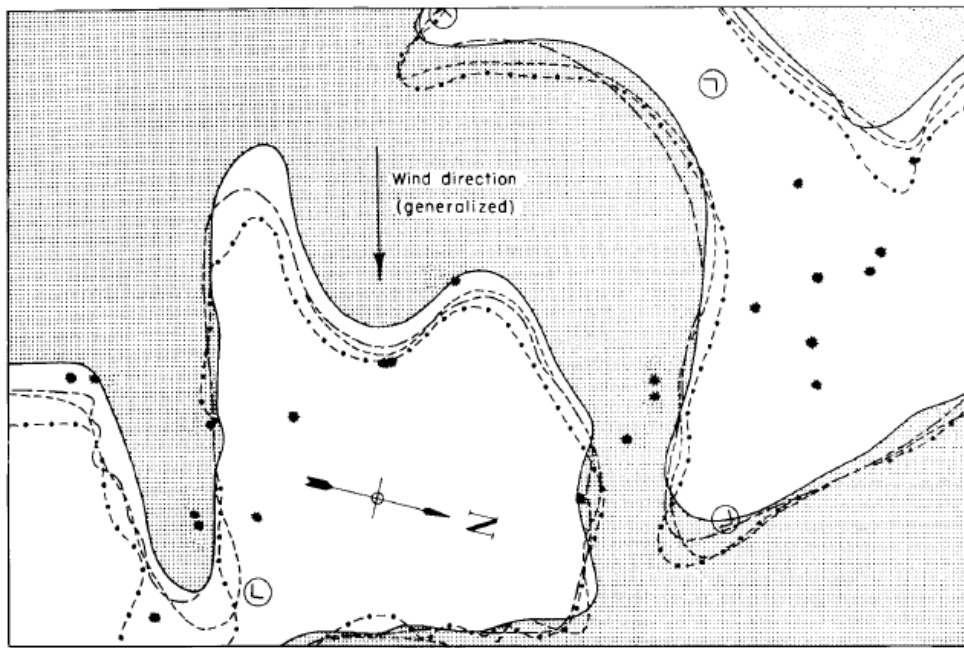
BARCHAN DUNE, NUMBER 6

0 25 50 75 100 125 150 175 200 225 250 FEET (Approx.)

Interdune area   Dune area (December 8, 1962)   Ⓛ Ground marker   ✸ Shrub

———— December 8, 1962   — — — July 8, 1963   - - - - - January 17, 1964   — • — June 22, 1964
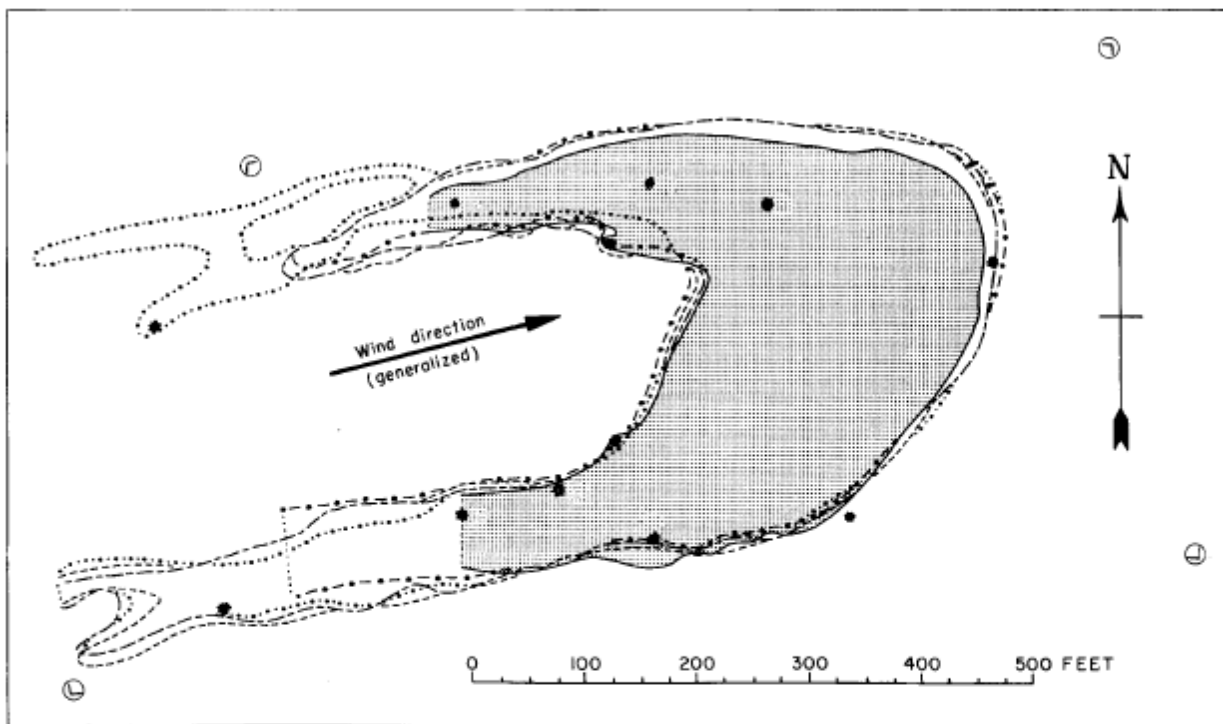
PARABOLIC DUNE, NUMBER 7

0   100   200   300   400   500 FEET

Interdune area   Dune area (December 8, 1962)   Ⓛ Ground marker   ✸ Shrub

———— December 8, 1962   — — — July 8, 1963   - - - - - January 17, 1964   — • — June 22, 1964   ·········· February 2, 1965

Figure 2: Migration of (a, top) barchan dune and (b, bottom) parabolic dune (McKee, 1966).
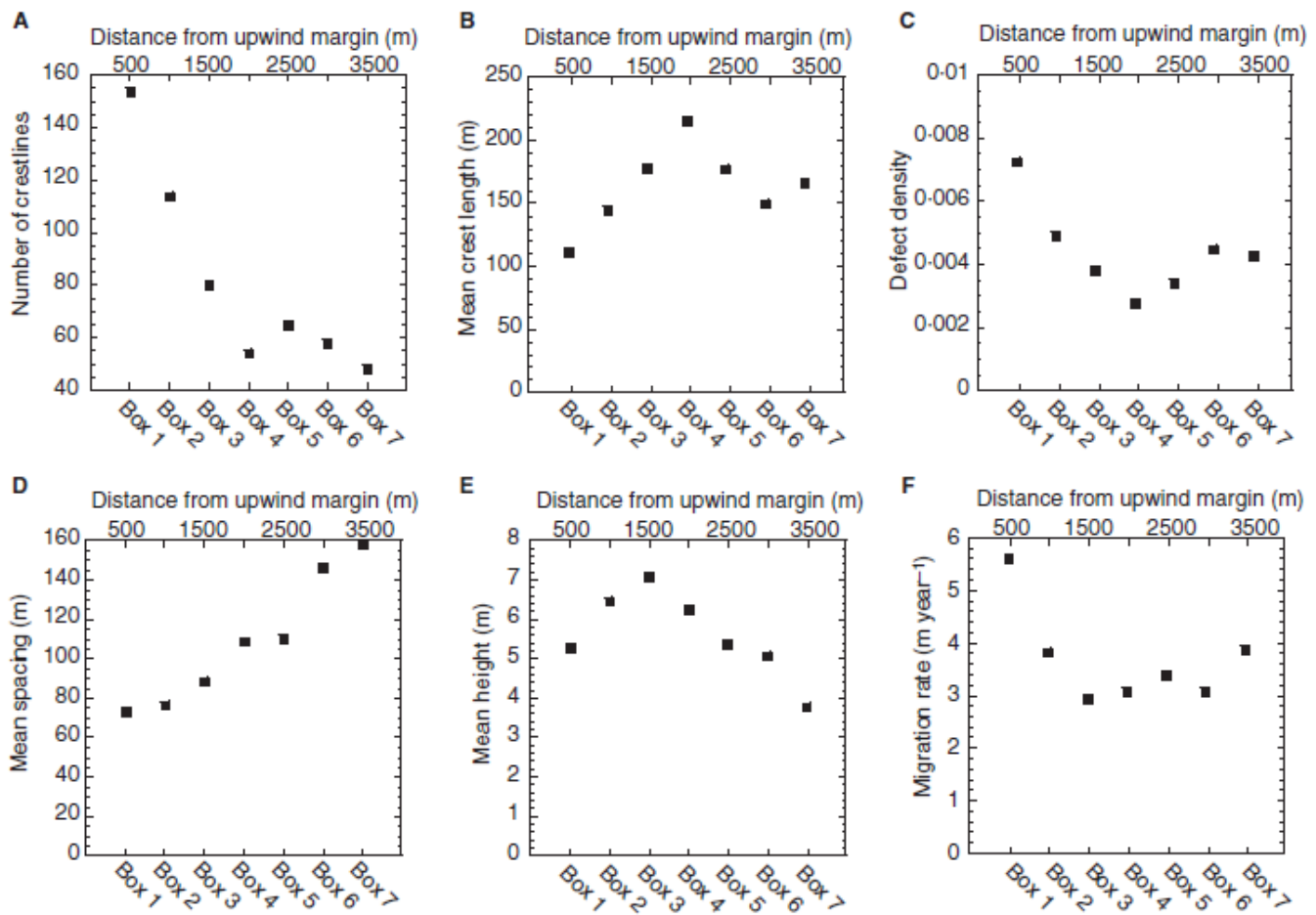
Figure 3: Variability of measured parameters over dune field (Ewing and Kocurek, 2010)

A subsequent study by Ewing and Kocurek (2010) expanded the dataset to include aerial photographs from 1985, digital orthophoto quarter quadrangles from 1996, 2003 and 2005, and a digital elevation model generated from a June 2007 airborne LiDAR survey. Large pedestal dunes, as permanent vegetated structures within the active dune field apparent in all images, were used as ground-control points. Dune crestlines were then manually digitized using GIS software. The authors had not only measured dune migration rates, but also characterized variations over the dune field, and described how differential migration rates over a single dune can result in constructive (resulting in fewer, larger dunes) and regenerative (resulting in more, smaller dunes) events.

Fig. 3 shows the results from the study. Measured migration rates of ~3 m/yr agree with those measured from the earlier McKee (1966) study. However, the additional details paint a more complex picture with three different regimes. At the upwind margin (Box 1) where both energy and sediment supply are high, dunes are smaller (smaller crest lengths and heights), denser and migrate faster. In the middle of the field (Box 3), dunes are the largest, and migration is the slowest. At the downwind margin (Box 7), dune size is even smaller than in Box 1, and migration rates are slower despite the smaller size. These variations across the regimes can be explained by the equation $M = Q/S$ presented earlier. At the upwind end, S is small and Q is large, and so M is large. In the middle of the field, S is large but Q is intermediate, giving a smaller M. At the downwind end, both S and Q fall. However, while S is comparable to that at the upwind end, Q is much smaller, and so after some fluctuations due to the competing effects of decreasing S and Q, M settles to a value lower than that at the upwind end.

The study also found that upwind dunes have higher densities of defects (ends of crestlines). These defects typically migrate faster than the rest of the dune, and thus this higher density makes the dunes more susceptible to reorientation by the northerly component of the wind regime. The resulting pattern at the upwind margin is that of more irregularly oriented and closely spaced crestlines, forming a network-type pattern. The pattern becomes more organized towards the center of the dune field where crestlines are more widely spaced and have fewer defects.
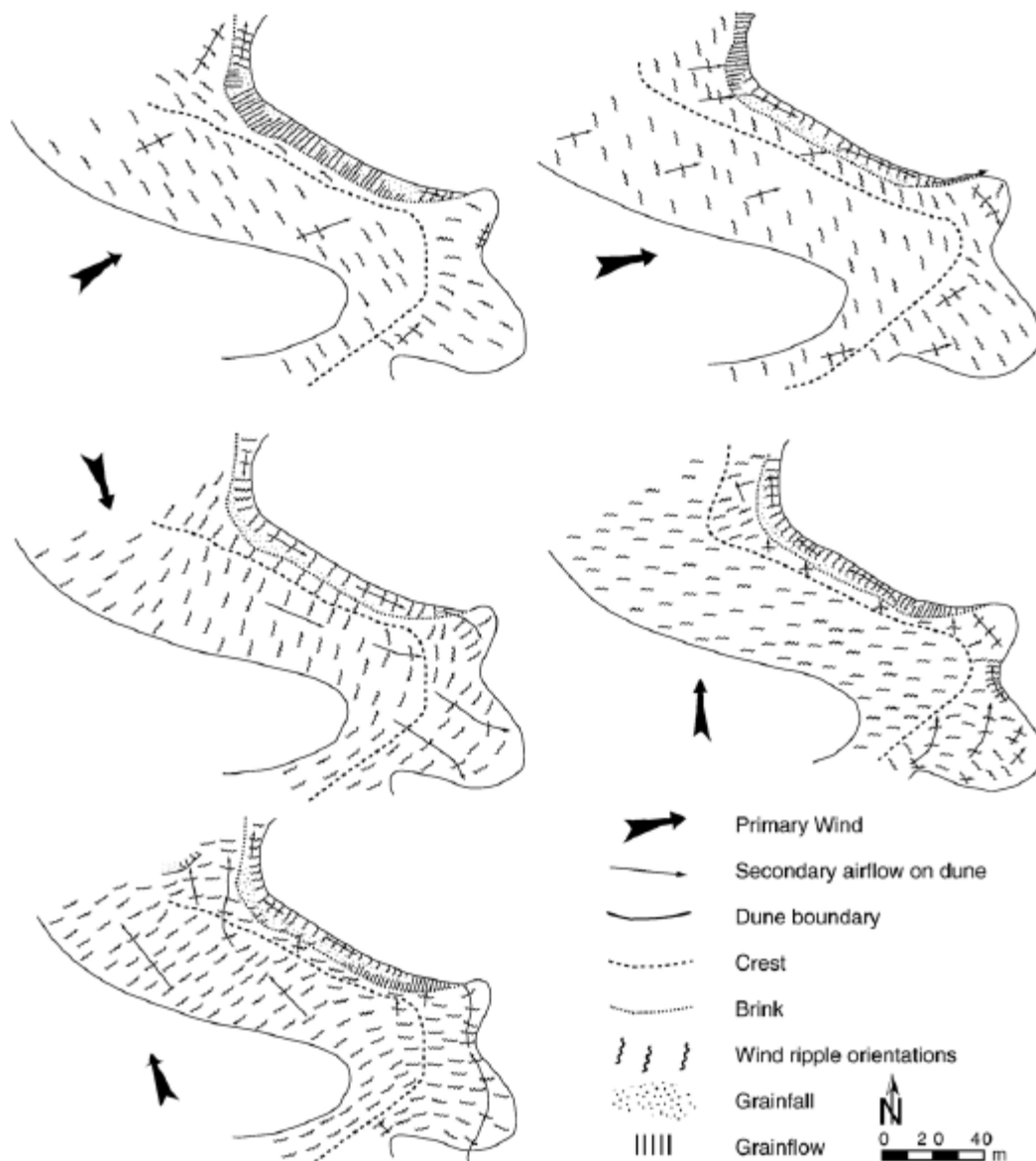
Figure 4: Response of dune to various wind regimes (Kocurek et. al. ,2007).

Studies on the ground complement the remote sensing studies. Kocurek et. al. (2007) monitored a crescentic dune over a year to document dune response to each significant wind direction (Fig. 4). The dunes are oriented most transverse to the southwest winds, and thus maximum sand transport and dune migration occurs during these winds. Wind ripples on the lee face are restricted to "turning points" where the wind incidence angle is oblique. Winds from the west, however, strike the dunes obliquely, resulting in deflected alongslope air flow on the lee face and predominantly wind ripples migrating to the southeast. A similar pattern of lee face ripples occurs with winds from the NNW. Winds from the north result in rounding of dune brinks and crests, minimal crest-normal migration, and lee face reactivation. A reversal in the direction of the deflected alongslope transport occurs with winds from the S-SE.

Dunes do not just migrate over the accumulation surface, but rather they leave sets of cross-strata that are progressively buried beneath interdune deposits, which in turn are buried beneath the prograding lee of the next upwind dune. Kocurek et. al. (2007) also dug trenches across three interdune areas and the basal portions of their associated dunes to study historical migration rates. This is possible because the interdune deposits exhibit banded laminae, which are interpreted to correspond to seasonal wetting cycle involving a rise of the capillary fringe through wind-blown sand, trapping sand by adhesion onto the damp surface, and the development of the organic mats during periods of maximum wetness. Counting the number of light/dark couplets, the authors deduced a migration rate of 4.5 m/yr. This unexpectedly high value is likely due to an incomplete record due to scouring during extended dry periods.

References

Ewing, R.C., Kocurek, G.A. *Aeolian dune interactions and dune-field pattern formation: White Sands Dune Field, New Mexico*. Sedimentology, 57(5): 1199-1219, 2010.

Kocurek, G., Carr, M., Ewing, R., Havholm, K.G., Nagar, Y.C., Singhvi, A.K. *White Sands Dune Field, New Mexico: Age, dune dynamics and recent accumulations*. Sedimentary Geology, 197(3): 313-331, 2007.

Livingstone, I., Wiggs, G.F., Weaver, C.M. *Geomorphology of desert sand dunes: A review of recent progress*. Earth-Science Reviews, 80(3): 239-257, 2007.

McKee, E.D. *Structures of dunes at White Sands National Monument, New Mexico (and a comparison with structures of dunes from other selected areas)*. Sedimentology, 7(1): 3-69, 1966.
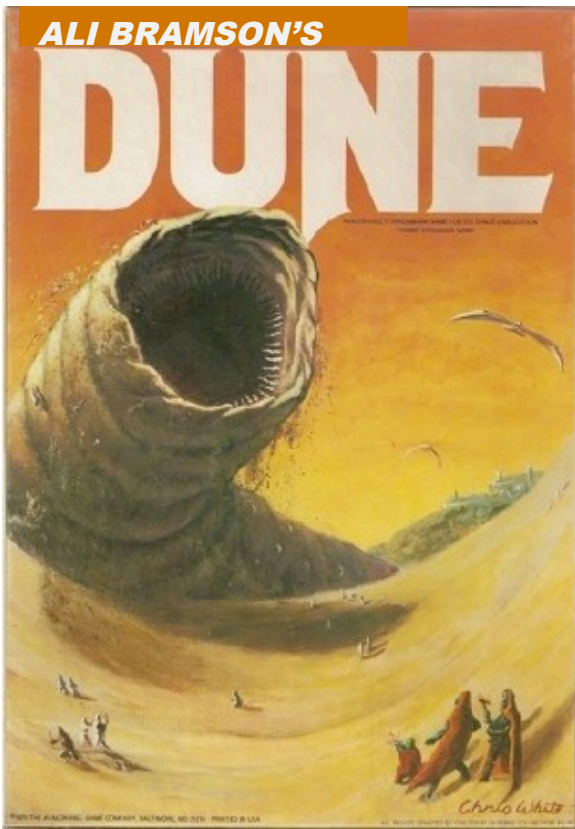
DUNE GEOMORPHOLOGY

Dune:

/d(y)o͞on/

noun
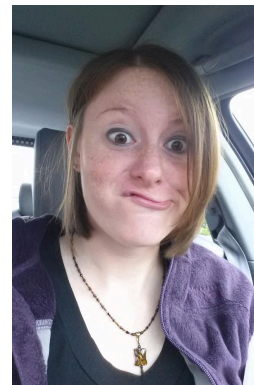
An elongated ridge of sand formed by wind or water
[Understanding Earth, 5th Edition]
ALSO
A movie where Sting wears really tight underwear
[Tanquary, personal communication]
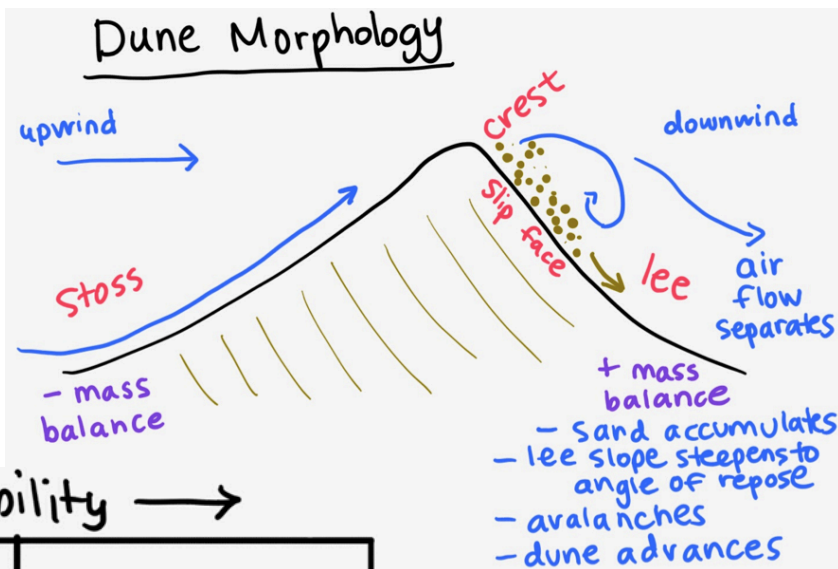
Dunes need: a supply of loose sand and wind. These factors determine which kind of dune forms.

Dune Morphology
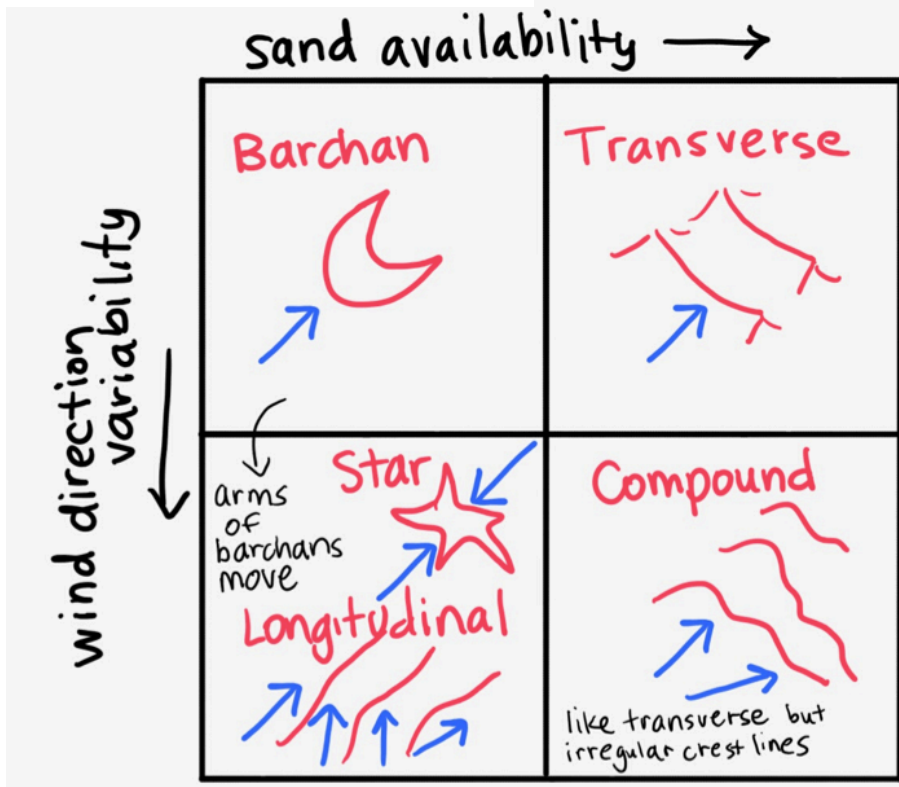
Sand dunes begin formation when sand encounters a rock or other obstacle. The wind streamlines separate on the lee side where eddies are weaker so sand grains can settle and pile up into a dune. Likewise, sand piles up on the lee side of the dune until it reaches the angle of repose and the sand avalanches down, advancing the dune.

52

Longitudinal Dunes: Barchans w/ subtle changes in winds

deposition

Parabolic dunes: Barchans when plants grow on the arms, prohibit sand movement

Wind cannot pick up wet materials very easily so dunes are generally found in dry climates. The exception is dunes along coasts where sand is so abundant dunes can form even in these humid environments. However, in these environments, soils and plants can cover the dunes making it more difficult for the sand to saltate.

Variations in sand availability, wind direction and vegetation allow dunes to morph between different types of dunes.

Vegetation slows down the sand but movement speed is also determined by size. Larger dunes move slower because of their smaller perimeter to area ratio meaning the sand requires more hops along the surface to move. This is also why barchans have arms which move faster than the middle of the dune.

Barchan Dunes

wind

Arms move faster
They peel away from center
Occurs when incomplete sand availability

Movement Speed

$\frac{perimeter}{area}$ large → move fast

$\frac{perimeter}{area}$ small → move slow
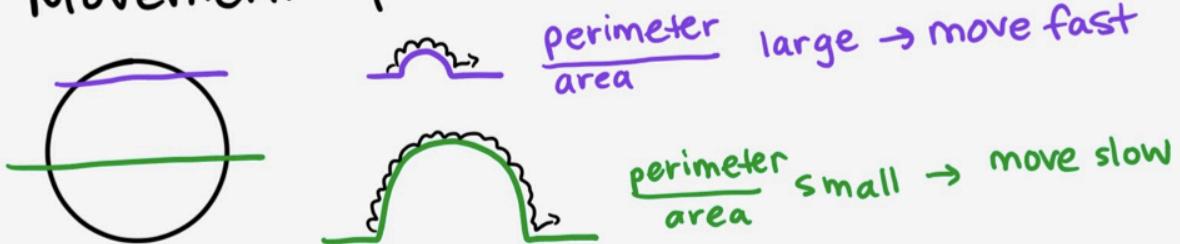
The size of the dune is related to wind speed and grain size. There are three sizes of sand features, with dunes being the middle size on the order of 10-100 meters. Smaller features are called ripples and large (>100s m) features are called megadunes or draa.
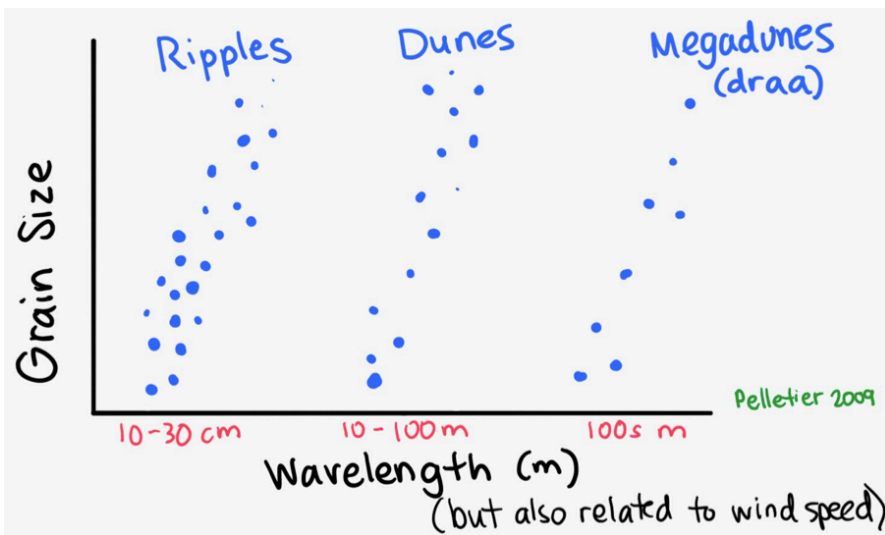
In general, dunes form from sand sized particles due to .1-1 mm sized particles being easiest to move.

sand sized (0.1 – 1 mm) particles easiest to move
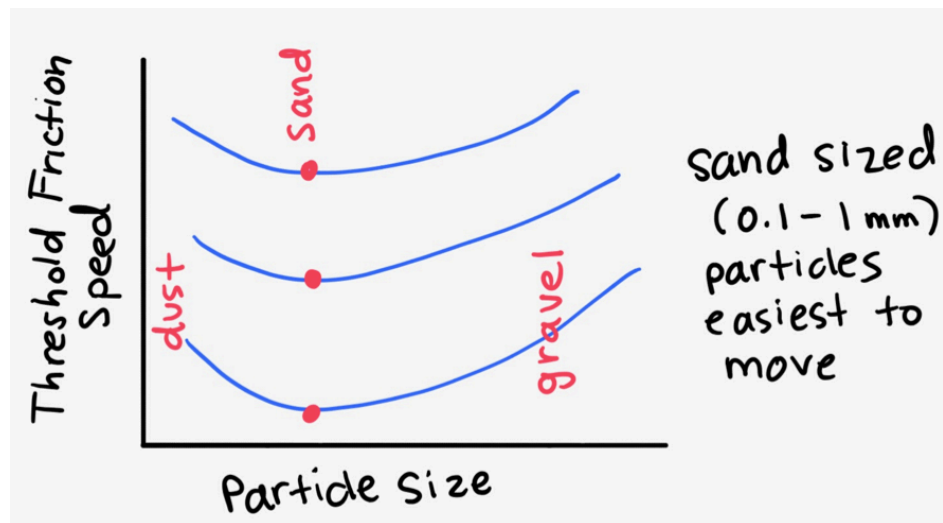
Dunes in the solar system

<u>Earth:</u> Dunes are found across the world and on every continent. The largest dune, Duna Federica Kirbus, is in Argentina and over 1200 m tall. Large sand seas of dunes (ergs) are most widespread at mid to low latitude deserts.


Brazil

Namibia

Mars:

Dunes are one of the most widespread aeolian features on Mars and HiRISE has taken beautiful pictures of many different varieties of dunes! Most of the sand ergs on Mars are in the north circumpolar regions and in crater floors. This difference from Earth's distribution is attributed to a difference in wind patterns. Dune morphology appears to be similar between Mars and Earth with dunes forming from saltation despite differences in grain size, composition, atmospheric density and wind speeds/patterns.

The saltation threshold friction velocity is about an order of magnitude larger (~100 kph) on Mars leading to average grain sizes of 0.16 mm (vs. 22 kph and .25 mm in the Sahara) [Breed et al. 1979]. Dunes on Mars have been found to change over the course of a couple years [Bourke et al. 2008].
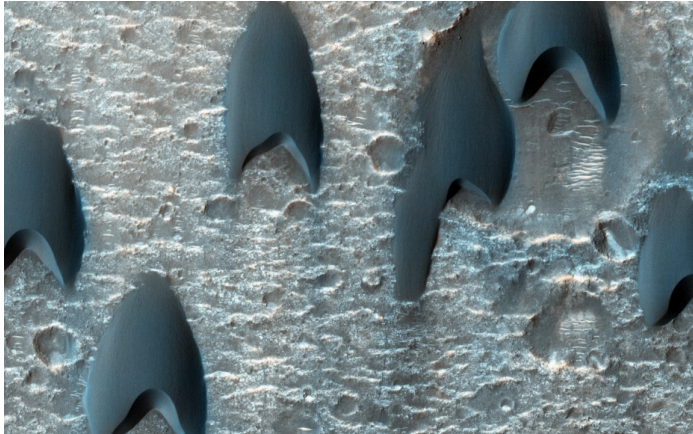
Titan:
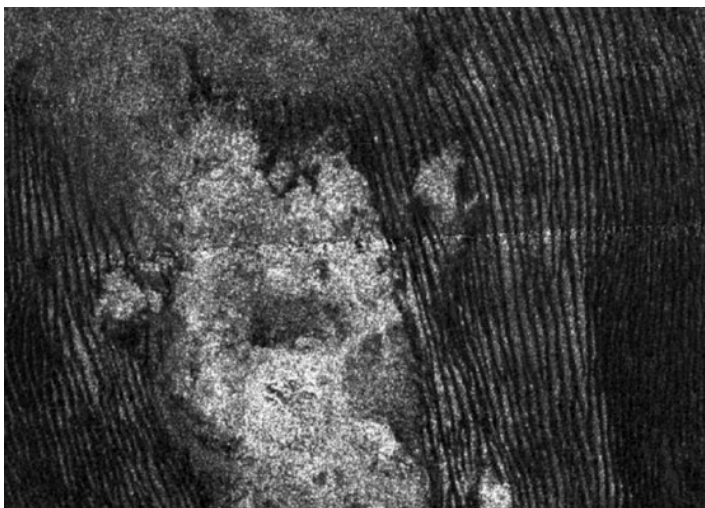
Dunes made of solid hydrocarbons are equatorward of 30° on Titan. Poleward has more moisture (there are liquid methane and ethane lakes and seas) so sand is less mobile there.
Dunes cover ~13% of surface (surface area ~ the size of the United States). On average they are 1-2 km wide, hundreds of km long and 100 m tall.

Cassini radar image of sand dunes on Titan. Credit: NASA/JPL–Caltech/ASI/ESA and USGS/ESA
[http://www.jpl.nasa.gov/news/news.php?feature=3261]

White Sands Missile Range:
The "Birthplace of America's Missile and Space Activity"
Sarah Peacock

General Background:

Nearly seventy years ago, the White Sands Missile Range (WSMR) went by a different name, the Alamogordo Army Airfield. It acted as a government military installation during the World War II. Due to disputes over the use of its airfield, Alamogordo Army Airfield was abandoned in the early-1940s. In the mid 1940s, it re-opened as the WSMR (or White Sands Proving Ground) and became the venue for a multitude of tests relating to the United States' retaliation against the Japanese. The most notable test was the detonation of the first atomic bomb on the missile range's Trinity Site in the mid 1940s.

Presently, the missile range is over 3,200 square miles, and covers five towns in the state of New Mexico. It is the largest military installation in the world. The site is used mostly by private clients who wish to test military or space exploration equipment far from civilization. The WSMR is the location of choice for landing spacecraft when they return home from outer space. It is also the location where most spacecraft parts are tested before a launch.

Rocket Launches:

The first rockets to launch from the WSMR Launch Complex 33 were WAC Corporals. These 16 foot, 660 pound rockets were designed to carry a 25 pound weather package to an altitude of 20 miles. During a series of tests in the mid 1940s, the WAC Corporal was very successful, ultimately attaining an altitude of 43 miles.

Figure 1: WAC Corporal rocket launch.

Soon after the WAC Corporals, the German V-2 brought a lot of attention to the WSMR. Standing 46 feet tall and weighing 28,000 pounds, these large rockets had the capability to reach altitudes exceeding 100 miles. During the first launch, the V-2 rose only 3.5 miles and then crashed in a large fireball. Luckily, for the second attempt, the rocket launched as expected and became the first successful launch of a large rocket on American soil and accelerated the US into the Space Age.

Figure 2: V-2 rocket.

Scientific Research Directive:

In addition to improving rocket technology, the military directed that all V-2s carry some sort of scientific payload. In July 1946, V-2s carried fruit flies and corn seeds to expose them to cosmic radiation. Some other studies include solar spectroscopy, solar radiation, artificial meteorites, temperatures, ambient pressures, winds, and atmospheric compositions at various altitudes. In March of 1947, a Naval Research Laboratory team put a camera aboard a V-2 that achieved a 100-mile altitude to bring back the first ever photo of Earth from "space."
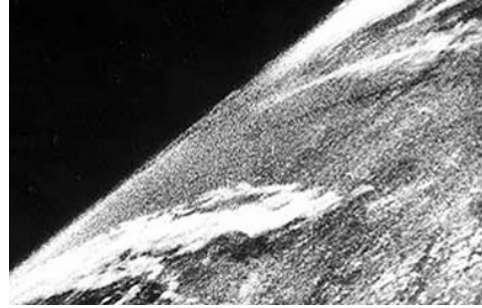
In 1948 and 1949, monkeys were placed into the payload compartment and wired to measure their heart and respiration rates. Luckily, this data was sent back to the ground during the flight, because the parachutes failed and the monkeys died on impact. Both measurements were normal during the acceleration forces during liftoff and weightlessness, giving scientists confidence that humans could safely ride a rocket.
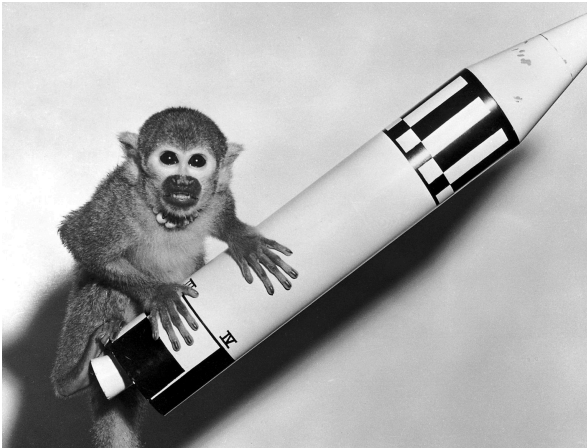
Figures 4 and 5: Monkeys who courageously gave their lives to science.

The WSMR played a key role with many tests for the Apollo program. From 1963 to 1966, a series of tests were conducted using a Little Joe II rocket to simulate the Saturn rocket in order to develop an escape system for the crew if there was a failure during launch. When the escape system was triggered, the capsule was released from rocket and parachuted safely back to the ground.

Figure 6: Little Joe rocket.

In the 1970s, NASA selected two old lakebeds at the WSMR as a space shuttle pilot training area. The two lakebed runways that were developed for training were lengthened to 35,000 feet to allow actual landings of returning shuttle orbiters, including Columbia's third landing in 1982. The site was chosen as a back-up landing site for Columbia in case of rain at Edwards Air Force Base, the primary landing site. Pilot training continues at the site with over 90% of shuttle training runs taking place at White Sands.

Figure 7: Columbia landing at White Sands.

Fun Facts:

Prior to 1961, every time a missile was fired, manned crews would spend hours combing the desert for parts they could attribute to the missiles success or failure. In order to expedite this process the WSMR started the Range Instrumentation Development Division "dog program." For up to a year before testing, crucial missile components were sprayed down with shark-liver oil that dogs are particularly sensitive to. After a missile firing, radar could be used to track the general area the missile parts had fallen onto, and dogs were sent to retrieve the parts covered in oil. The dogs were equipped with terrycloth jackets that housed ice-cubes to cool them down during the summer. The dog program was immensely successful (the canines had a 96% recovery rate), but the WSMR was forced to discontinue the program in 1965 due to the perceived inhumane nature of the program.

Figure 8: Two of the dogs in the Range Instrumentation Developments Division "dog group," Dingo and Count, after recovering a piece of a missile launched in the early 1960s at the WSMR.

References:
White Sands Missile Range
http://www.nasa.gov/pdf/449089main_White_Sands_Missile_Range_Fact_Sheet.pdf
White Sands Missile Range History
http://www.wsmr-history.org/History.htm

Common Rock Forming Minerals

Dark-Colored minerals

| Hardness	Cleavage	Physical Properties	Name
Hardness >5	Excellent or good	Dark gray, Blue-gray or black. May be iridescent. Cleavage in 2 planes at nearly right angles, Striations. Hardness-6	Plagioclase Feldspar
		Brown, gray, green or red. Cleavage in 2 planes at nearly right angles. Exsolution Lamellae. Hardness-6	Potassium Feldspar
		Opaque black. 2 cleavage planes at 60° and 120°. Hardness- 5.5	Hornblende (Amphibole)
	Poor or absent	Opaque red, gray, hexagonal prisms with striated flat ends. Hardness- 9	Corrundum
		Gray, brown or purple. Greasy luster. Massive or hexagonal prisms and pyramids. Transparent or translucent. Hardness- 7	Quartz Black or brown- Smoky , Purple- Amethyst
		Opaque red or brown. Waxy luster. Hardness- 7. Conchoidal Fracture	Jasper
		Opaque black. Waxy luster. Hardness- 7	Flint
		Transparent- translucent dark red to black. Hardness- 7	Garnet
Hardness < 5	Excellent or good	Colorless, purple, green, yellow, blue. Octahedral cleavage. Hardness- 4	Flourite
		Green. Splits along 1 excellent cleavage plane. Hardness- 2-3	Chlorite
		Black to dark brown. Splits along 1 excellent cleavage plane. Hardness- 2.5-3	Biotite mica
	Poor or absent	Opaque green, yellow or gray. Silky or greasy luster. Hardness- 2-5	Serpentine
		Opaque white, gray or green. Can be scratched with fingernail. Soapy feel. Hardness- 1	Talc
		Opaque earthy red to light brown. Hardness- 1.5-6	Hematite

Light-colored minerals

Hardness	Cleavage	Physical Properties	Name
Hardness >5	Excellent or good	White or gray, Cleavage in 2 planes at nearly right angles, Striations. Hardness-6	Plagioclase Feldspar
		Orange, brown, white, gray, green or pink. Cleavage in 2 planes at nearly right angles. Exsolution Lamellae. Hardness-6	Potassium Feldspar
		Pale brown, white or gray. Long slender prisms. Cleavage in 1 plane. Hardness- 6-7	Sillimanite
	Poor or absent	Opaque red, gray, white hexagonal prisms with striated flat ends. Hardness- 9	Corrundum
		Colorless, white, gray or other colors. Greasy luster. Massive or hexagonal prisms and pyramids. Transparent or translucent. Hardness- 7	Quartz White-Milky, Yellow-Citrine, Pink- Rose
		Opaque gray or white. Waxy luster. Hardness- 7. Conchoidal Fracture	Chert
		Colorless, white, yellow, light brown. Translucent opaque. Laminated or massive. Cryptocrystalline. Hardness- 7	Chalcedony
		Pale olive green. Conchoidal fracture. Transparent or translucent. Hardness- 7	Olivine
Hardness < 5	Excellent or good	Colorless, white, yellow, blue, green. Excellent cleavage in 3 planes. Breaks into rhombohedrons. Effervesces in HCl. Hardness- 3	Calcite
		Colorless, white, yellow, blue, green. Excellent cleavage in 3 planes. Breaks into rhombohedrons. Effervesces in HCl only if powdered. Hardness- 3.5-4	Dolomite
		White with tints of brown. Short tabular crystals or roses. Very heavy. Hardness- 3-3.5	Barite
		Colorless, white or gray. Massive or tabular crystals, blades or needles. Can be scratched by fingernail. Hardness- 2	Gypsum
		Colorless, white. Cubic crystals. Salty taste. Hardness- 2.5	Halite
		Colorless, purple, green, yellow, blue. Octahedral cleavage. Hardness- 4	Flourite
		Colorless, yellow, brown. Splits along 1 excellent cleavage plane. Hardness- 2-2.5	Muscovite mica
	Poor or absent	Yellow crystals or earthy masses. Hardness 1.5-2.5	Sulfur
		Opaque green, yellow or gray. Silky or greasy luster. Hardness- 2-5	Sepentine
		Opaque white, gray or green. Can be scratched with fingernail. Soapy feel. Hardness- 1	Talc
		Opaque earthy white to light brown. Hardness- 1-2	Kaolinite

Metallic

	Streak	Physical Properties	Name
Hardness > 5	Dark Gray	Brass yellow	Pyrite
		Dark gray-black, attracted to magnet	Magnetite
	Brown	Silvery black to black tarnishes gray	Chromite
Harness < 5	Red-Red/Brown	Silvery gray, black, or brick red	Hematite
	Dark Gray	Brass yellow, tarnishes dark brown or purple	Chalcopyrite
		Iridescent blue, purple or copper red, tarnishes dark purple	Bornite
		Silvery gray, tarnishes dull gray Cleavage good to excellent	Galena
		Dark gray to black, can be scratched with fingernail	Graphite

Sedimentary Rocks

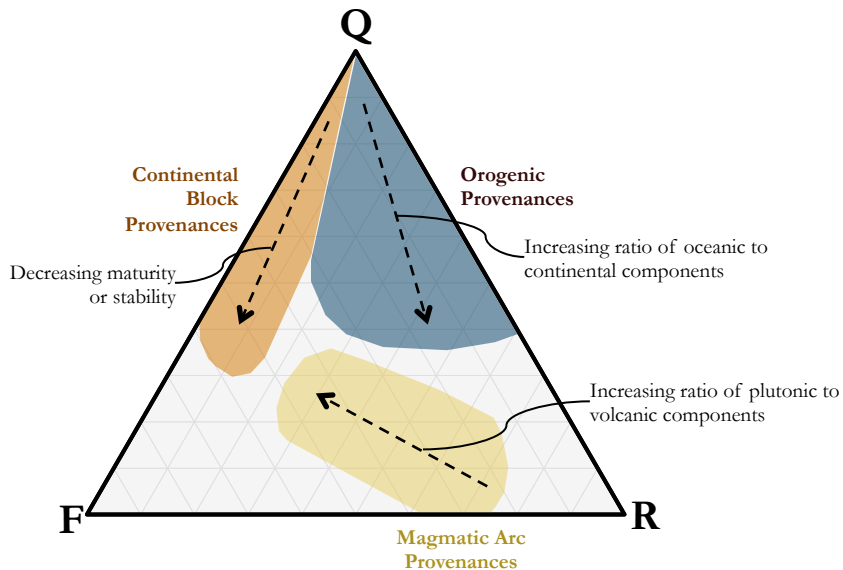## McBride, 1963 & Dott, 1964 Classification Scheme for
Clastic Sedimentary Rocks

Scheme based on the normalized percentages of the visible grains:
quartz and chert(Q), feldspar (F), and lithic rock fragments (R) – as
well as the percent composed of matrix (mud & silt)
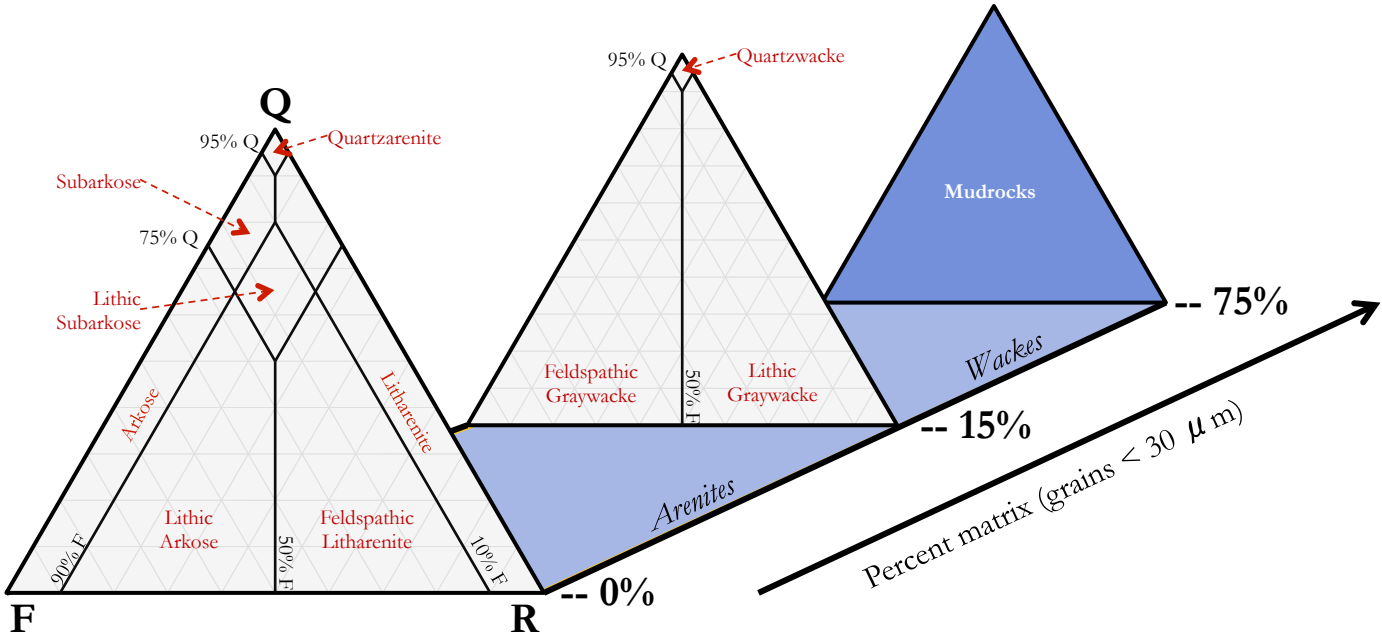
Tectonic Setting for Clastic Sedimentary Rocks

Scheme based on the normalized percentages of the visible grains: quartz and
chert(Q), feldspar (F), and lithic rock fragments (R) – as well as the percent composed
of matrix (mud & silt). Regions based upon field data.

Sedimentary Rocks

	Mudrocks (containing > 50% mud)			Rocks with <50%mud
	Silt dominant (> 2/3 of rock)	Clay and Silt	Clay dominant (> 2/3 of rock)	Sand-sized or larger grains dominant
Non-laminated	Siltstone	Mudstone	Claystone	Conglomerates, Breccias, Sandstones, etc.
Laminated	Laminated Siltstone	Mudshale	Clayshale	

Classification Scheme for **Mudrocks**

Scheme based on clay/silt content, and whether the rock is laminated (layered) or not.

Classification Scheme for **Sub-Conglomerates and Sub-Breccias**

Scheme based on percent of a rock composed of: gravel or pebbles (size >2 mm), sand (2 mm > size > 1/16 mm), and mud (size < 1/16 mm).

Gravel/Pebbles

- Well-sorted Conglomerate or Breccia
- 75% Pebbles
- Conglomerate or Breccia
- 50% Pebbles
- Muddy Conglomerate or Breccia
- Sandy Conglomerate or Breccia
- 25% Pebbles
- Pebbly Mudstone
- 50% Sand
- Pebbly Wacke
- 90% Sand
- Pebbly Arenite

Mud   **Sand**

Very well sorted   Well sorted   Moderately sorted

Poorly sorted   Very poorly sorted
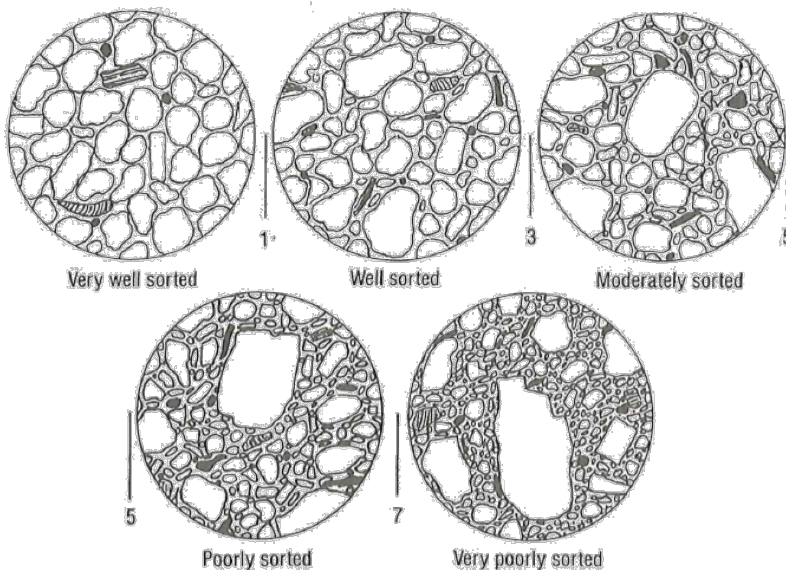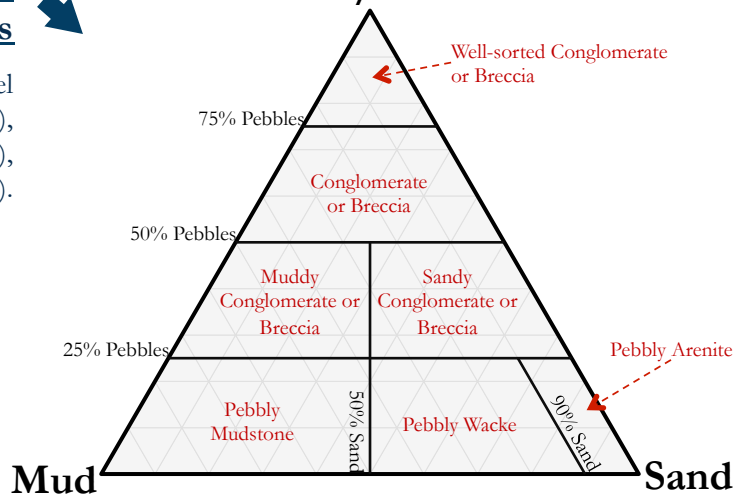
Estimating Sorting

Example hand-lens view of detritus. From Compton, 1985

Sedimentary Rocks

Degrees of Rounding

Example hand-lens view of detritus of varying degrees of roundedness. The top row are equidimensional (spherical) grains, while the lower row are elongated grains. From Compton, 1985 and Davis & Reynolds, 1996, respectively.
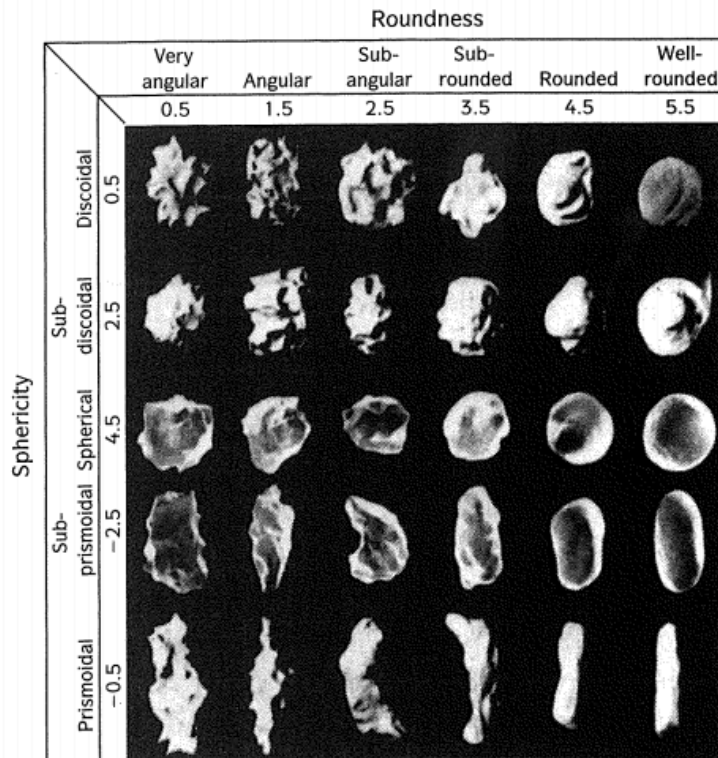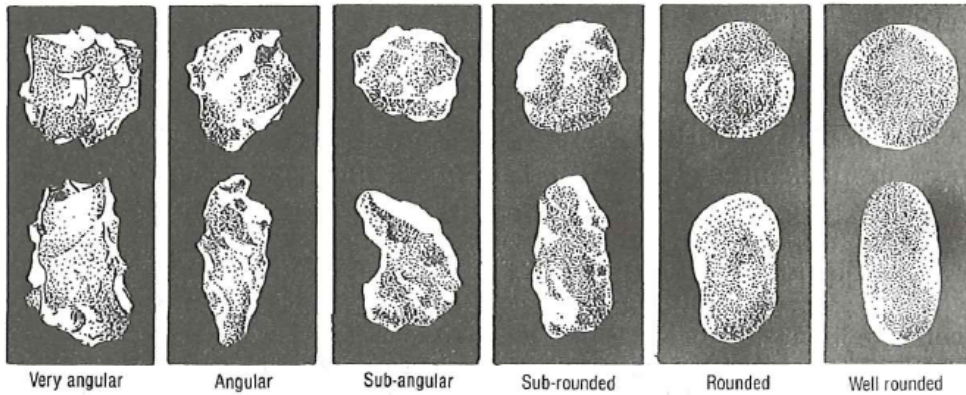
Sedimentary Rocks

Percentage Diagrams for Estimating Composition by Volume

Example hand-lens view of rocks with varying composition. To find weight percents, simply multiply each volume percent by the specific gravity of that mineral, and re-normalize. Compton, 1985

Sedimentary Rocks

Actual size	mm	ϕ	Wentworth size class	
	1000	−10 (1024 mm)		
	900 800 700			
	600		Boulder	
	500	−9		
	400			
	300			
		−8 (256 mm)		
	200			
		−7	Cobble	
	100 90 80 70	−6		
	60			Gravel
	50			
	40			
	30	−5	Pebble	
	20	−4		
	10 9 8 7 6 5	−3		
	4	−2		
	3		Granule	
	2	−1		
	1	0	Very coarse sand	Sand

Actual size	mm	ϕ	Wentworth size class	
	1 0.9 0.8 0.7 0.6	0	Coarse sand	
	0.5	1		
	0.4		Medium sand	
	0.3	2		Sand
	0.2		Fine sand	
		3 (125 µm)		
	0.1 0.09 0.08 0.07		Very fine sand	
	0.06	4 (62.5 µm)		
	0.05		Coarse silt	
	0.04			
	0.03	5 (31.3 µm)		
	0.02		Medium silt	
		6 (15.6 µm)		
	0.01 0.009 0.008 0.007	7 (7.8 µm)	Fine silt	Mud
	0.006		Very fine silt	
	0.005			
	0.004	8 (3.9 µm)		
	0.003			
	0.002	9 (1.95 µm)	Clay	
	0.001	10		

Sedimentary Rocks: Carbonates

Folk Classification Scheme for **Carbonate Rocks**

Folk's classification scheme is based upon the composition (and type of allochems) within a limestone. Figures from Prothero and Schwab, 2004

Principle Allochems in Limestone	Limestone Type			
	Cemented by Sparite		Cemented by Micritic Matrix	
Skeletal Grains (Bioclasts)	Biosparite		Biomicrite	
Ooids	Oosparite		Oomicrite	
Peloids	Pelsparite		Pelmicrite	
Intraclasts	Intrasparite		Intramicrite	
Limestone formed in place	Biolithite		Terrestrial Limestone	

Dunham Classification Scheme for **Carbonate Rocks**

Dunham's classification scheme is based upon depositional textures within a limestone.

Allochthonous Limestone (original components not organically bound during deposition)						Autochthonous Limestone (original components organically bound during deposition; reef rocks)		
Of the allochems, less than 10% are larger than 2 mm				Of the allochems, greater than 10% are larger than 2 mm				
Contains carbonate mud			No mud	Matrix supported	Grain supported	Organisms acted as baffles	Organisms are encrusting and binding	Organisms building a rigid framework
Grain supported		Grain supported						
Less than 10% grains	More than 10% grains							
Mudstone	Wackestone	Packstone	Grainstone	Floatstone	Rudstone	Bafflestone	Bindstone	Framestone

Igneous Rocks

IUGS Classification Scheme for
Phaneritic Igneous Rocks

Phaneritic: most crystals are visible to the naked eye; rock appears granular.

Scheme based on the normalized percentages of the visible mineral grains: quartz (Q), plagioclase (P), alkali feldspar (A), and feldspathoids (foids, F).

Q

typically not igneous

60% Q

Alkali Feldspar Granite

Granite

Granodiorite

Tonalite

Alk.-Feld. Quartz Syenite

20% Q

Alk.-Feld. Syenite

5% Q

A

10% P · 35% P · 65% P · 90% P

Quartz Syenite
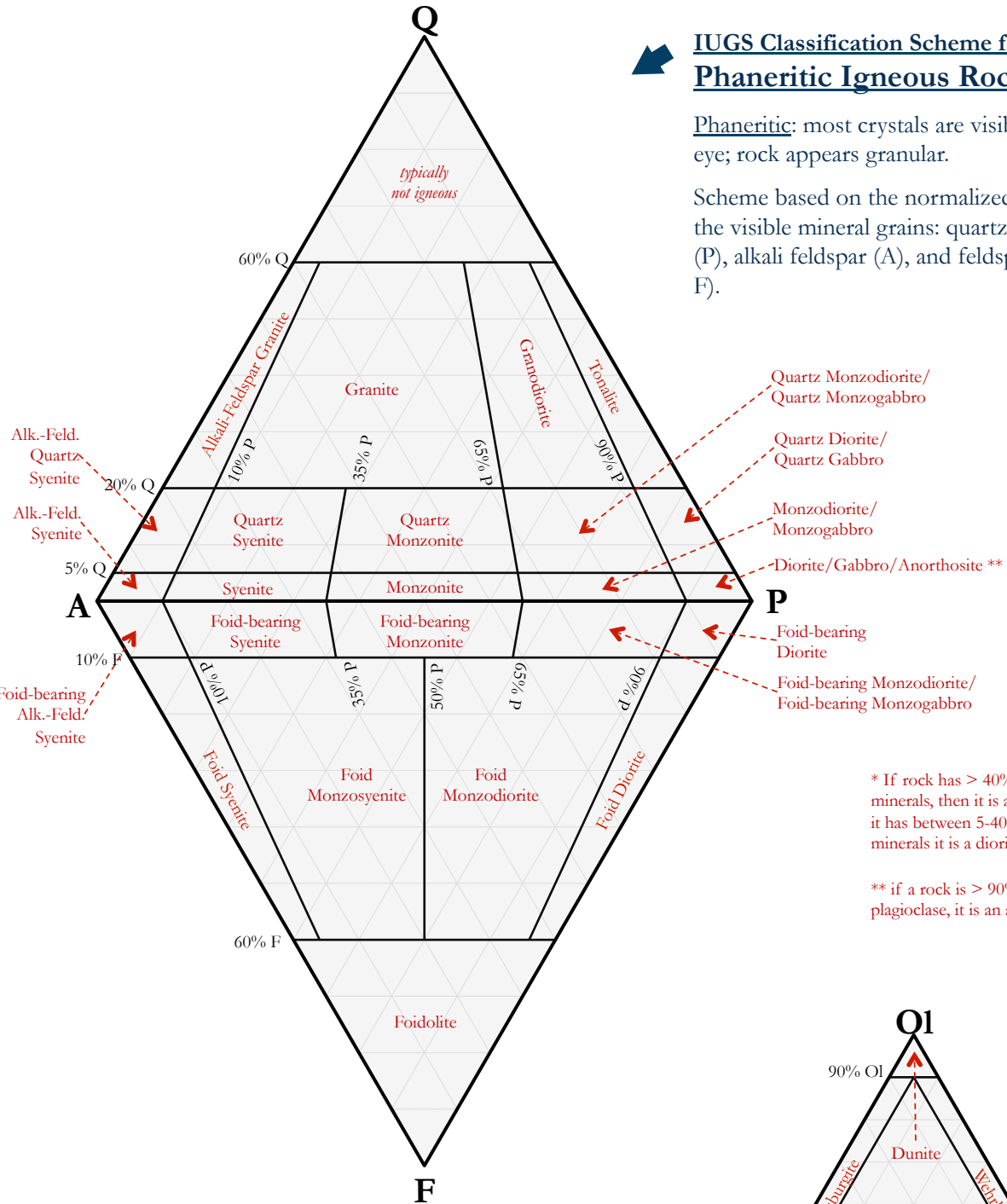
Quartz Monzonite

Quartz Monzodiorite/ Quartz Monzogabbro

Quartz Diorite/ Quartz Gabbro

Monzodiorite/ Monzogabbro

Syenite

Monzonite

Diorite/Gabbro/Anorthosite **

Foid-bearing Syenite

Foid-bearing Monzonite

Foid-bearing Diorite

10% F

Foid-bearing Alk.-Feld. Syenite

Foid-bearing Monzodiorite/ Foid-bearing Monzogabbro

P

10% P · 35% P · 50% P · 65% P · 90% P

Foid Syenite

Foid Monzosyenite

Foid Monzodiorite

Foid Diorite

60% F

Foidolite

F

* If rock has > 40% mafic minerals, then it is a gabbo. If it has between 5-40% mafic minerals it is a diorite.

** if a rock is > 90% plagioclase, it is an anorthosite

IUGS Classification Scheme for
Phaneritic Ultramafic Igneous Rocks (1)

Ultramafic: more than 90% of the total minerals are mafic.

Scheme based on the normalized percentages of the visible minerals: olivine (Ol), orthopyroxene (Opx), and clinopyroxene (Cpx).

Ol

90% Ol

Dunite

Harzburgite

Wehrlite

5% Cpx

Lherzolite

95% Cpx

40% Ol

Olivine Orthopyroxenite

Olivine Websterite

Olivine Clinopyroxenite

10% Ol

Orthopyroxenite

5% Ol

Clinopyroxenite

Websterite

Opx

Cpx
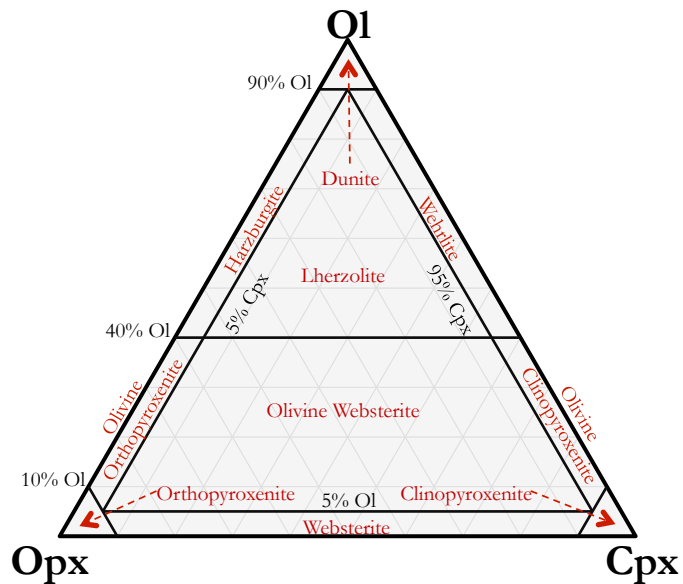
Igneous Rocks

IUGS Classification Scheme for **Aphanitic Igneous Rocks**

Aphanitic: the majority of crystals are not visible to the naked eye.

Aphanetic rocks are hard to classify due to the lack of visible minerals. However, you may still be able identify them based on phenocryst content, if phenocrysts are present. Scheme based on the normalized percentages of the visible phenocrysts: quartz (Q), plagioclase (P), alkali feldspar (A), and feldspathoids (foids, F).

Q

typically not igneous

60% Q

Alkali Feldspar Rhyolite

Rhyolite

Dacite

10% P

35% P

65% P

Quartz Alkali Trachyte

20% Q

Alkali Trachyte

5% Q

Quartz Trachyte

Quartz Latite

Andesite/Basalt*

Trachyte

Latite

A

Foid-bearing Syenite

Foid-bearing Latite

Foid-bearing Andesite/Basalt*

P

10% F

Foid-bearing Alk.-Feld. Syenite

10% P

35% P

50% P

65% P

90% P

Phonolite

Tephritic Phonolite

Phonolitic Tephrite (Basanite)

Tephrite/Basanite

60% F

Foidite

F
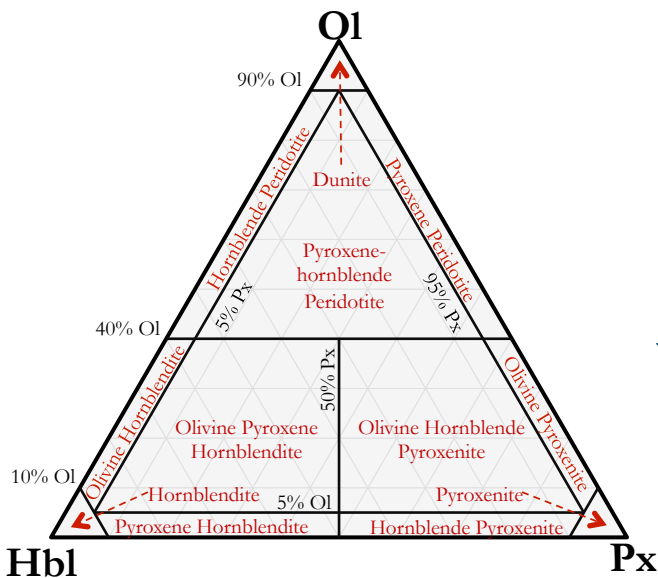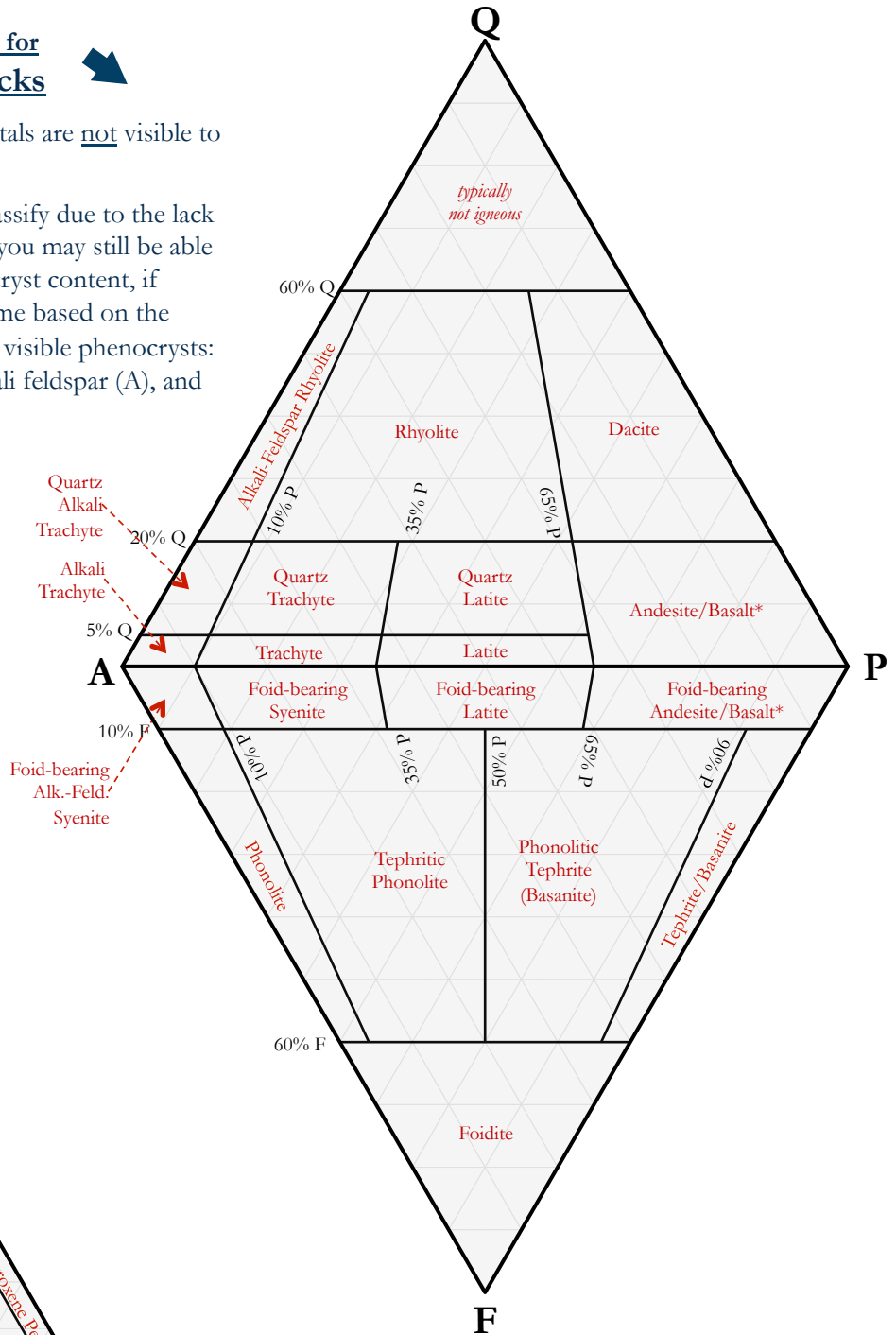
IUGS Classification Scheme for **Phaneritic Ultramafic Igneous Rocks (2)**

Ultramafic: more than 90% of the total minerals are mafic.

Scheme based on the normalized percentages of the visible minerals: olivine (Ol), hornblende (Hbl), and pyroxene (Px).

Ol

90% Ol

Dunite

Hornblende Peridotite

Pyroxene Peridotite

5% Px

95% Px

Pyroxene-hornblende Peridotite

40% Ol

50% Px

Olivine Hornblendite

Olivine Pyroxenite

Olivine Pyroxene Hornblendite

Olivine Hornblende Pyroxenite

10% Ol

Hornblendite

5% Ol

Pyroxenite

Pyroxene Hornblendite

Hornblende Pyroxenite

Hbl

Px

Igneous Rocks

Blocks & Bombs

Classification Scheme for
Pyroclastic Igneous Rocks

Pyroclastic rocks are formed via the accumulation of fragments of volcanic rock scattered by volcanic explosions. They are frequently classified based upon the size distribution of clasts.

Pyroclastic Breccia

75%

Tuff-Brecia

25%

Lapilli-Stone

Lapilli-Tuff

Tuff

Lapilli

Ash

Sizes

256 mm

64 mm

2 mm

1/16 mm

Classification

Coarse bombs and blocks

Fine bombs and blocks

Lapilli

Coarse ash

Fine ash
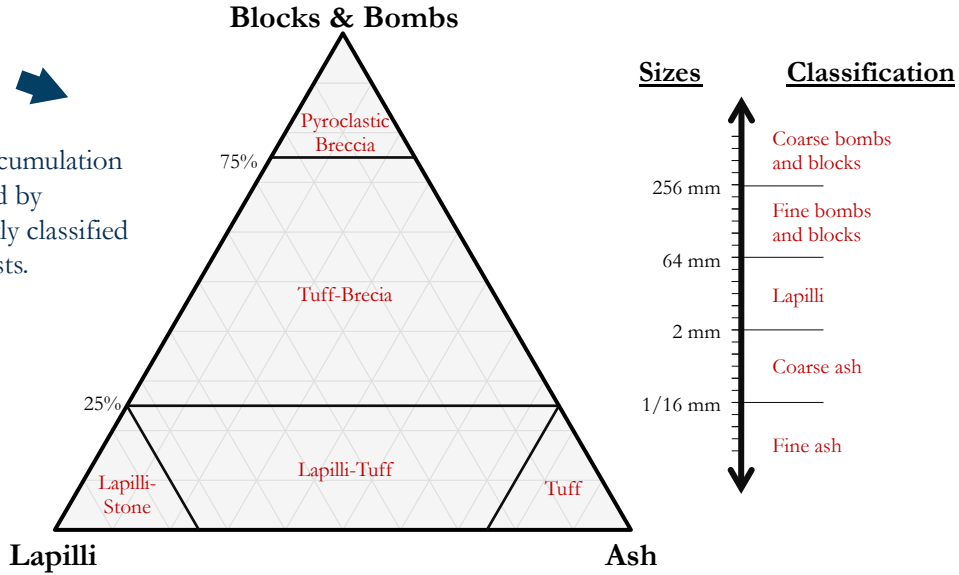
Types of Tephra (Pyroclasts)

In each row, the viscosity of the lava increases to the right. From Compton, 1985.

BLOCKS AND BOMBS (X0.1 or less)

Cowdung bomb   Ribbon bombs   Spindle (fusiform) bomb   Partly shaped scoria lump   Breadcrust bomb   Block

LAPILLI (X1)

Agglutinated spatter   Glass drops   Round-bubble pumice   Long-tube pumice   Glassy and stony lithic lapilli   Accretionary lapilli   Cross section

ASH (X10)

Droplets (Pele's tears)   Threads (Pele's hair)   Globules   Shards   Pumice   Lithic ash   Crystal ash   Broken   px   fld   qz   hbl   bio

Vitric ash

olivine

Mg-pyroxene

Mg-Ca-pyroxene

amphibole

biotite

Calcic plagioclase

Calcic-alkalic plagioclase

alkali-calcic plagioclase

alkalic plagioclase

K-feldspar
muscovite
quartz

Temperature

Bowen's Reaction Series

From Winter, 2010.

Metamorphic Rocks

⬇ ### Classification Scheme for
Metamorphic Rocks

Based upon texture and mineralogical composition.

Structure & Texture		Characteristic Properties	Characteristic Mineralogy	Rock Name
Foliate (layered)	Increasing grain size, and degree of metamorphism ⬇	Dull luster; very flat fracture surface; grains are too small to readily see; more dense than shale	No visible minerals	Slate
		Silky sheen; Crenulated (wavy) fracture structure; A few grains visible, but most are not	Development of mica and/or hornblende possible	Phyllite
		Sub-parallel orientations of individual mineral grains; wavy-sheet like fracture; often contains porphyroblasts; thinly foliated	Abundant feldspar; Quartz and mica are common; hornblende possible	Schist
		Sub-parallel, alternating bands or layers of light and dark material; coarsely foliated; blocky fracture	Abundant feldspars; Quartz, mica, and hornblende are common	Gneiss
Foliate (layered)		Interlocking crystals; effervesces in dilute HCl; softer than glass	Calcite	Marble
		Nearly equigranular grains; fracture across grains (not around them); sub-vitreous appearance; smooth feel compared to sandstone	Quartz	Quartzite

⬇ ### Mineralogy for
Metamorphic Rock Facies

Facies	Definitive Mineral Assemblages in Mafic Rocks
Zeolite	zeolites: especially laumontite, wairakite, analcime (in place of other Ca-Al silicates such as prehnite, pumpellyite and epidote)
Prehnite-Pumpellyite	prehnite + pumpellyite (+ chlorite + albite)
Greenschist	chlorite + albite +epidote (or zoisite) + actinolite ± quartz
Amphibolite	hornblende + plagioclase (oligoclase, andesine) ± garnet
Granulite	orthopyroxene + clinopyroxene + plagioclase ± garnet
Blueschist	glaucophane + lawsonite or epidote/zoisite (± albite ± chlorite ± garnet)
Eclogite	pyralspite garnet + omphacitic pyroxene (± kyanite ± quartz), no plagioclase
Contact Facies	mineral assemblages in mafic rocks of the facies of contact metamorphism do not differ substantially from those of the corresponding regional facies at higher pressure

Metamorphic Rocks

Metamorphic Rock Facies, P vs. T diagram

From Winter, 2010
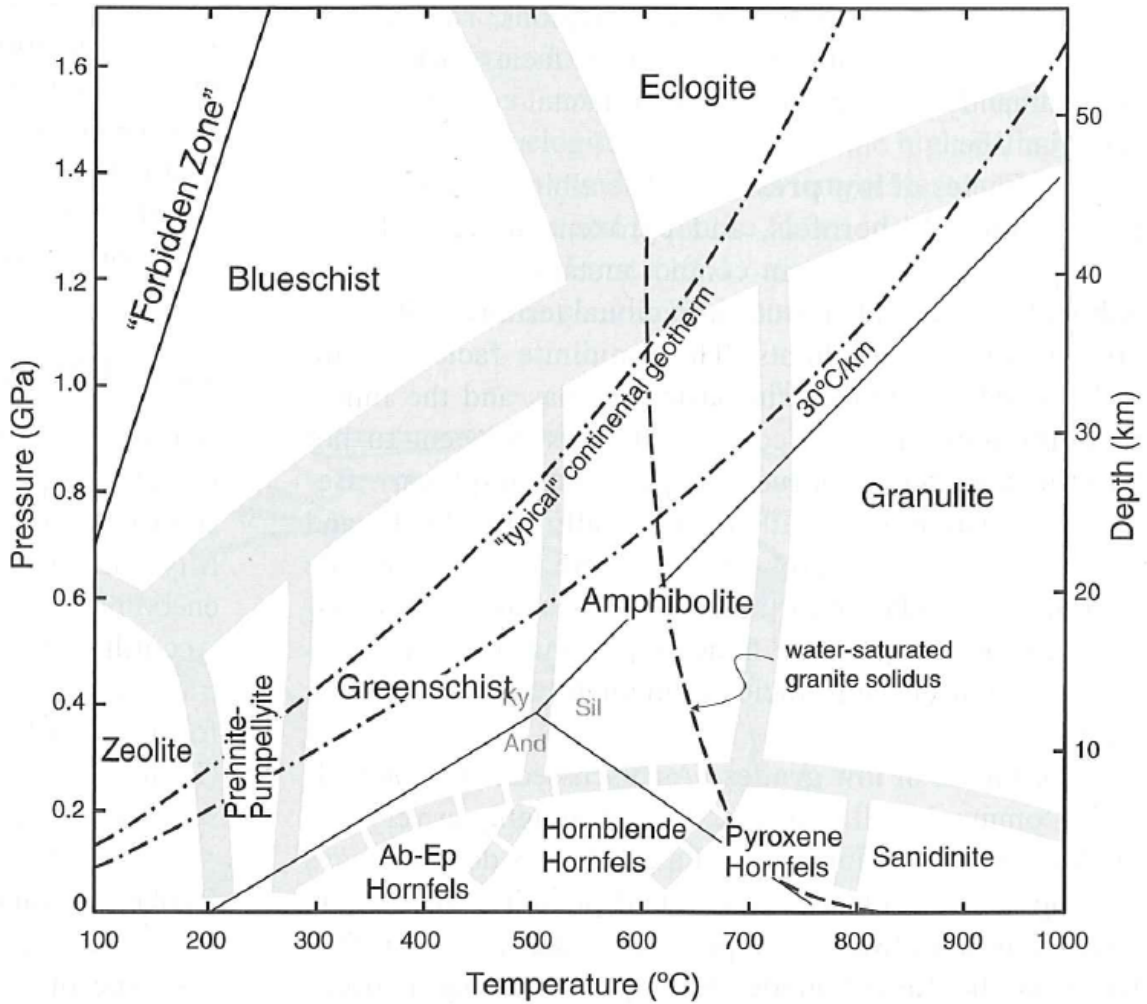
Schematic of Island Arc, and the origins of Metamorphic Facies

A schematic cross section of an island arc. Light gray lines are isotherms. From Winter, 2010

(1) zeolite
(2) prehnite-pumpellyite
(3) blueschist
(4) eclogite
(5) greenschist
(6) ab-ep amphibolite
(7) amphibolite
(8) granulite
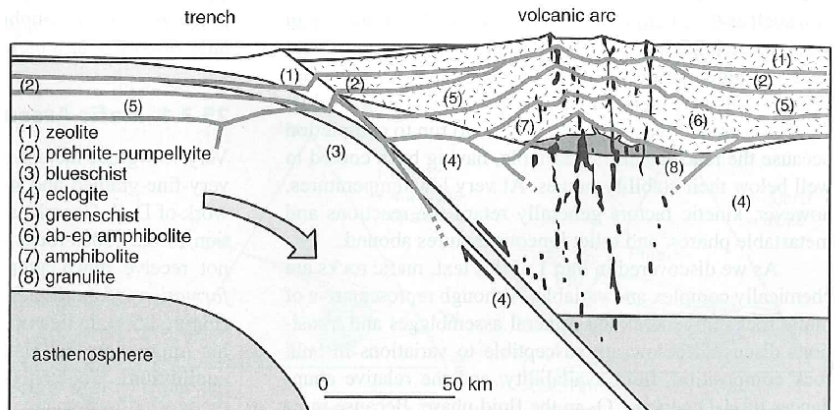
Structural Geology: Normal Faults

Normal Faults ➡

In normal faults, the footwall goes up with respect to the hanging wall. Normal faults are indicative of extension. Figures from Davis & Reynolds, 1996.

Fault Surface, with slickenlines indicating direction of motion

Footwall

Hanging Wall

Low-angle Normal Slip Fault

Normal Slip Fault
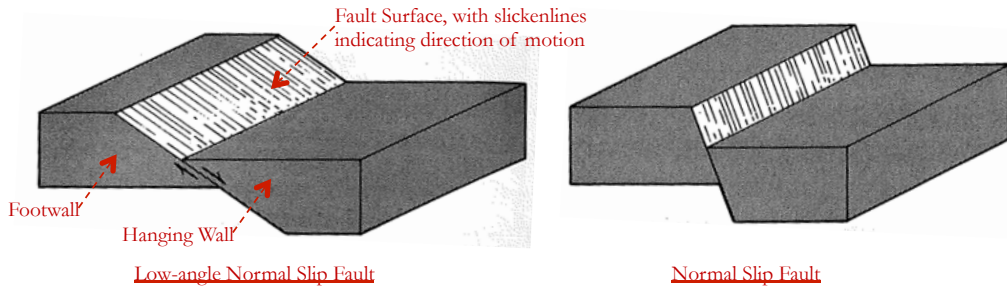
Effects of Brittle or Ductile Shear in Normal Faults ⬇

The block diagrams below illustrate the effects of changing the nature of deformation, between brittle deformation (which results in clear fault planes, fractures and fault rocks), ductile deformation (which causes deformation over a larger shear zone). Often, strata of different rheologies will behave differently, as is shown in the figure at right. The dashed layer was weak and deformed ductilely, while the middle grey layer was rigid and formed boudins. Figures from Davis & Reynolds, 1996.
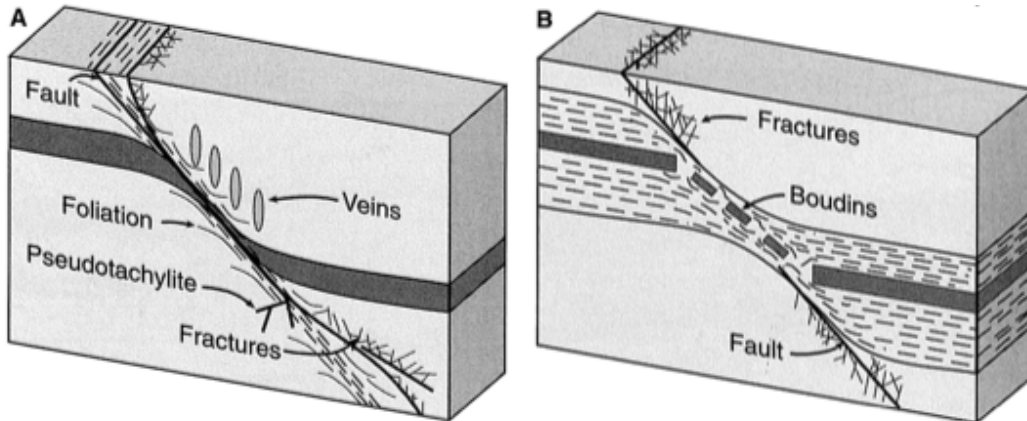
Inversion Tectonics ⬇

If the regional stresses change, previously inactive faults can reactivate, and change their sense of motion. In the figure at left, layer-A was formed prior to the formation of a normal fault. Layer-B and layer-C were deposited after the formation, and shut down of the fault. In the figure at the right, the fault has reactivated, though as a reverse fault. The resulting stratigraphic sequence is a combination of effects one would expect from both normal and reverse faults. Figures from Davis & Reynolds, 1996.
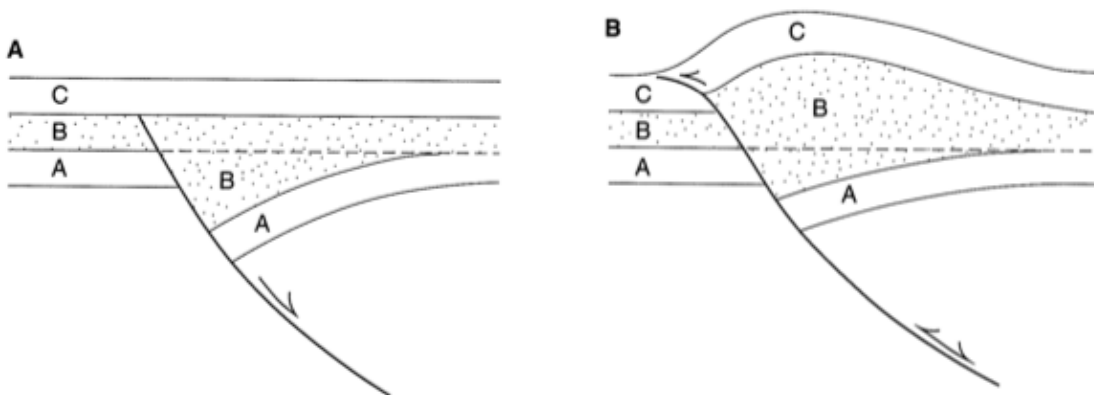
Structural Geology: Normal Faults

Normal Faults Geometries

Various normal fault geometries are possible. They all allow for lithospheric extension. (A) Domino style faulting. (B) Listric normal faulting with reverse drag. (C) Imbricate listric normal faulting. Note that listric faulting can cause extreme rotation of faulted blocks. (D) Listric normal faulting bounding a family of planar normal faults. Figures from Davis & Reynolds, 1996.
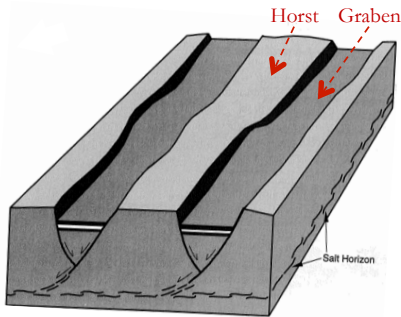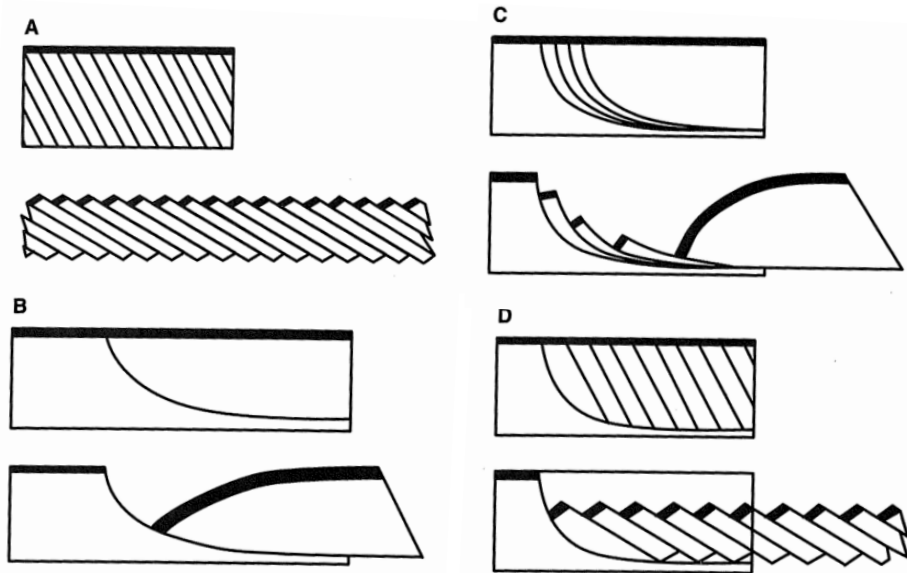
Horsts & Grabens

Classical formation describing fault-bounded uplifted (horsts) and down-dropped blocks (grabens). Figures from Davis & Reynolds, 1996.

Drag Folds, Reverse Drag, and Step Faulting

Faulting does not always produce clean displacement along the fault surface. Fault blocks are frequently folded or fractured, and the nature of these deformations are non-trivial. Figures from Davis & Reynolds, 1996.
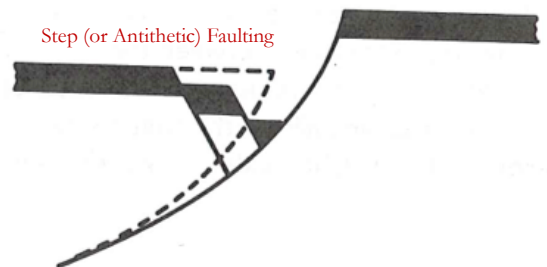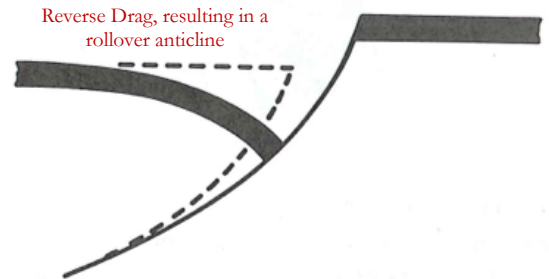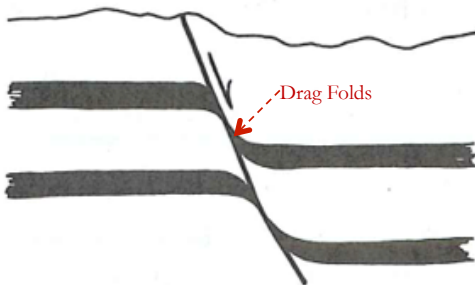
Structural Geology: Reverse & Thrust Faults

Reverse Faults ➡️

In reverse faults, the footwall goes down with respect to the hanging wall. Normal faults are indicative of compression. Thrust faults are reverse faults with fault dips <45 degrees. Figures from Davis & Reynolds, 1996.


Hanging Wall

Footwall

Fault Surface, with slickenlines indicating direction of motion

Reverse Slip Fault

Thrust Slip Fault
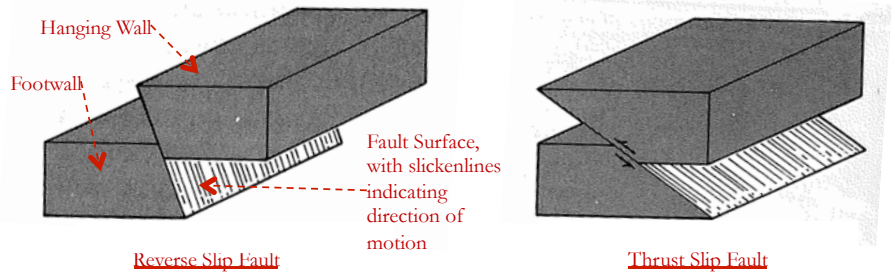
"Ramp-Flat" Geometry of Typical Thrust Fault Systems ⬇️

In a regional thrust, faulted blocks are "thrust" on top of younger strata. The exact geometry of these thrust systems can vary significantly. Figures from Davis & Reynolds, 1996.

Ramp

Flat
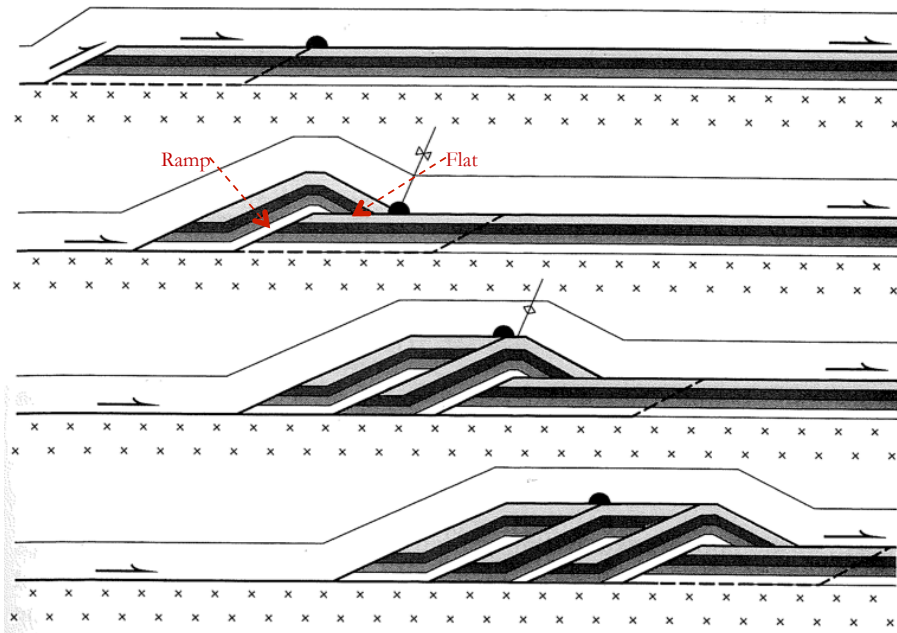
Klippe & Windows ⬇️

Thrust faults move large blocks of non-indigenous rock (referred to as "allochthonous" rock) over emplaced rock (referred to as "autochthonous" rock). If the overlying allochthonous rock is eroded, it can create windows into the lower underlying autochthonous rock. Erosion can also create islands of isolated allochthonous rock, called klippe. Figures from Davis & Reynolds, 1996.

Klippe

Allochthonous Rocks

Window

5 km

Autochthonous Rocks
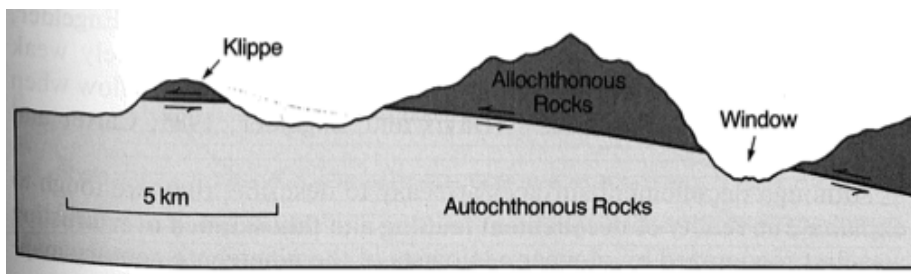
Structural Geology: Reverse & Thrust Faults
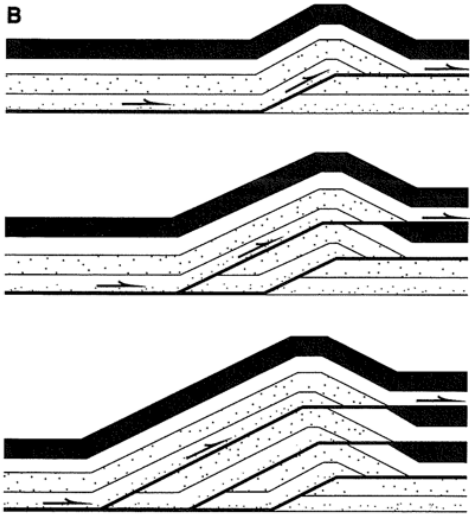
Out-of-Sequence Thrust Fault System

Unlike "in-sequence" thrust fault systems (as shown on the previous page, the "roof" of the thrust block in an out-of-sequence system becomes the "flat" for subsequent fault blocks. Figures from Davis & Reynolds, 1996.

Imbricate Fans vs. Duplexes

Two thrust fault geometries: imbricate fans (top) and duplexes (bottom). Figures from Davis & Reynolds, 1996.
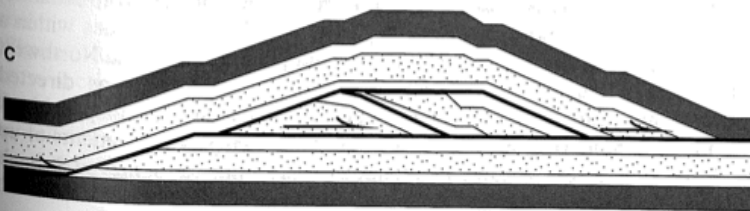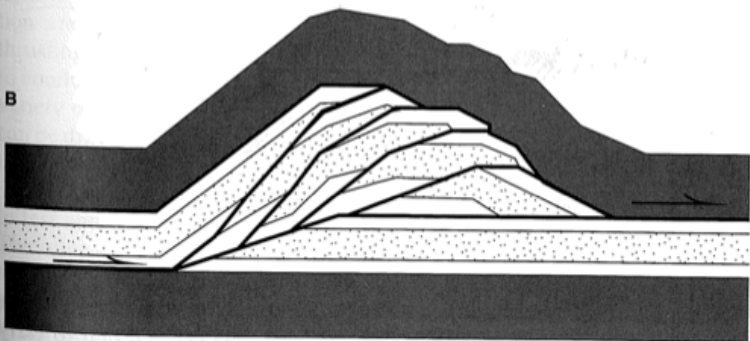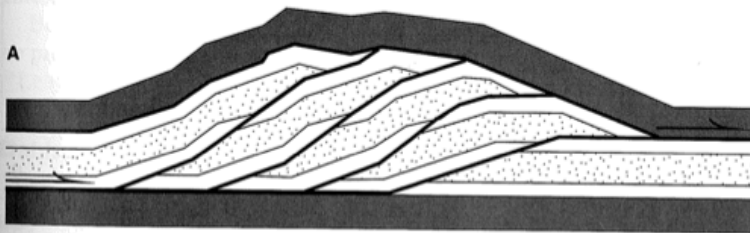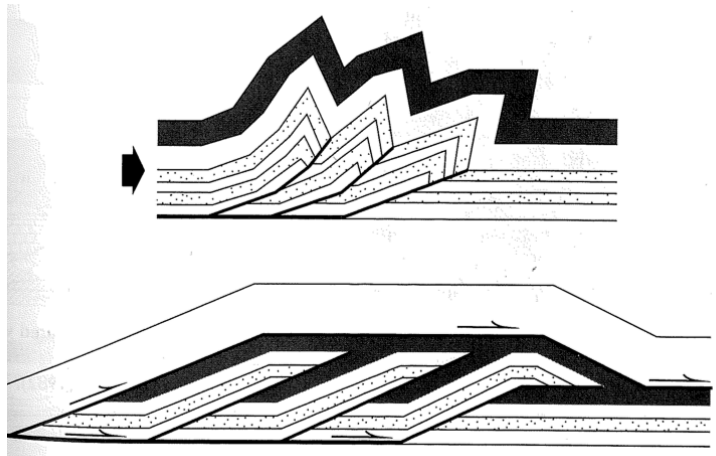
Forms of Duplexes

The exact form of a duplex or imbricate fan depends on the spacing of ramps and the amount of slip. (A) A normal duplex develops when slice length exceeds the fault slip. (B) An antiformal duplex develops when slice length and fault slip are effectively equal. (C) A forward-dipping duplex develops when the fault slip is greater than the slice length. Figures from Davis & Reynolds, 1996.

Structural Geology: Strike-Slip or Transform Faults

Strike-Slip Faults ➡

In reverse faults, the footwall goes down with respect to the hanging wall. Normal faults are indicative of compression. Thrust faults are reverse faults with fault dips <45 degrees. Figures from Davis & Reynolds, 1996.

Fault Surface, with slickenlines indicating direction of motion
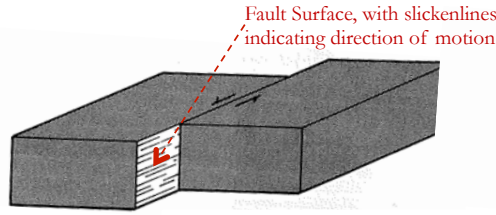
Left Lateral (Sinistral) Strike-Slip Fault
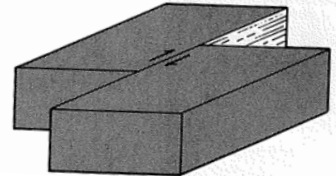
Right Lateral (Dexteral) Strike-Slip Fault
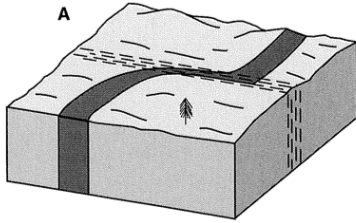
Continuous Shear Zone
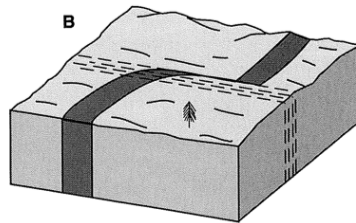
Discontinuous Shear Zone

⬅ Ductile Shear Zones

Shear in a strike-slip fault is not always located in a single plane. Sometimes, shear takes place over an extended region. Figures from Davis & Reynolds, 1996.

Brittle Shear Zones ⬊

Figures from Davis & Reynolds, 1996.

A
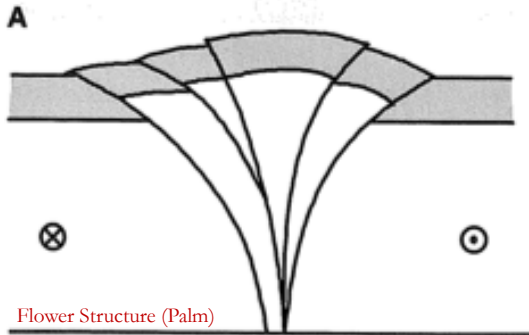
Flower Structure (Palm)

B
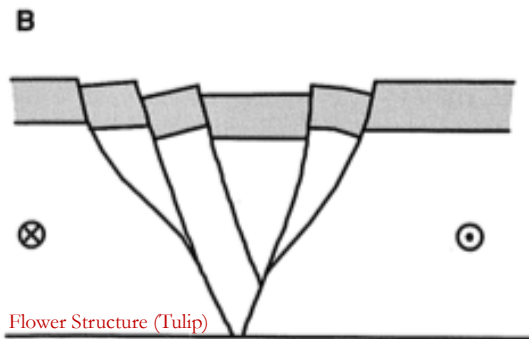
Flower Structure (Tulip)

A

Parallel Faults

B
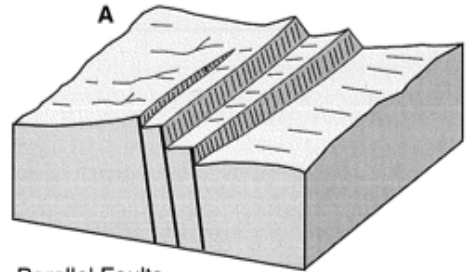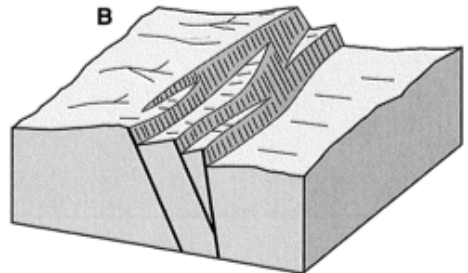
Anastomosing Faults

C
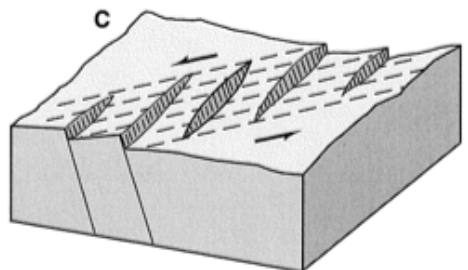
En Echelon Faults

Structural Geology: Strike-Slip or Transform Faults

Bends in Strike-Slip Faults

Strike-slip faults along irregularly curved faults creates localized regions of extension and compression. Figures from Davis & Reynolds, 1996.
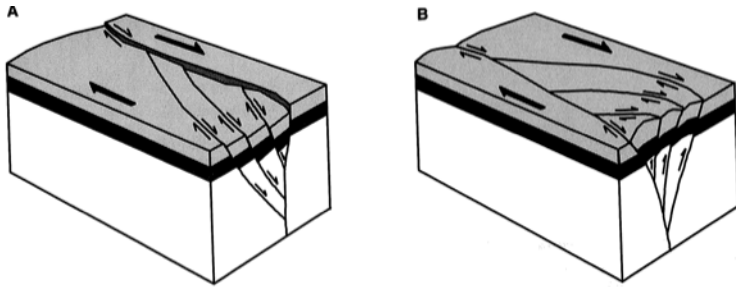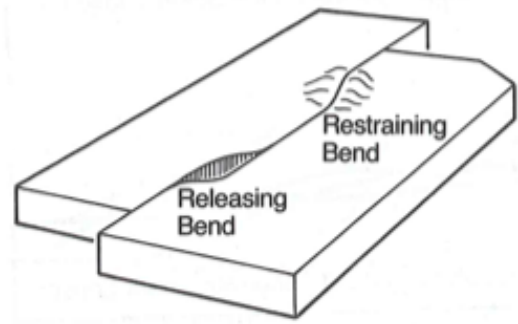
Strike-Slip Duplexes

(A) Extensional duplexes can form at releasing bends. (B) Compressional duplexes can form at restraining bends. Figures from Davis & Reynolds, 1996.

Slip Indicators in Strike-Slip Systems

In strike-slip systems, the maximum (S_1) and minimum compressional stresses (S_3) are at an angle with respect to the sense of shear. This can lead to the formation of both large scale folds and faults, or small scale fractures or veins, which are indicative to the sense of motion. Figures from Davis & Reynolds, 1996.
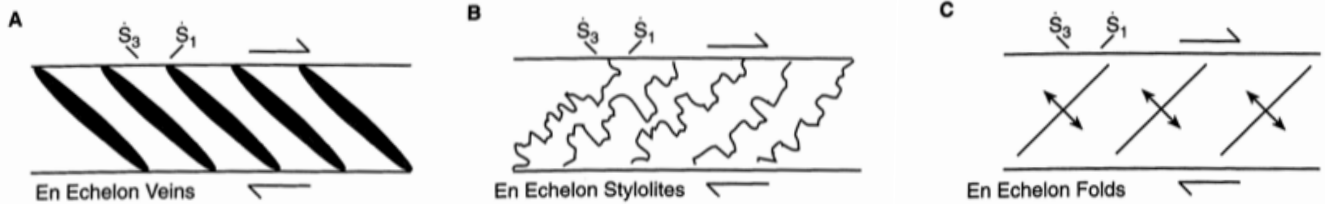
Even more Geometric Arrangements of Strike-Slip Faults

Figures from Davis & Reynolds, 1996.
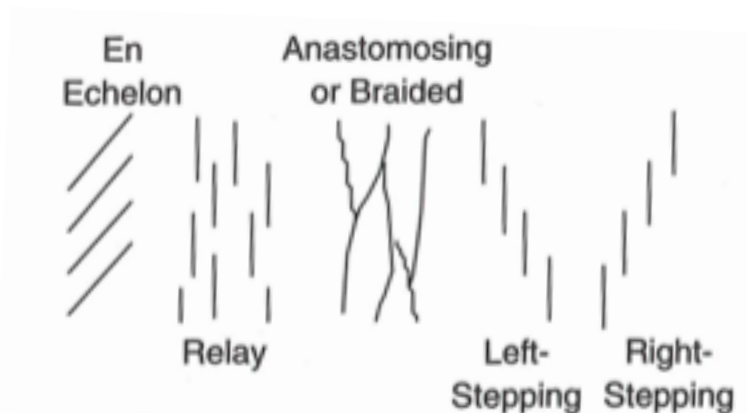
Structural Geology: Strike-Slip or Transform Faults

Riedel Shears

When under compression, rocks tend to form fail with faults forming 30° from the primary compressional stress. In a strike-slip fault, the primary compressional stress (σ_1) is 45° away from the plane of strike-slip shearing. The combination of these two facts results in fractures at interesting angles with respect to the motion of shear. These are called Riedel shears. The figure below shows a left-handed strike-slip zone. Figures from Davis & Reynolds, 1996.
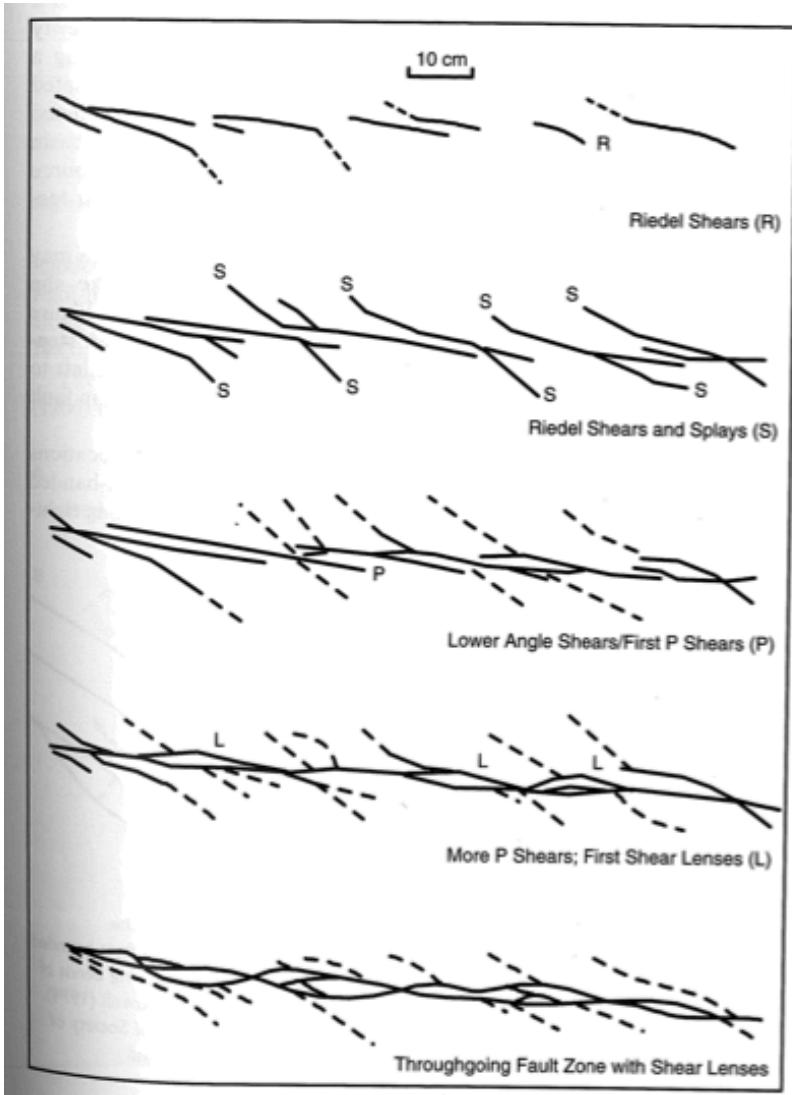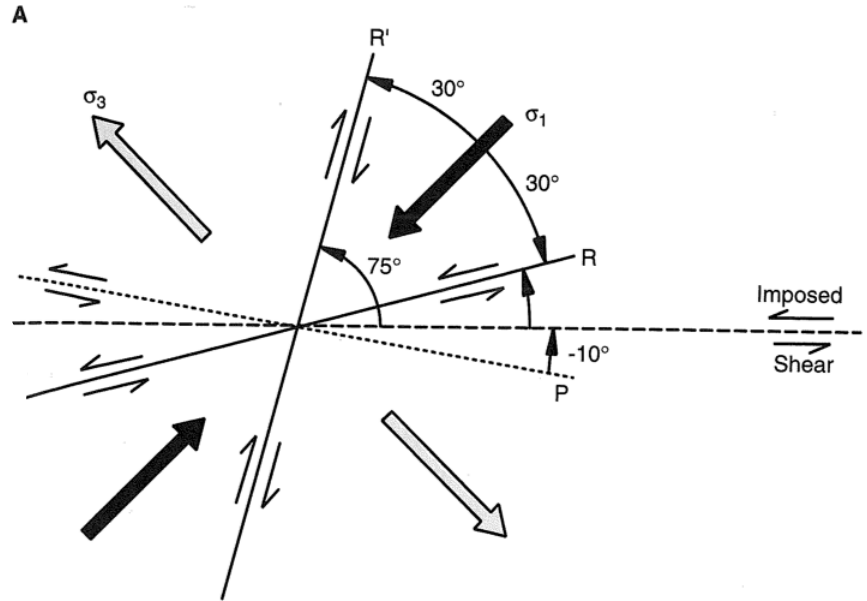
The figure at left illustrate the formation sequence of Riedel shears and other splays and shears in a right-handed strike-slip zone. Figures from Davis & Reynolds, 1996.

Structural Geology: Folds

Anticlines & Antiforms, and Synclines & Synforms

Antiforms are concave-down folds, while Synforms are concave-up folds. Anticlines are antiforms were we <u>know</u> that the younger strata lie on top of older strata. Similarly, Synclines are antiforms where younger strata lie on top of older strata. Figures from Davis & Reynolds, 1996.

Anticline

Syncline

Antiform

Synform
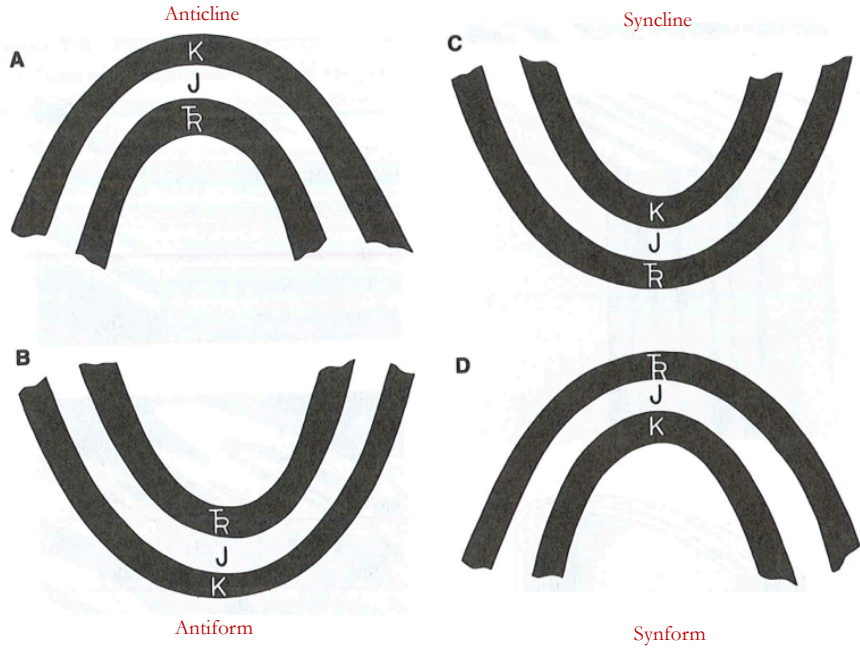
Plunging Folds

Folds (defined by hinge lines and axial surfaces) are not necessarily perpendicular to the Earth's surface. They can be dipping into or out of the surface. This can create interesting patterns of exposed surface rock, or even topography. Figures from Jones, 2001.

Non-plunging antiform

Non-plunging synform

Plunging antiform

Plunging synform
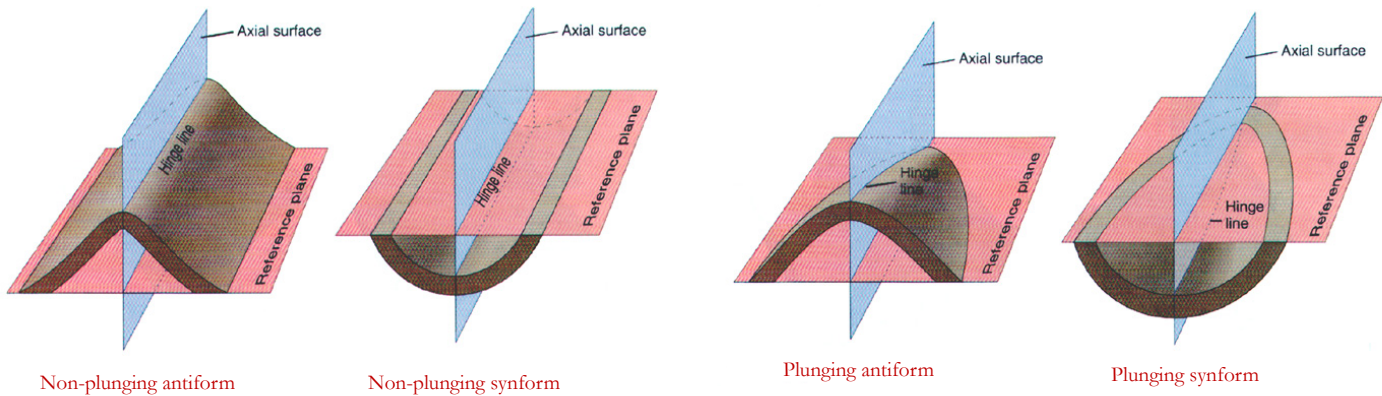
Fold Shapes

Folds can come in a variety of shapes. Davis & Reynolds, 1996.

A
B
C
Chevron
Cuspate
Circular

D
E
F
Elliptical
Box (Conjugate)
Teardrop
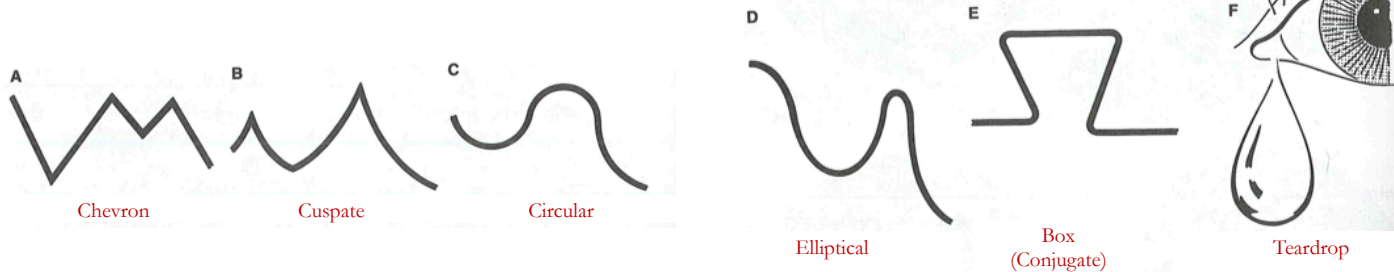
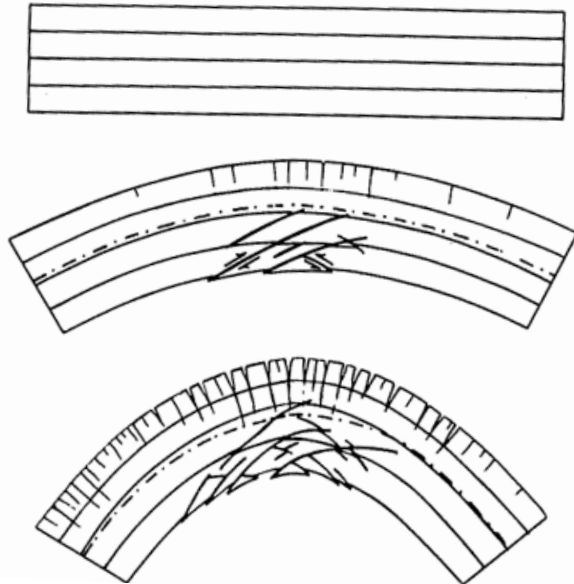# Structural Geology: Folds

Fold Tightness

Fold tightness is based upon the size of the inter-limb angle. Figures from Davis & Reynolds, 1996.
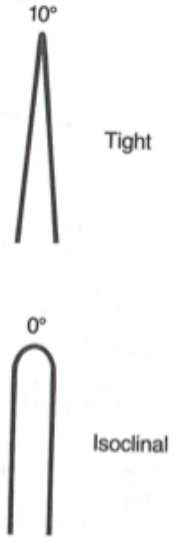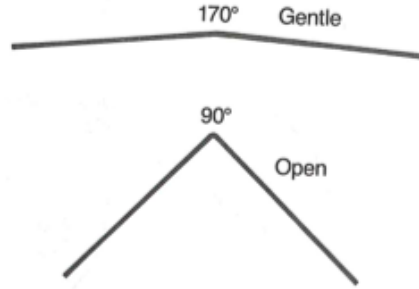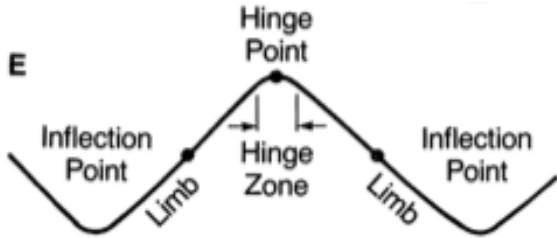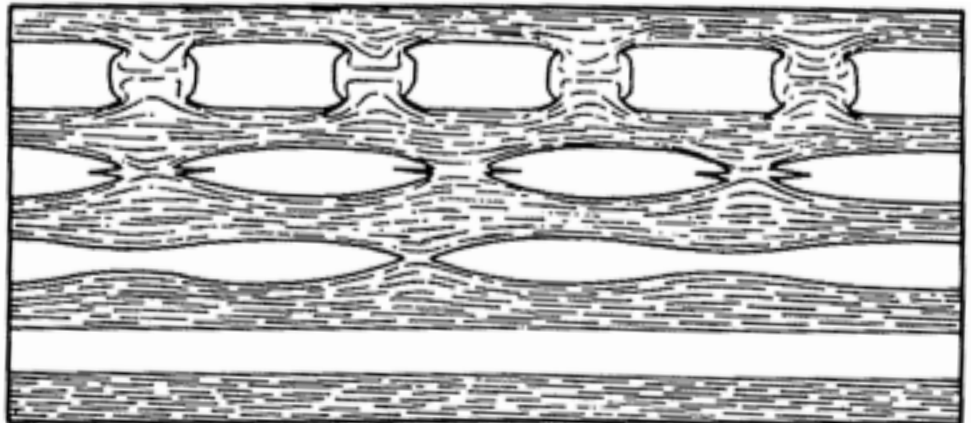

Minor Structures in Folds

When folding layers of strata, layer-parallel stretching occurs in the outer arc of a folded layer, while layer-parallel shortening occurs in the inner arc. Figures from Davis & Reynolds, 1996.

Boudins

Layer-parallel stretching can pinch off layers of strata, depending on the ductility contrast between layers. This can result in pinch-and-swell structures or boudins (where the pinching completely pinches off portions of a given strata). Figures from Davis & Reynolds, 1996.

Geologic Map Symbols

#	Description
1	Contact, showing dip where trace is horizontal, and strike and dip where trace is inclined
2	Contact, located approximately (give limits)
3	Contact, located very approximately, or conjectural
4	Contact, concealed beneath mapped units
5	Contact, gradational (optional symbols)
6	Fault, nonspecific, well located (optional symbols)
7	Fault, nonspecific, located approximately
8	Fault, nonspecific, assumed (existence uncertain)
9	Fault, concealed beneath mapped units
10	Fault, high-angle, showing dip (left) and approximate dips
11	Fault, low-angle, showing approximate dip and strike and dip
12	Fault, high-angle normal (D or ball and bar on downthrown side)
13	Fault, reverse (R on upthrown side)
14	Fault, high-angle strike-slip (example is left lateral)
15	Fault, thrust (T on overthrust side)
16	Fault, low-angle normal or detachment (D on downthrown side)
17	Fault, low-angle strike-slip (example is right lateral)
18	Fault, low-angle, overturned (teeth in direction of dip)
19	Optional sets of symbols for different age-groups of faults
20	Fault zone or shear zone, width to scale (dip and other accessory symbols may be added)
21	Faults with arrows showing plunge of rolls, grooves or slickensides
22	Fault showing bearing and plunge of net slip
23	Point of inflection (bar) on a high-angle fault
24	Points of inflection on a strike-slip fault passing into a thrust
25	Fault intruded by a dike
26	Faults associated with veins
27	Anticline, showing trace and plunge of hinge or crest line (specify)
28	Syncline (as above), showing dip of axial surface or trough surface
29	Folds (as above), located approximately
30	Folds, conjectural
31	Folds beneath mapped units
32	Asymmetric folds with steeper limbs dipping north (optional symbols)
33	Anticline (top) and syncline, overturned
34	Antiformal (inverted) syncline
35	Synformal (inverted) anticline
36	Antiform (top) and synform (stratigraphic sequence unknown)
37	Separate dome (left) and basin
38	Culmination (left) and depression
40	Vertically plunging anticline and syncline
41	Monocline, south-facing, showing traces of axial surfaces
42	Steeply plunging monocline or flexure, showing trace in horizontal section and plunge of hinges
43	Plunge of hinge lines of small folds, showing shapes in horizontal section
44	Strike and dip of beds or bedding
45	Strike and dip of overturned beds
46	Strike and dip of beds where stratigraphic tops are known from primary features
47	Strike and dip of vertical beds or bedding (dot is on side known to be stratigraphically the top)
48	Horizontal beds or bedding (as above)
49	Approximate (typically estimated) strike and dip of beds
50	Strike of beds exact but dip approximate
51	Trace of single bed, showing dip where trace is horizontal and where it is inclined
52	Strike and dip of foliation (optional symbols)
53	Strike of vertical foliation
54	Horizontal foliation
55	Strike and dip of bedding and parallel foliation
56	Strike and dip of joints (left) and dikes (optional symbols)
57	Vertical joints (left) and dikes
58	Horizontal joints (left) and dikes
59	Strike and dip of veins (optional symbols)
60	Vertical veins
61	Horizontal veins
62	Bearing (trend) and plunge of lineation
63	Vertical and horizontal lineations
64	Bearing and plunge of cleavage-bedding intersection
65	Bearing and plunge of cleavage-cleavage intersections
66	Bearings of pebble, mineral, etc. lineations
67	Bearing of lineations in plane of foliation
68	Horizontal lineation in plane of foliation
69	Vertical lineation in plane of vertical foliation
70	Bearing of current from primary features; from upper left: general; from cross-bedding; from flute casts; from imbrication
71	Bearing of wind direction from dune forms (left) and cross-bedding
72	Bearing of ice flow from striations (left) and orientation of striations
73	Bearing of ice flow from drumlins
74	Bearing of ice flow from crag and tail forms
75	Spring
76	Thermal spring
77	Mineral spring
78	Asphaltic deposit
79	Bituminous deposit
80	Sand, gravel, clay, or placer pit

Geologic Map Symbols

81	⚒	Mine, quarry, or open pit
82	▫ ▱ ▱	Shafts: vertical, inclined, and abandoned
83	⊱ ⊶	Adit, open (left) and inaccessible
84	⊷ ✕	Trench (left) and prospect
85	● ○ ⦶	Water wells: flowing, nonflowing, and dry
86	● ✵	Oil well (left) and gas well
87	◈	Well drilled for oil or gas, dry
88	⊖ ✵	Wells with shows of oil (left) and gas
89	◇ ⊙	Oil or gas well, abandoned (left) and shut in
90	⊙	Drilling well or well location
91		Glory hole, open pit, or quarry, to scale
92		Dump or fill, to scale

Fossil and Structural Symbols for Stratigraphic Columns

	Algae		Tree trunk fallen	⅜	Foraminifers, general		Scour casts
	Algal mats		Trilobites	◖	Foraminifers, large		Convolution
	Ammonites		Vertebrates		Fossils		Slumped beds
	Belemnites		Wood		Fossils abundant	⅏	Paleosol
	Brachiopods		Beds distinct	(⅋)	Fossils sparse		Mud cracks
	Bryozoans	(=)	Beds obscure		Gastropods	□ □□	Salt molds
	Corals, solitary	≠	Unbedded		Graptolites		Burrows
	Corals, colonial		Graded beds	♤	Leaves	○	Pellets
	Crinoids		Planar cross-bedding		Ostracodes	⊙	Oolites
	Echinoderms		Trough cross-bedding		Pelecypods	◎	Pisolites
	Echinoids		Ripple structures		Root molds		Intraclasts
	Fish bones		Cut and fill	⅄	Spicules		Stylolite
	Fish scales		Load casts		Stromatolites	⊖	Concretion
					Tree trunk in place		Calcitic concretion

Lithologic Patterns for Stratigraphic Columns & Cross Sections

1. Breccia
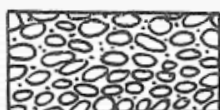
2. Clast-supported conglomerate

3. Matrix-supported conglomerate

4. Conglomeratic sandstone

5. Coarse sandstone
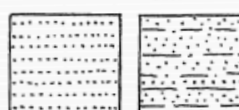
6. Fine sandstone
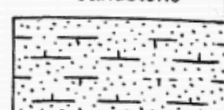
7. Feldspathic sandstone

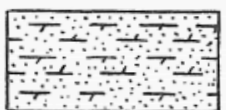8. Tuffaceous sandstone
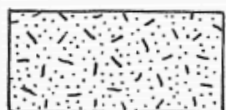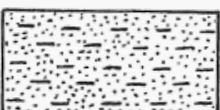
9. Graywacke
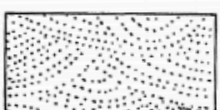
10. Cross-bedded sandstone
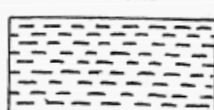
11. Bedded sandstone

12. Calcite-cemented sandstone

13. Dolomite-cemented sandstone

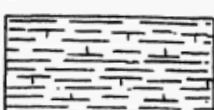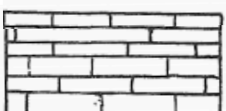14. Silty sandstone

15. Siltstone
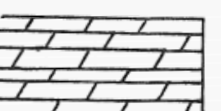
16. Mudstone

17. Shale

18. Coal bed with carbonaceous shale

19. Pebbly mudstone

20. Calcareous shale
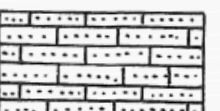
21. Limestone

22. Cross-bedded limestone

23. Dolomite (dolostone)
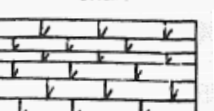
24. Dolomitic limestone

25. Calcitic dolomite
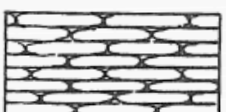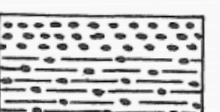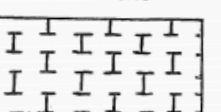
26. Sandy limestone

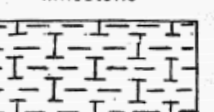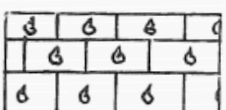27. Clayey limestone

28. Cherty limestone

29. Bedded chert

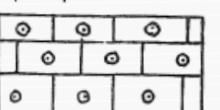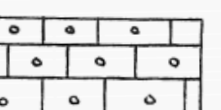30. Phosphorite, phosphatic shale

31. Chalk

32. Marl

33. Fossiliferous limestone
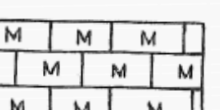
34. Oolitic limestone

35. Pelletal limestone

36. Intraclastic limestone

37. Crystalline limestone

38. Micritic limestone

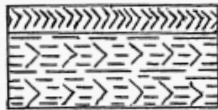39. Algal dolomite

40. Limestone conglomerate

Lithologic Patterns for Stratigraphic Columns & Cross Sections

41. Limestone breccia

42. Algal dolomite breccia

43. Gypsum bed, gypsiferous shale
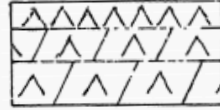
44. Anhydrite, anhydritic dolomite

45. Rock salt, salty mudstone
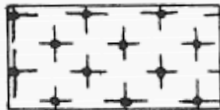
46. Peridotite
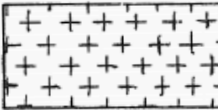
47. Gabbro
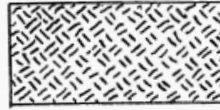
48. Mafic plutonic rock
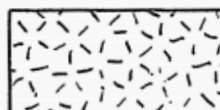
49. Coarse granitic rock
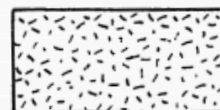
50. Fine granitic rock
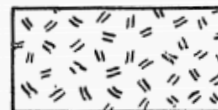
51. Porphyritic plutonic rock

52. Porphyritic plutonic rock

53. Mafic lava
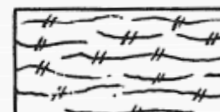
54. Silicic lava
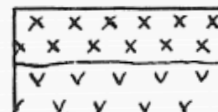
55. Intrusive volcanic rocks

56. Pillow lava
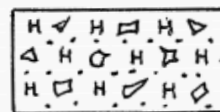
57. Hyaloclastite
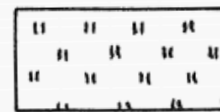
58. Tuff
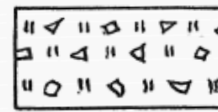
59. Tuff-breccia
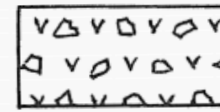
60. Volcanic breccia
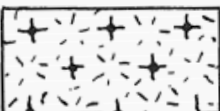
61. Massive serpentinite
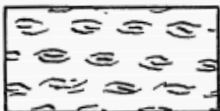
62. Foliated serpentinite
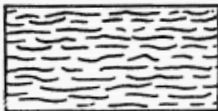
63. Schist
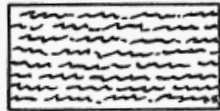
64. Crenulated schist

65. Folded schist
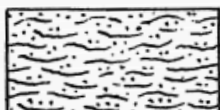
66. Semischistose sandstone
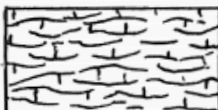
67. Semischistose limestone

68. Semischistose gabbro

69. Greenstone
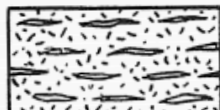
70. Silicic gneiss
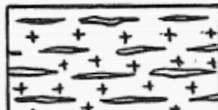
71. Mafic gneiss
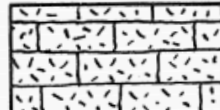
72. Marble
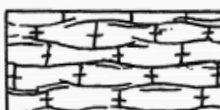
73. Foliated marble
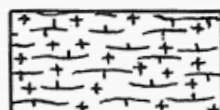
74. Foliated calc-silicate rock
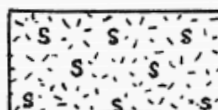
75. Massive skarn
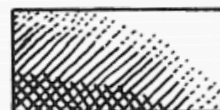
76. Alteration zones
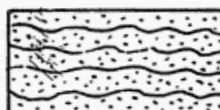
77. Quartzite

78. Quartzite

79. Silicic migmatite

80. Mafic migmatite

From Compton, 1985

Geologic Timescale

PRECAMBRIAN

EON	ERA	PERIOD	BDY. AGES (Ma)
PROTEROZOIC	NEOPROTEROZOIC	EDIACARAN	542
		CRYOGENIAN	630
		TONIAN	850
	MESOPROTEROZOIC	STENIAN	1000
		ECTASIAN	1200
		CALYMMIAN	1400
	PALEOPROTEROZOIC	STATHERIAN	1600
		OROSIRIAN	1800
		RHYACIAN	2050
		SIDERIAN	2300
ARCHEAN	NEOARCHEAN		2500
	MESOARCHEAN		2800
	PALEOARCHEAN		3200
	EOARCHEAN		3600
HADEAN			3850

PALEOZOIC

PERIOD	EPOCH	AGE	PICKS (Ma)
PERMIAN	L	CHANGHSINGIAN	251
		WUCHIAPINGIAN	254
	M	CAPITANIAN	260
		WORDIAN	266
		ROADIAN	268
	E	KUNGURIAN	271
		ARTINSKIAN	276
		SAKMARIAN	284
		ASSELIAN	297
CARBONIFEROUS	PENNSYLVANIAN	GZHELIAN	299.0
		KASIMOVIAN	304
		MOSCOVIAN	306
		BASHKIRIAN	312
	MISSISSIPPIAN	SERPUKHOVIAN	318
		VISEAN	326
		TOURNAISIAN	345
DEVONIAN	L	FAMENNIAN	359
		FRASNIAN	374
	M	GIVETIAN	385
		EIFELIAN	392
	E	EMSIAN	398
		PRAGHIAN	407
		LOCKHOVIAN	411
SILURIAN	L	PRIDOLIAN	416
		LUDFORDIAN	419
		GORSTIAN	421
	M	HOMERIAN	423
		SHEINWOODIAN	426
	E	TELYCHIAN	428
		AERONIAN	436
		RHUDDANIAN	439
ORDOVICIAN	L	HIRNANTIAN	444
		KATIAN	446
		SANDBIAN	455
	M	DARRIWILIAN	461
		DAPINGIAN	468
	E	FLOIAN	472
		TREMADOCIAN	479
CAMBRIAN*	Furongian	STAGE 10	488
		STAGE 9	492
		PAIBIAN	496
	Series 3	GUZHANGIAN	501
		DRUMIAN	503
		STAGE 5	507
	Series 2	STAGE 4	510
		STAGE 3	517
	Terreneuvian	STAGE 2	521
		FORTUNIAN	535
			542

MESOZOIC

| PERIOD	EPOCH	AGE	PICKS (Ma)
CRETACEOUS	LATE	MAASTRICHTIAN	65.5
		CAMPANIAN	70.6
		SANTONIAN	83.5
		CONIACIAN	85.8
		TURONIAN	89.3
		CENOMANIAN	93.5
	EARLY	ALBIAN	99.6
		APTIAN	112
		BARREMIAN	125
		HAUTERIVIAN	130
		VALANGINIAN	136
		BERRIASIAN	140
JURASSIC	LATE	TITHONIAN	145.5
		KIMMERIDGIAN	151
		OXFORDIAN	156
	MIDDLE	CALLOVIAN	161
		BATHONIAN	165
		BAJOCIAN	168
		AALENIAN	172
	EARLY	TOARCIAN	176
		PLIENSBACHIAN	183
		SINEMURIAN	190
		HETTANGIAN	197
TRIASSIC	LATE	RHAETIAN	201.6
		NORIAN	204
		CARNIAN	228
	MIDDLE	LADINIAN	235
		ANISIAN	241
	EARLY	OLENEKIAN	245
		INDUAN	250
			251.0

Magnetic Polarity: RAPID POLARITY CHANGES

CENOZOIC

PERIOD	EPOCH	AGE	PICKS (Ma)
NEOGENE (TERTIARY)	HOLOCENE		0.01
QUATER-NARY	PLEISTOCENE	CALABRIAN / GELASIAN	1.8 / 2.6
	PLIOCENE	PIACENZIAN	3.6
		ZANCLEAN	5.3
	MIOCENE (L)	MESSINIAN	7.2
		TORTONIAN	11.6
	MIOCENE (M)	SERRAVALLIAN	13.8
		LANGHIAN	16.0
	MIOCENE (E)	BURDIGALIAN	20.4
		AQUITANIAN	23.0
PALEOGENE (TERTIARY)	OLIGOCENE (L)	CHATTIAN	28.4
	OLIGOCENE (E)	RUPELIAN	33.9
	EOCENE (L)	PRIABONIAN	37.2
		BARTONIAN	40.4
	EOCENE (M)	LUTETIAN	48.6
	EOCENE (E)	YPRESIAN	55.8
	PALEOCENE (L)	THANETIAN	58.7
	PALEOCENE (M)	SELANDIAN	61.7
	PALEOCENE (E)	DANIAN	65.5

BATTLESHIP

	1	2	3	4	5	6	7	8	9	10
A										
B										
C										
D										
E										
F										
G										
H										
I										
J										

Outline the ships listed below on your grid (horizontally or vertically). Have a friend outline their ships on their grid (don't peak!). Guess at coordinates (mark their guesses on your grid). When someone hits all the squares of their opponent's ship, it's been sunk. Game goes until all of one players' ships have been sunk!

1 carrier (5 squares)
2 battleships (4 squares each)
3 destroyers (2 squares each)
2 cruisers (3 squares each)
1 submarine (3 squares)

Fun Geology Word Search

```
T  E  C  T  O  N  I  C  S  B  A  S  I  N
P  R  E  C  A  M  B  R  I  A  N  R  G  M
T  F  I  R  V  O  L  C  A  N  I  S  M  I
E  E  S  T  R  A  T  I  G  R  A  P  H  Y
R  P  L  A  Y  A  A  A  G  Y  P  S  U  M
R  L  A  N  I  D  U  T  I  G  N  O  L  D
A  M  I  S  S  I  L  E  S  F  A  I  M  U
I  E  E  R  A  C  I  O  Z  O  N  E  C  N
N  I  A  N  O  L  L  A  R  A  F  I  N  E
H  M  T  I  A  N  E  B  A  R  G  I  L  S
S  E  E  T  I  H  W  O  A  S  A  N  D  S
O  G  S  E  D  I  M  E  N  T  A  R  Y  O
J  E  A  E  A  L  A  M  O  G  O  R  D  O
N  A  I  L  O  E  A  L  I  R  R  O  O  T
```

Word List:

RIFT	BASIN	PLAYA	WHITE
SANDS	MISSILES	PRECAMBRIAN	CENOZOIC
JOSH	TECTONICS	FARALLON	DUNE
TERRAIN	AEOLIAN	STRATIGRAPHY	GYPSUM
VOLCANISM	SEDIMENTARY	ALAMOGORDO	MARS
LONGITUDINAL	GRABEN		

Field Trip Bingo

Everyone is cold	Somebody's talk runs longer than 15 minutes (wrap it up)	Wildlife sighting!	Someone takes a selfie with Shane	Someone takes a selfie
You arrived at camp after sunset	Drinking around the campfire	Car trouble (oh no!)	It rained or snowed	Your phone has no reception
Shane uses a pop culture reference	Someone locks the keys in the car	**Everyone wishes Hannah were here Free Space**	A car gets separated from the caravan	Stop for gas (hooray coffee and plumbing!)
Someone teaches Shane a new pop culture reference	Somebody cited Wikipedia in the field trip guide	You see a license plate from East of the Mississippi River	Somebody poses a geology question that stumps everyone	Your radio doesn't work
You see a license plate from East of the Continental Divide	Someone's tent was pitched on top of a cactus (or some equally uncomfortable thing)	Somebody calls Jon "The Bapst"	We're lost	Somebody gets a minor injury while hiking

Field Trip Bingo

Car trouble (oh no!)	Your radio doesn't work	Somebody calls Jon "The Bapst"	You arrived at camp after sunset	Somebody gets a minor injury while hiking
Someone locks the keys in the car	Wildlife sighting!	Someone takes a selfie with Shane	Your phone has no reception	Someone teaches Shane a new pop culture reference
Everyone is cold	We're lost	**Everyone wishes Hannah were here Free Space**	You see a license plate from East of the Continental Divide	You see a license plate from East of the Mississippi River
Somebody's talk runs longer than 15 minutes (wrap it up)	Somebody cited Wikipedia in the field trip guide	Shane uses a pop culture reference	Someone takes a selfie	Drinking around the campfire
A car gets separated from the caravan	Stop for gas (hooray coffee and plumbing!)	Somebody poses a geology question that stumps everyone	Someone's tent was pitched on top of a cactus (or some equally uncomfortable thing)	It rained or snowed

Field Trip Bingo

Drinking around the campfire (hooray coffee and plumbing!)	Stop for gas	We're lost	Your radio doesn't work	Someone teaches Shane a new pop culture reference
Someone locks the keys in the car	It rained or snowed	Someone's tent was pitched on top of a cactus (or some equally uncomfortable thing)	Somebody poses a geology question that stumps everyone	You arrived at camp after sunset
Your phone has no reception	Someone takes a selfie	Everyone wishes Hannah were here Free Space	You see a license plate from East of the Mississippi River	Somebody's talk runs 15 minutes longer than (wrap it up)
Wildlife sighting!	You see a license plate from East of the Continental Divide	Car trouble (oh no!)	Someone takes a selfie with Shane	Somebody cited Wikipedia in the field trip guide
Somebody gets a minor injury while hiking	Everyone is cold	Shane uses a pop culture reference	A car gets separated from the caravan	Somebody calls Jon "The Bapst"

Field Trip Bingo

Someone's tent was pitched on top of a cactus (or some equally uncomfortable thing)	Everyone is cold	Your phone has no reception	Somebody cited Wikipedia in the field trip guide	Car trouble (oh no!)
Your radio doesn't work	You see a license plate from East of the Continental Divide	You see a license plate from East of the Mississippi River	Somebody gets a minor injury while hiking	We're lost
A car gets separated from the caravan	Wildlife sighting!	Everyone wishes Hannah were here Free Space	Drinking around the campfire (hooray coffee and plumbing!)	Stop for gas
Someone takes a selfie	Shane uses a pop culture reference	Somebody poses a geology question that stumps everyone	Somebody's talk runs 15 minutes longer than (wrap it up)	You arrived at camp after sunset
Someone teaches Shane a new pop culture reference	Someone locks the keys in the car	It rained or snowed	Someone takes a selfie with Shane	Somebody calls Jon "The Bapst"